NASA CR-135407
PWA-5512-24

NASA

EFFECT OF STEADY FLIGHT LOADS ON JT9D-7 PERFORMANCE DETERIORATION

JT9D JET ENGINE DIAGNOSTICS PROGRAM

A. Jay and E. S. Todd

UNITED TECHNOLOGIES CORPORATION
Pratt & Whitney Aircraft Group
Commercial Products Division

Prepared for

NATIONAL AERONAUTICS AND SPACE ADMINISTRATION

NASA Lewis Research Center
Contract NAS3-20632

1. Report No.	2. Government Accession No.	3. Recipient's Catalog No.
CR-135407		

4. Title and Subtitle	5. Report Date
Effect of Steady Flight Loads on JT9D-7 Performance Deterioration	June 9, 1978
	6. Performing Organization Code

7. Author(s)	8. Performing Organization Report No.
A. Jay and E. S. Todd	PWA-5512-24
	10. Work Unit No.

9. Performing Organization Name and Address	11. Contract or Grant No.
UNITED TECHNOLOGIES CORPORATION Pratt & Whitney Aircraft Group Commercial Products Division East Hartford, Connecticut 06108	NAS3-20632
	13. Type of Report and Period Covered

12. Sponsoring Agency Name and Address	Sub-Element Task 3A.3
NATIONAL AERONAUTICS AND SPACE ADMINISTRATION Lewis Research Center Cleveland, Ohio 44135	14. Sponsoring Agency Code

15. Supplementary Notes

Project Manager, Joseph A. Ziemianski
NASA Lewis Research Center
Cleveland, Ohio 44135

Project Engineer, Edward G. Stakolich
NASA-Lewis Research Center
Cleveland, Ohio 44135

16. Abstract

Escalating fuel costs and the need to meet national energy conservation goals have led to a new industry awareness of the importance of maintaining good fuel consumption throughout the life-cycle of an engine. However, higher fuel consumption is only part of the overall engine deterioration picture which consists of reduced surge margin, higher exhaust gas temperature, and other hot section distress. Engine deterioration characteristics can, in general, be divided into two time periods. The first, called short-term deterioration, occurs in less than 250 flights on a new engine and in the first few flights following engine repair. Engine deterioration in the second time period, characterized as long-term, involves primarily hot section distress and compression system losses which occur at a somewhat slower rate than short-term deterioration.

It is generally accepted that the causes for short-term deterioration are associated with clearance changes which occur in the flight environment. In this report, the analytical techniques utilized to examine the effects of flight loads and engine operating conditions on performance deterioration are presented. The role of gyroscopic, gravitational, and aerodynamic loads are discussed along with the effect of variations in engine build clearances. These analytical results are compared to engine test data along with the correlation between analytically predicted and measured clearances and rub patterns. Conclusions are drawn and important issues are discussed.

17. Key Words (Suggested by Author(s))	18. Distribution Statement
Engine Performance Deterioration Steady Flight Loads Analytical Model Blade-Tip/Rub-Strip Damage Thrust Specific Fuel Consumption (TSFC)	

19. Security Classif. (of this report)	20. Security Classif. (of this page)	21. No. of Pages	22. Price*
Unclassified	Unclassified	108	

* For sale by the National Technical Information Service, Springfield, Virginia 22161

PREFACE

The requirements of NASA Policy Directive NPD 2220.4 (September 14, 1970) regarding the use of SI Units have been waived in accordance with the provisions of paragraph 5d of that Directive by the Director of Lewis Research Center.

TABLE OF CONTENTS

TABLE OF CONTENTS (Cont'd)

LIST OF TABLES

LIST OF TABLES (Cont'd)

LIST OF ILLUSTRATIONS

LIST OF ILLUSTRATIONS (Cont'd)

LIST OF ILLUSTRATIONS (Cont'd)

LIST OF ILLUSTRATIONS (Cont'd)

SECTION 1.0

SUMMARY

An analytical model for predicting the effects of quasi-steady (slowly varying with time) flight loads on gas turbine performance deterioration has been completed. The flight loads considered are steady state aerodynamic loads, steady state maneuver loads, internal engine loads due to thrust, gyroscopic loads, thermal loads, and engine thrust reverse loads. The model derives from the observation that engine performance is strongly dependent on gas-path seal clearances and relates permanent changes in these clearances to structural deformations and seal rubs which occur within the operating environment. Other factors such as erosion which alter clearances much more gradually than seal rubs are excluded from the present model.

Functionally, the model is used to compute the change in thrust specific fuel consumption (TSFC) that results from the sequence of events which defines an engine flight profile or mission. A given flight profile is broken down into a large number of short segments, called time points, for which airplane and engine operating conditions are known. Internal and external flight loads that act at each time point give rise to structural deflections which may or may not exceed the local gap between static and rotating seal components. When an interference (rub) is found to occur, damage to both blade tips and rub strips is calculated and added to the clearances available for succeeding time points. After all time points in a given flight profile have been considered, average clearance changes for all stages are computed and combined with performance influence coefficients to produce ΔTSFC values for standard steady state engine operating conditions such as sea level take-off and cruise.

The process described above has been applied in detail to the JT9D-7 engine in the 747 nacelle. Missions which have been treated include the production engine acceptance test, the airplane flight acceptance test, and an idealized representation of revenue service. Flight loads for the airplane acceptance test and revenue service simulations were provided by The Boeing Commercial Airplane Company (BCAC). Results from the model strongly reinforce the conclusion that flight induced seal rubs are the primary cause of short-term (150 flights or less) engine performance deterioration and are a significant contributor to the additional deterioration accumulated over the long term. Specifically, predicted changes in take-off TSFC due to flight loads only for the JT9D-7 engine (+1.1, +1.65, +1.9 percent after one, 150, and 1,000 flights, respectively) were found to agree favorably with 747 fleet experience.

Close scrutiny of results from the model reveals that, in general, calculated average clearance changes for the individual stages also correlate well with JT9D-7 experience. Except for the fan stage, however, predicted and observed circumferential rub damage distributions do not compare satisfactorily. Before the model can be upgraded to remove this discrepancy, a comprehensive test program of a flight dressed engine must be conducted to identify discrepancies between calculated and measured deflection characteristics. Such a program will be proposed as part of the JT9D Jet Engine Diagnostics Program.

SECTION 2.0

INTRODUCTION

2.1 PROBLEM DESCRIPTION

The current and projected high cost of fuel for gas turbine engines places a premium on incorporation of design features which increase the operating efficiency of aircraft propulsion systems. One such feature, universally recognized to be of major importance, is the maintenance of tight operating clearances between static and rotating components of flow-path seals. In practice, this is difficult to accomplish since the individual seal components and their supporting structures experience wide excursions in temperatures, rotational speeds, and other loadings at different points in the flight cycle which give rise to relative deflections that can lead to contact, wear, and increased clearances between seal parts. Early gas turbine designs accounted for these time varying loads and associated deflections as part of the standard design process and attempted to tune rotor and case growths such that tight clearances (maximum efficiency) would occur during steady-state operation (climb, cruise) without introducing damaging rubs during transient conditions (take-off, landing). In view of the ready availability of inexpensive fuel and other factors, designs which dropped a few percent in efficiency after a year or two in service were considered adequate at that time.

Today's situation is quite different as a consequence of two factors. First, fuel costs have more than doubled and are expected to continue to rise, and second, higher bypass ratio engines are more susceptible to structural deformations which can cause tight seal clearances to be degraded by rubs. The second factor follows from the larger size (increased thrust and air loads) and increased thrust-to-weight ratio (lightweight, flexible structures) characteristic of the turbofan engines which power current commercial transports. In order to define powerplant configurations which will meet the more stringent performance retention requirements of tomorrow's marketplace, today's designer must have at his disposal a more advanced set of analytical tools with which to anticipate the response (deflections) of an engine to its flight environment (loads) than was previously necessary.

This report describes progress that has been made toward development of a comprehensive analytical procedure for predicting the effects of flight loads on gas turbine performance deterioration. The damage mechanism considered is wear of flow-path outer air seals due to interference of rotating (blade tip) and stationary (rub strip) seal components. Wear behavior of inner air seals is more complex and has been omitted from the current model. Other mechanisms such as erosion and contamination which decrease engine efficiency more gradually than seal rubs are deemed to be of secondary importance and have been excluded. At this point, the model assumes that the loads vary slowly with time and are treated as static. Extension of the model to include dynamic effects is in process and will be the subject of a future report.

2.2 PREVIOUS STUDIES

The design procedure employed to account for the effects of structural deformations on blade tip clearances traditionally splits the associated loads into two distinct groups for computational convenience. The first group is considered to be axisymmetric with respect to the engine centerline and includes thermal, pressure, and centrifugal effects. Accounting for these loads entails construction of detailed time histories of corresponding rotor and case growths which reflect the transient as well as

steady state conditions that occur during test and flight operation. Adequate analytical tools in the form of shell of revolution and body of revolution computer programs have been available and utilized to predict this class of engine deflections for many years. The second group is comprised of loads which are asymmetrically distributed about the engine centerline and includes external air loads (e.g., inlet lift), maneuver loads (G's, gyros), thrust (including thrust reverse), and mount reactions. Until recently, the effects of these loads on seal clearances were predicted by application of equivalent forces and moments to a beam model of the engine rotor/frame structure. Deflections in the vertical and horizontal planes were computed for load combinations expected to occur at crucial points in the flight profile and compared to the available gaps to determine if damaging rubs should occur.

When early JT9D engine designs were found to experience seal rubs and performance losses due to case bending and ovalization, more sophisticated analytical tools were brought into the design analysis process to describe shell (as opposed to beam) deflections associated with the major asymmetric loads (thrust, inlet lift). A significant advance toward improved performance deterioration prediction was made by a Pratt & Whitney Aircraft (P&WA) study in 1973 which utilized results from a general purpose finite element structural analysis program (ASKA) [1]* to account for case deflections induced by thrust and cowl moments. Axisymmetric growths as well as closures due to maneuver loads were treated in the same way as before. By symmetrically dealing with loads, deflections, gap closures, blade/seal damage, and clearance increases for representative stages from each module of the engine (fan, low- and high-pressure compressors, and high- and low-pressure turbines), the 1973 study projected performance credits/debits which could be assigned to various mounting schemes for the JT9D-70 engine and, in so doing, laid the groundwork for the analytical model that is the subject of this report.

Basic assembly of the current system was accomplished as part of an internally funded cooperative Engine/Airframe Structural Integration Program with Boeing Commercial Airplane Company (BCAC) in 1976. Essentially automating the 1973 approach, a special computer program was constructed to track the effects of loads on seal clearance changes and performance losses in detail for arbitrary flight profiles and to reduce the labor required to manipulate the data from the previous two months to only a few days (see Section 3.7). With the availability of the program, the number of time points in the flight cycle which could be examined was increased by an order of magnitude, all engine stages could be included rather than representative ones from each module, and hand calculations of local interferences, blade/seal damage, and ΔTSFC changes were eliminated. The system was exercised with the full complement of data for a simplified flight profile (snap acceleration to steady state take-off, snap deceleration to ground idle) and released for production use at the conclusion of the cooperative P&WA/BCAC 1976 program.

2.3 SCOPE OF CONTRACT EFFORT

Application and extension of the 1976 performance deterioration analytical model was included as part of the JT9D Jet Engine Diagnostics Program (contract NAS3-20632). Application of the model contains those activities related to updating the inputs for the

*Numbers in brackets, [ ], indicate references listed in Section 8.0

JT9D-7 engine and rigorous simulation of load-induced performance losses which occur during 747 acceptance test flights. Virtually all of the primary inputs were updated, involving detailed definition of the typical airplane acceptance test profile, specification of pressure distributions and load factors for time points of interest, construction of corresponding base-line clearance curves, and revision of tables of abradability factors and performance influence coefficients for all 21 stages of the engine. The first two of these five items were provided as part of a Boeing subcontract effort, while the last three were generated by P&WA. Other input data, such as offset grind depths for the fan and high-pressure turbine, and NASTRAN* [2] deflections for thrust and maneuver loads, were carried over without change from the 1976 effort. Detailed input data and results from simulation of the flight acceptance test are discussed in Section 4.0. Simulation of subsequent service experience was not originally planned to be a part of the contract effort but was added in response to requests by program managers. Results of that investigation are described in Section 5.0.

External loads were assumed to vary slowly with time so that dynamic effects could be neglected and deflection calculations made with conventional static analysis tools. Some uncertainty as to the acceptability of this assumption has always been present in view of the transient form of gusts and maneuver loads (landing jolts) encountered in most if not all revenue flights. Consequently, provision was made within the Diagnostics Contract to extend the deterioration model to include dynamic effects. Work toward that end is currently underway.

*The acronym NASTRAN is formed from NAsa STRuctural ANalysis. NASTRAN is a general purpose digital computer program for the analysis of large complex structures and has its origin in the research councils of NASA.

SECTION 3.0

ANALYTICAL MODEL

3.1 OVERVIEW

This section provides a general description of the analytical procedure employed to assess the effects of steady flight loads on short-term performance deterioration of the JT9D-7/747 propulsion system. In essence, the model provides a vehicle for predicting blade tip rub damage caused by structural deformations which occur during flight operation and relates the corresponding enlarged seal clearances to increases in engine thrust specific fuel consumption. While most of the data used by the model is generated within P&WA powerplant analysis groups (Structures, Systems, Performance, etc.), the airframe manufacturers (BCAC, DAC*) must also be looked to for accurate representations of their hardware and externally applied flight loads. Inputs from the individual analysis groups stem from specialized solutions for smaller parts of the gas turbine problem and combine to give the model its foundation in thermodynamics, aerodynamics, solid mechanics, and other technical disciplines. A rough idea of the manner in which these inputs are combined to relate causes and effects for the problem at hand can be formed by examination of Figure 1. Detailed information on each item in this flow chart is given below.

3.2 FLIGHT PROFILE DEFINITION

The starting point for all deterioration predictions to be discussed in this report is a description of the sequence of operating conditions or events which comprise a engine mission or flight profile. The cycle may be relatively simple in terms of power level changes and exposure to external loads, as is the case for standard production engine acceptance tests on the ground, or may encompass load spectra from run-way roughness to clear air turbulence which are commonly encountered by commercial airlines. Each such cycle is constructed from a series of time segments (start-up, taxi, take-off, climb, cruise, descent approach, landing, shutdown), the end points of which can be characterized by unique combinations of aircraft and engine operating parameters (gross weight, altitude, attitude, Mach number, rotor speeds, temperatures, pressures, flows) that serve to define boundary conditions for subsequent aerodynamic, thermodynamic, and structural analyses. For the purposes of this report, attention has been primarily focused on the airplane acceptance test flight, chiefly because the profile is well defined and reasonably controlled. Ground tests and fleet service which precede and follow the flight acceptance test, respectively, have also been included but in a less rigorous fashion. Quantitative information on idealization of these cycles for the JT9D-7 engine is given later in the text (see Subsections 4.2 and 5.2).

3.3 AXISYMMETRIC LOADS AND DEFLECTIONS

Temperature, pressure and centrifugal force fields play an important role in determining internal seal clearances. Perhaps the most convenient feature of this set of forces is the common assumption that circumferential variations in these fields are small and, for the purposes of deflection analysis, can be neglected. The second important characteristic is that each field varies appreciably in response to changes in power level and requires a transient analysis for proper representation. Specialized computational procedures have evolved at P&WA to perform the secondary flow, heat transfer, and other analyses that define temperature, pressure, and rotor speed time histories for desired flight profiles. These loads are input to

*DAC-Douglas Aircraft Company

axisymmetric structural analysis programs which generate corresponding histories of relative deflections (gap closures) between static and rotating components of the gas-path seals (Figure 2-A). Combination of the axisymmetric closures with values for the initial build clearances (cold gaps, also assumed to be uniform) then provides the sought after hot clearances as functions of time. Since they essentially indicate the gaps available for accommodation of additional deflections due to external flight loads, plots of these data will hereafter be referred to as base-line clearance curves. A full set of outer air-seal curves for the JT9D-7 airplane acceptance test flight was generated as part of the contract effort and is discussed in Subsection 4.2.

3.4 ASYMMETRIC LOADS AND DEFLECTIONS

The second set of structural deformations is related to loads which are not uniformly distributed with respect to the engine centerline. Generally, the set arises from external motions or restraints imposed by the flight environment and is composed of air loads (inlet lift), maneuver loads (G's and gyros), and thrust (including thrust reverse). Asymmetric cowl loads occur as pressure distributions around the inlet which is bolted to the engine. As would be expected, consideration of these loads and their contribution to the performance deterioration problem presents a greater challenge than was the case for the previous group. For ease of analysis, these asymmetric loadings may be decomposed into symmetric (Figure 2-C) and antisymmetric components (Figure 2-B). This aspect allows only a half model of the JT9D-7 to be used with proper symmetric or antisymmetric boundary conditions applied at the symmetry plane (vertical plane through the engine centerline).

The burden of defining cowl pressure distributions (air loads) and maneuver load factors for candidate flight missions has traditionally been borne by the airframe manufacturers. Since these data are usually supplied to P&WA only in gross form (force/moment resultants, design limits/envelopes), provision was made for BCAC to generate detailed aerodynamic load descriptions for the flight acceptance test as part of their coordinated subcontract effort. That task was accomplished quite satisfactorily for all time points of immediate interest, and the results are discussed in Subsection 4.2. Conversion of internal and external pressure distributions into appropriate descriptions of thrust and thrust reverse loads was also performed by P&WA and BCAC, respectively.

The fundamental nature of this class of loads leads to axial and circumferential variations in engine case deformations that can differ significantly from patterns which can be predicted with the classical beam model approach. In order to allow for case ovalization, local distortion around thrust pick-ups and mount points, and other shell-like effects, advanced analytical tools must be employed. While some success in dealing with ovalization effects has been achieved with shell-of-revolution formulations, only the finite element discretization in the circumferential direction has been found to provide the modeling flexibility required to obtain accurate deflection solutions.
Since calculation of circumferential rub damage distributions was desired for this effort, the NASTRAN finite element model of a flight-dressed JT9D-7 available from earlier studies [2] was adopted for description of asymmetric structural deflections (Figure 3). For a more detailed description of the NASTRAN model, see Subsection 3.8. Nodal forces consistent with inlet cowl pressure distributions, internal thrust build-up, maneuvers, and thrust reverse loadings were applied to the NASTRAN model, and corresponding rotor/case displacement solutions were obtained. Model data as well as all nodal deflections were stored on magnetic tape for later use in seal rub and performance deterioration analyses (see Subsection 3.7).

3.5 BLADE-TIP/RUB-STRIP DAMAGE CALCULATION

The process by which structural deflections are translated into blade-tip/rub-strip damage is schematically indicated in Figure 4. Results of a calculation for both symmetric and antisymmetric loadings is shown in Table I. As already seen (Figure 1), the procedure involves calculations for a sequence of time points selected from the given flight profile. For each time point, the effects of axisymmetric loads (baseline clearances), offset grinds and rub damage from previous time points are first combined to establish the circumferential variation of clearance that is available for accommodation of nonaxisymmetric structural deformations (Figure 4-A). Asymmetric rotor/case deflections are then introduced, and when the relative closures exceed the available gap, the extent of local interference is recorded (Figure 4-B). Finally, wear characteristics of the contacting materials (abradability factors, see Section 4.3) are brought in to determine the trade-off between blade-tip/rub-strip damage due to the interference (Figure 4-C). Gap changes caused by shortened blades and the worn rubstrip are in turn carried forward to appear as increased initial clearances for the next time point. At the end of the cycle, the accumulated damage for each rub strip is circumferentially averaged (Fourier decomposition) and added to blade-tip wear to provide the average clearance change for the stage.

3.6 PERFORMANCE DETERIORATION DUE TO CLEARANCE CHANGES

The final step to be taken involves conversion of permanent clearance changes for the total cycle to increases in TSFC under standard performance conditions. This is accomplished by simply summing the contributions from each stage, or,

$$(\Delta TSFC)_i = \sum_{\substack{\text{all} \\ \text{stages}}} \zeta_{ij}\, \bar{c}_j$$

where

ζ_{ij} = performance influence coefficient for stage j, condition i

$\bar{c}_j$ = average clearance change for stage j

Influence coefficients are unique to a particular engine model and are provided by the Powerplant Performance Group at P&WA. The values used for the JT9D-7 at take-off and cruise are shown later in the report (see Subsection 4.4).

3.7 NASTRAN PERFORMANCE DETERIORATION POST-PROCESSOR

The NASTRAN performance deterioration post-processor was developed as part of the BCAC and P&WA 1976 cooperative effort.

The program computes clearance increases and performance deterioration resulting from blade-tip/rub-strip interferences. The program accepts NASTRAN deflection output in card image format. Three NASTRAN internal data blocks are used to define case and rotor geometry, and these must also be obtained from the NASTRAN run. The program performs the functions described in Section 3.0 of this report. It eliminates the large amount of hand work that would be required to perform these calculations for each stage in the engine. The flow of the program is depicted in Figure 1.

3.8 NASTRAN STRUCTURAL MODEL OF THE JT9D-7/747

The mathematical model was jointly developed by P&WA and BCAC and began with an identi-

fication of below-the-wing propulsion system substructures, which were provided by each party. Since, primary emphasis in the study was on behavior of the engine, the wing was not included. By excluding the wing, the nacelle/strut combination could reasonably be assumed to be symmetric about a vertical plane through the engine centerline. Symmetric and antisymmetric behavior could then be calculated with a half model for much less cost than a full model.

Substructure interfaces were chosen where subassemblies were mechanically joined (i.e., mount points, flanges, etc.), Figures 5 and 6. Detailed finite-element models of the engine static structure (cases and bearing support frames), rotors, and thrust yoke were provided by Pratt & Whitney Aircraft. Rotors were modeled as beams with discrete masses input directly. Boeing provided the inlet, strut, and tailcone models.

Secondary structural components (fan and core cowls, fan and turbine reversers, stator assemblies), accessories, and plumbing were included as discrete or distributed masses as appropriate to bring the mass properties of the model to within 5 percent of the actual hardware. The final static model consisted of eight substructures with approximately 11,000 freedoms as shown in Figure 7 and summarized in Table II.

SECTION 4.0

SIMULATION OF ACCEPTANCE TESTS/FIRST FLIGHT

4.1 OVERVIEW

The production flight acceptance test mission was selected for simulation because every 747 off the assembly line is tested this way, according to a routine that is kept as standard as possible. The purpose of the flight acceptance test is to check out airplane internal systems. Airplane take-off gross weight, air speed, and throttle setting vary somewhat from test to test because pilot instructions are given in terms of obtaining a signal from a warning or control instrument rather than in terms of achieving a specified flight condition.

Operating conditions to be considered as part of the flight acceptance test are defined in terms of rotor speeds, pressures, and temperatures from engine performance tables along with flight-related parameters such as attitude, altitude, inlet Mach number, airplane weight, and fuel distribution in the wing. Air loads present on the inlet are described for the flight acceptance profile. Thermal, pressure, and centrifugal loadings are accounted for by the use of base-line clearance curves. These curves describe axisymmetric clearances between rotating and stationary seal components as functions of time for the flight acceptance profile. Inertia (G's) and gyroscopic effects as a function of time are also characterized for the acceptance profile.

The computer simulation of the flight acceptance profile incorporates the proper combination of nacelle loadings, engine thrust, inertia and gyroscopic effects, base-line clearances, and air-seal/blade abradability factors. Exposure to thrust and maneuver loads results in deformation of propulsion system structural members and leads to relative motion between static and rotating components of flow-path seals (this is termed closure). If the motions are larger than can be accommodated by the available clearances, rubs and wear (air-seal/blade damage) will occur and result in a loss in performance. A more detailed description of each of the elements of the flight acceptance profile follows.

4.2 FLIGHT PROFILE

4.2.1 Production Acceptance Test

Each engine is tested according to an accurately controlled set of specifications. Included as part of these specifications are:

1. Engine start up
2. Maximum reverse bleed test
3. Snap accelration from flight idle (to 95 percent thrust)
4. Snap deceleration to ground idle
5. Performance calibrations
6. T_{T6} temperature checks
7. Wet trim
8. Wet take-off including smoke measurement
9. Other data checks

If an engine fails to meet any of its requirements on test, corrective action is taken to overcome the trouble and the engine begins the acceptance test again. After an engine has met the requirements of the test, it is either shipped or disassembled, inspected,

rebuilt, retested and then shipped. These so-called "audit engines" are torn down at a rate of either one every other month or one in every twenty engines, whichever is limiting. Ordinarily, no rub measurements are made during this teardown, but early in the JT9D-7 program, several engines were examined after the production acceptance test and found to have air-seal rubs. One significant point to make is that air seals are rubbed in several stages prior to the airplane acceptance test. This damage prior to the flight acceptance test is accounted for by the NASTRAN Performance Deterioration Post-Processor.

4.2.2 Airplane Flight Acceptance Test

The rationale for the selection of the flight acceptance test has been discussed in a previous section. It should be stressed that the flight profile is kept virtually identical for all airplanes and all customers. The representative 747 used for generation of this profile has the following characteristics:

Airplane gross weight at take-off = 500 Kips

Fuel: 168.8 Kips

The sequence of events for the flight test is as follows:

1. Normal Start.

   Static ground runs.
   Run each engine at dry T.O. power for 30 to 45 sec.
   Snap decelerate to idle.
   Accelerate to 95 percent of static T.O. N_1.
   Snap decelerate to idle.

2. Taxi Out and Take-off.

   Use dry rolling EPR with three air conditioning packs on (approx. 20 minutes at maximum continuous thrust (MCT)).
   Use wet rolling EPR if water injection is installed.
   Typical T.O. gross weight 523,000 lb.

3. Climb at maximum continuous thrust about 20 minutes.

   Check engine and wing anti-icing.

4. Cruise at 35,000 ft., M_n = 0.84 to 0.86, EPR = 1.22 to 1.27 (cruise thrust).

5. Slow down to M_n = 0.77 at 35,000 ft.

   Individually check each engine.
   Air bleed off. Slowly decelerate to check pressure ratio bleed control (PRBC) open.
   Slowly accelerate to check PRBC close.
   Set no-bleed maximum continuous power (MCP) (EPR = 1.68 to 1.70).
   Snap decelerate from N_2 = 95 percent to idle, taking 1.5 sec. to move throttle, and monitor the rpm rate of decay.

6. Set MCP for 3 to 4 minutes, above 30,000 ft., to approach M_{MAX} = 0.92.
   Decelerate to 280 KIAS.

7. While descending to 25,000 ft.:
   Shut down each engine after 2 minutes cool down.
   Windmilling start after approx. 1 minute shutdown time.

8. Increase airspeed to maximum dynamic pressure (q) by setting MCT for about 2 minutes while descending from 22,000 to 19,000 ft.

9. At 17,000 ft. slow down to less than 200 KIAS.
   Check stall warnings at 0, 10, 30-degree flap angles.
   Engine to MCT after each stall warning for about 30 to 45 sec.

Check alternate flaps and alternate landing gear for 10 to 15 minutes at moderate thrust (285 KIAS).
With flaps at 30 degrees, check flap load relief. MCT for about 1 min., while descending to 15,000 ft.

10. Idle descent to 3000 ft.
Normal automatic approach ILS landing.
Make one touch-and-go approach with acceleration to go-around thrust.

11. Reverse thrust to FAA limit and modulate to reverse idle.
Then put on forward thrust and taxi in.

12. Normal engine shutdown accomplished at idle thrust.

Total time for flight acceptance test is about 165 minutes. All throttle maneuvers are carried out in conformity with P&WA restrictions on throttle rates.

This analysis covers the following 16 conditions sampled along the mission profile (Figure 8):

100. Take-off roll

101. Lift-off rotation

102. Climb at 3000 ft.

103. Climb at 17,500 ft.

104. Cruise at 35,000 ft., Mach 0.86

105. Cruise at 35,000 ft., Mach 0.77

106. Mach max. (0.92) at 32,000 ft.

107. Shutdown and restart at 27,500 ft.

108. Max. q (372.3 KEAS) at 20,000 ft. (speed brakes)

109. 1.3 V_s at 17,000 ft., 0° flap

110. 1.3 V_s at 17,000 ft., 10° flap

111. 1.3 V_s at 17,000 ft., 30° flap

112. Descent at 8500 ft.

113. Approach at 3000 ft., 20° flap

114. Touch down

115. Full thrust reverse

A summary of relevant flight parameters is given in Table III.

4.2.3 Flight Loads: Magnitude and Distribution

Inlet pressure distributions were obtained as follows:

For each flight condition the following inputs were supplied for the steady state aerolastic program at Boeing:

> Altitude, equivalent air speed, Mach number, total airplane weight and fuel distribution in the wing, maneuver load factor, upward gust velocity, flap setting, and thrust.

The aeroelastic solution gives the following output:

> Airplane load factor, lift coefficient, wing root angle of attack, wing section angle of attack at the nacelle stations.

Next, the aerodynamic pressure distribution on the nacelle for each flight condition was obtained. This was done by matching as closely as possible the aeroelastic C_L and Mach number with an available flight test for which nacelle static pressures were measured.

The set of flight tests shown in Table IV was available. All blow-in door (BID) inlets had extensive instrumentation on the external surface of the inlet, core cowl, tailcone, and strut. Fixed lip inlets were instrumented only at two azimuth stations (15 and 180 degrees) on the inlet, both externally and internally (Figure 9).

The pressure distribution about the inlet was calculated by curve fitting the function:

$$\frac{P}{P_\infty} = A + B \cos(\theta - 30^\circ)$$

to the experimental points (θ = 15 and 180 degrees). Inside the inlet the pressure distribution had to be extrapolated to the fan face (s/c = 1) from the last experimental point (s/c = 0.224 at θ = 15 degrees and s/c = 0.569 at θ = 180 degrees). This was done by means of the compressible flow relation [3]

$$\dot{m} = 0.579\, \rho_T\, a_T A^*$$

where $\dot{m}$ is the mass flow through the fan. Solving for A^*, one obtains the ratio A_f/A^* (A_f = 40.5 ft^2 = inlet area available to the flow at the fan face). Entering the subsonic flow tables with this ratio, one obtains P/P_T at the fan face and consequently P since P_T is known.

The pressure curves are then extrapolated to this asymptote. The pressure distribution inside and outside the inlet was used as input for the NASTRAN model, together with the resultant loads on fan cowl, fan thrust reverser cowl, and core cowl.

All pressures were integrated to obtain resultant loads and moments for comparison with wind tunnel force data. These data yield forces and moments which are somewhat smaller than those obtained by flight pressures integration. The reason for this is that the wind tunnel data were obtained with flow-through models rather than powered ones, so that the effect of strongly asymmetrical internal pressure distributions in the inlet is not accounted for.

The aeroelastic solution gives airplane C.G. load factors (g's). To determine the load factor on the nacelle, it was noticed that the ratio $\Delta g_{nac}/\Delta g_{airplane}$ was nearly independent of the magnitude of airplane load factor and equal to 2.58 for the outboard nacelle and 1.4 for the inboard nacelle. The lateral load factors on the nacelle were obtained from a two-hour fatigue analysis with flight conditions close to the acceptance test profile.

Airplane pitch rates were calculated from the formula:

$$\dot{\theta} = \frac{32.2\sqrt{\sigma}\,(n_z - 1)}{1.688\, V_e}$$

where σ is the ambient density ratio, n_z is the airplane load factor, and V_e is the equivalent air speed. Yaw rates are assumed to be roughly the same order of magnitude as pitch rates.

This formula simply equates the incremental load factor (n_z-1) to the centrifugal acceleration caused by moving with angular velocity $\dot{\theta}$ in the vertical plane. Nacelle pitch and yaw rates associated with the dynamic excitation of the wing-nacelle system can be evaluated only through a complete dynamic analysis.

4.2.4 Basic Load Cases

Basic loads which were used to simulate the flight acceptance test are given in Table V. These basic loadings represent the following load types which are present in this test:

1) Steady state aerodynamic loads (inlet air loads).

2) Steady state maneuver loads (inertia loads).

3) Loads due to gusts; these are, of course, superimposed on 1) and 2).

4) Internal engine loads due to thrust, centrifugal and gyroscopic forces, and thermal transients.

5) Engine thrust reverse.

The procedures that were used to prepare load magnitudes and distributions are described in Subsection 4.2.2. Figures 10 through 21 depict the inlet air-load pressure distributions, and their resultants are shown in Table VI. These inlet air-load distributions are not symmetric about the vertical axis and hence symmetric and antisymmetric components (for the NASTRAN analysis) were used (Table V). NASTRAN FORCE cards were provided by Boeing for all inlet air-load basic load cases. Inertia load values are given in Table VII for each time point used in the flight acceptance flight profile. Values are given for both inboard and outboard engines. Inertia load values are handled automatically by the NASTRAN program merely by the use of the GRAV bulk data card. The user needs to give only direction and magnitude of the load.

The distributed thrust basic load case was constructed as part of the 1976 P&WA/BCAC Cooperative Structural Integration Program. The load case accounts for thrust build-up due to pressure drops or increases, strut loadings due to air flow, and bearing thrust loadings. These internal loadings were converted to NASTRAN FORCE cards for the analysis. The effects of these basic load cases are all analyzed with the NASTRAN analytical model of the JT9D-7/747 and the engine case and rotor deflections are stored for later use.

Tables VIII through XI depict closures throughout the engine for the previously mentioned load types. These closure maps do not represent damage, as damage is related to both closure and available clearance. These closure maps are produced by the NASTRAN Performance Deterioration Post-Processor which was described in Subsection 3.7 of this report.

4.2.5 Combined Load Cases

The basic load cases are linearly combined with load factor multipliers as shown below for the various time points within the flight acceptance profile, and the resultant damage and deterioration (Δ TSFC) are obtained. Load factor multipliers are used in conjunction with the basic load cases discussed in the previous section to obtain the proper load magnitudes required at each time point within the flight profile. Tables XII and XIII indicate the load factor multipliers used for the flight acceptance profile. As an example, the applied thrust load for flight condition 104 may be derived as:

45,000 x 0.1126 = 5067 pounds

Basic	Load	Applied
Load	Factor	Load

This value is combined with the axial force component of the air loads (Table VII) to yield a total applied load of 1000 pounds (Table III).

4.2.6 Base-Line Clearances

Pressures and centrifugal and thermal growth characteristics of the rotating and static components of gas-path seals must be considered when designing the initial cold seal gap at engine assembly. Since one seal component is rotating and the other is static, centrifugal growth incompatibility simply reflects the

growth of the rotating component. Thermal incompatibilities arise from the fact that the thermal response of the rotating seal component is influenced by the response of the disks. Since most compressor and turbine disks are fatigue-limited structures, to achieve life requirements they must be designed to ensure low stresses, resulting in massive structures that respond slowly to thermal variations. The static component thermal response is influenced by the response of the engine cases. These cases are lightweight structures that encompass large surface areas, hence they respond rapidly to thermal changes. Compressor cases are exposed directly to the primary gas path, whereas turbine cases are exposed to a combination of primary and cooling secondary gas, resulting in a more complex thermal analysis.

Base-line clearance curves which represent these different growth characteristics for all stages of the JT9D-7 were generated as part of the modeling effort required for the airplane flight acceptance test. Base-line clearance values at the representative time points are shown in Table XIV and base-line clearance curves for several stages are given in Figures 23 through 28. Base-line clearances which are functions of engine power settings, etc. are dependent upon build cold clearances. Table XV has been included to show cold clearance values and acceptable build tolerances.

4.3 ABRADABILITY FACTORS

When the relative closure between static and rotating seal components exceeds the available gap, rub damage is introduced to accommodate the interference. In general, the damage occurs in two forms: circumferentially uniform wear of the blade tips, and local (crescent-shaped) machining of the rub strip. The trade-off between blade-tip/rub-strip damage is dictated by the wear characteristics of the contacting materials and appears in the model through parameters called abradability factors (Figures 1 and 4). Values are assigned to these parameters on the basis of experimentally determined volume wear ratios for each material pair involved. The abradability factors used to calculate JT9D-7 rub damage due to flight loads are given in Table XVI.

4.4 PERFORMANCE INFLUENCE COEFFICIENTS

Performance influence coefficients have been developed for the JT9D-7 with the knowledge that increased tip clearance reduces efficiency and flow capacity according to a paired relationship. These coefficients relate blade-tip/rub-strip average damage to performance loss (ΔTSFC). In the flight acceptance profile, the stage average damages for the engine are computed and this damage is transformed into performance loss (ΔTSFC) values for steady state engine operating conditions such as sea level take-off and cruise. Values for these influence coefficients are given in Table XVII.

4.5 RESULTS:

4.5.1 Local Damage Maps/Plots

Results achieved by computer simulation of the JT9D-7/747 airplane acceptance test are discussed in this section. Table XVIII depicts the local damage in mils for the outboard side of the simulated "typical" engine (No. 1 or No. 2). This engine is referred to as typical because the air loads applied are, in general, combinations of both inboard and outboard distributions. The local damage depicted in this table occurs primarily in the fan, low-pressure compressor, and high- and low-pressure turbines with only minimal damage in the high-pressure compressor. Fan stage damage is primarily sidewise (Figure 29) due to the effect of airplane pitch up or down which causes the rotors to move laterally (gyroscopic effects). Damage in the high- and low-pressure turbines is shown to be occurring in both the rub strip and the blade tip due to rub-strip/blade-tip abradability effects. Figures 30 through 38

show circumferential damage distributions for the low-pressure compressor and high- and low-pressure turbine stages. These damage distributions are as viewed from the front of the engine, looking aft.

4.5.2 Average Damage Table

Stage average damages are shown in Table XIX. These values are obtained by circumferentially averaging the local values obtained for the airplane acceptance profile. The fan stage shows relatively small average damage due in part to the fact that the rub strip is relatively soft compared to the blade, and the damage is local in nature. The inclusion of a fan offset grind minimizes bottom damage.

4.5.3 ΔTSFC Prediction and Correlation with Short-Term Experience

The average damage discussed above is linearly converted to ΔTSFC using the performance influence coefficients given in Table XVII. The predicted value of 1.13 percent at static sea level take-off conditions is shown in Table XIX. From Figure 39 it can be seen that the NASTRAN prediction of airplane acceptance test deterioration for the JT9D-7 is quite good when compared to short-term deterioration engine data.

SECTION 5.0

SIMULATION OF JT9D-7/747 SERVICE EXPERIENCE

5.1 OVERVIEW

A new awareness of the importance of minimizing fuel consumption throughout the life cycle of an aircraft engine has led to this simulation of JT9D-7/747 service experience. Historically, it was believed that in the short term (less than 150 flights), the deterioration was primarily due to load-induced opening up of clearances. This belief is confirmed by the simulation of the acceptance test described in Section 4.0 of this report. In the long term, the belief was held that subsequent deterioration was primarily due to erosion, blade foreign object damage (FOD), and other hot section distress, but that no additional contribution was due to load. In this simulation of JT9D-7/747 service experience, an attempt is made to quantify the contribution of the loads to the long-term deterioration picture.

Subsequent subsections of this document describe in more detail the load-related items which were investigated by using the NASTRAN analytical model of the JT9D-7/747. In part, the effects of an engine's exposure to increasingly larger load levels is investigated with the use of 747 airplane load exceedance curves. The relative contribution of various loads to the overall engine deterioration picture is also discussed along with the effects of engine build clearance tolerances, differences between inboard and outboard engine loads and deterioration, and the effects of module reoperation or replacement where initial running clearances are restored part way through an engine's life.

5.2 FLIGHT PROFILE

5.2.1 Specialization of Acceptance Profile

In the simulation of the 747 service experience, it was necessary to specialize the previously defined flight acceptance test profile to include only those maneuvers which are typical of a revenue flight. Airplane stall checks are not part of a 747 revenue flight, so those time points were deleted. The relative values of the load combinations remain unchanged, but the absolute values are increased to account for the probability of encountering larger loads in the life of the 747 airplane. The next subsection of this report describes these load exceedance values

5.2.2 Load Exceedances

Loads described in the previous sections, i.e., air loads plus conservative values of gusts and maneuver intensity, are very unlikely to be exceeded during the flight acceptance test missions and can therefore be identified with the once-per-flight loads. Exceedance data for inlet air loads were obtained from BCAC (Figure 40) based on a three-hour mission. Exceedance data for G loads were obtained from a curve (Figure 41) generated by BCAC for a three-hour flight mission. Exceedance data for pitch and yaw rates were supplied by P&WA (Figure 42). These curves were used to determine ratios of once-per-flight to once-per-several flights loads. Exceedance data for G loads and air loads are considered reliable down to the once-per-thousand flights level. More uncommon load intensities are open to some question. For missions longer than three hours, only the cruise segment would be substantantially different. It is felt that these load intensities, at a given exceedance level, would be very close to the three-hour values, since most turbulence occurs at low altitude (climb and descent segments).

5.2.3 Results

Results achieved by computer simulation of

JT9D-7/747 service experience are discussed in this subsection. The simulation of 747 service experience has been accomplished at several discrete times in the lifetime of the airplane. The significant trend observed to date is that, in the lifetime of the airplane, an ever-increasing exposure to increasing load levels causes engine deterioration. Hence, loads are a contributing factor to engine long-term deterioration as well as short-term deterioration. Figures 43 through 50 show a comparison of sample rub depths measured from engine P-695743 [4] and those predicted by the NASTRAN computer simulation. Table XX summarizes local and average rub depths for all stages of the engine as predicted by NASTRAN and as measured on P-695743. Scrutiny of these figures and Table XX reveals that, in general, the NASTRAN predicted average clearance changes for the individual stages correlate well with P-695743 observations. The high-pressure compressor module is virtually devoid of rub damage in the NASTRAN model, however, the P-695743 engine shows substantial high-pressure compressor rub damage. At present, it is not known whether engine P-695743 exhibits typical or atypical rub patterns. As can be seen in Figure 51, the rub of the first-stage high-pressure turbine outer air seal of P-695743 is not typical when compared to a sample of 149 service engines. Similar data is not available for other stages of the JT9D. Except for the fan stage, predicted (NASTRAN) and observed (P-695743) circumferential rub damage distributions do not compare satisfactorily. The fan stage shows good correlation (Figure 43) with engine P-695743 [4] and with BCAC observations made during 747 airplane certification testing. Figure 44 depicts NASTRAN predicted fan rub damage as a function of the number of flights. NASTRAN model predicted average clearance changes and the resulting change in take-off TSFC is presented in Table XXI for various numbers of flights. These changes in TSFC are also shown in Figure 52 and are compared to actual 747 fleet experience in Figure 53. The NASTRAN model deterioration results are based on quasi-steady flight loads only and, as can be seen in Figure 53, are somewhat lower than the fleet average values. The fleet average values include dynamic load effects, blade and seal erosion, and blade surface roughness, which can account for the differences. Also shown in Figure 53 is the measured ΔTSFC obtained from engine P-695743 after 141 flights.

Knowing that loading induced seal rubs are significant contributors to the long-term engine deterioration, it is essential to further extend the application of the NASTRAN engine model to investigate the effects of differing load levels and their overall contribution to engine deterioration. This work is described in the next section of this report.

5.3 EFFECTS OF VARIABLE LOAD LEVELS ON PERFORMANCE

5.3.1 Thrust

From the computer simulation previously done, it was determined that it would be useful to "split-out" the effects of various loads (thrust, air loads, g loads, and gyro loadings) on engine deterioration. Tables XXII through XXV show the results of this study.

It was found that the contribution of thrust to additional damage was zero. The explanation for this is that during the production acceptance test an engine is run to higher thrust levels than it would ordinarily encounter in the flight acceptance test or service. Any damage occurring due to thrust alone occurs during the production acceptance test with no further damage in the flight acceptance test due to thrust only. During the flight acceptance test, thrust contributes to closure (Figure 54), but there is enough available clearance (previous damage and base-line clearance) to prevent additional damage due to thrust alone.

5.3.2 Air Loads

As can be seen from Tables XXII through XXV, air loads contribute heavily to overall engine deterioration. Air loads account for approximately 80 percent of the overall "loads contribution" to deterioration. With air loads contributing this large portion of deterioration, it is obvious that, if a performance deterioration improvement is desired, revised installation designs are required to improve engine load paths or increase the effective stiffness. This improvement would be accomplished by new mounting concepts, increasing the engine stiffness, or utilizing nacelle load sharing, i.e., stiffening the engine with nacelle structure, e.g. cowls. The most effective solution is yet to be determined.

5.3.3 G Loadings

From Tables XXII through XXV, it can be seen that gravitational (G) loadings effect the two high-pressure turbine stages from a damage standpoint. Also, from Table IX, it can be seen that only the fan, low-pressure compressor, and high-pressure turbine closures are affected by G loadings. For the cycles considered, only the two high-pressure turbine stages, and the two low-pressure compressor stages are affected. The high-pressure turbine stages contribute to the deterioration of the engine with the overall contribution to deterioration being approximately 8 percent of the ΔTSFC. Both cases and rotors respond to G loadings and there is very little that can be done to recover this 8 percent, short of a major engine redesign.

5.3.4 Gyro Loadings

Gyroscopic loadings primarily affect the fan stage of the JT9D-7 engine from the standpoint of damage, due to the fact that the fan is a massive overhung stage and the gyroscopic effects are large (Table X). In terms of deterioration, the effects of gyro loadings amount to approximately 13 percent of the total ΔTSFC. The recovery of this percentage of deterioration would necessitate major design changes such as the addition of bearings to the engine.

5.4 OTHER CONSIDERATIONS

5.4.1 Effects of Build Clearance Tolerances

Ultimately the rate of deterioration of the engine is a function of its design. An engine built with open clearance will deteriorate at a slower rate than an engine with tight clearances. An engine with loose clearances has a high initial fuel consumption, but shows little deterioration with time. An engine with tight clearances starts off with a low initial fuel consumption, but it exhibits a much greater deterioration rate. Modeling studies have shown that although an engine built with tight clearances deteriorates at a greater rate, it still exhibits better fuel consumption than a nominally built engine over its life cycle. This is true, in part, because rubs are local and the stage is still tighter on the average.

The effects of build clearance tolerances were investigated by using the tolerance values given in Table XV in conjunction with the previously mentioned base-line clearance curves (Figures 23 through 28). Figure 55 depicts the results obtained from this investigation. The engine built with open clearances shows less deterioration with time than an engine built with tight clearances. No attempt has been made to bias the curves due to initially higher fuel consumption or initially lower fuel consumption.

5.4.2 Differences in Inboard vs. Outboard Engines

The basic differences between the inboard and outboard engines are the position on the wing and the nacelle angle of attack. The position of the engine on the wing affects the airload distributions due to interaction of the flow field with the fuselage. The G loads are larger on the outboard nacelle, primarily due to wing elasticity. The outboard nacelle has

a lower angle of attack than the inboard nacelle which can result in a larger pitch moment on the inboard nacelle. These differences can, in general, only be characterized in an empirical sense. The loads described in the previous sections of this document represent a hybrid of inboard and outboard values and, hence, the engine in the simulation is termed "typical". Also, engines in service do not usually remain in any single position on any single aircraft, nor do all engines remain intact. An inboard high-pressure turbine module could be swapped for another high-pressure turbine module from an engine that was mounted in the outboard position. Most engines in service become "typical" or multiposition engines in their lifetime.

5.4.3 Correlation with Other Damage Data

As part of an in-house study of engine gapping practices, rub data from JT9D-7 flight engines were obtained from P&WA Engineering and Product Support groups in East Hartford and Southington. The data received was for engines with 2000 to 3000 cycles of service time. Data were obtained for the fan, high-pressure compressor, and the first stage of the high-pressure turbine Figure 56 depicts NASTRAN predicted fan average damage through time versus the 67 mils observed in the 2000 to 3000 engine cycle range. Fan damage is very sensitive to gyro loading magnitudes (see subsection 5.3.4), and for this reason the NASTRAN correlation with observation is felt to be reasonably good.

5.4.4 Reoperation or Module Replacement Effects

In the past, maintenance practices have been directed toward repair of damaged parts, restoration of clearances, and recovery of exhaust gas temperature (EGT) or surge margin at minimum cost for the repair. These maintenance actions were partly directed toward recovering hot section performance losses. Historically, it has been found that these hot section maintenance actions were often ineffective because only a small amount of TSFC was restored and the TSFC recovered was lost again in a short time (Figure 57). The NASTRAN JT9D-7/747 structural model has been used to confirm this effect by simulating 1/1000 flight load levels and restoring high-pressure turbine clearances in the model, and then proceeding with the flight simulation. Since air loads, G's, and gyros all affect high-pressure turbine closures, the high-pressure turbine air seal showed new damage early in the subsequent flight simulation. Reoperation or module replacement (where only build clearances are restored) only temporarily improves TSFC, because as the engine re-enters service and encounters flight loadings, the air-seals in the restored module (high- or low-pressure turbine) once again experiences rub damage and deterioration within a short time frame. When further hot section maintenance is performed, the deterioration repeats itself; hence the "sawtooth" nature of the deterioration curve (Figure 57). As long as the air loads, etc., must be carried by the engine cases, then restoration of clearances will provide only temporary TSFC improvements because the cases will ovalize, the rotors will deflect, and the air seal rub damage will, once again, occur.

SECTION 6.0

CONCLUSIONS

An analytical procedure for assessing the effects of flight loads on engine performance deterioration has been developed and applied to predict short- and intermediate-term changes in TSFC for the JT9D-7/747 installation. Good correlation between predicted and observed values for ΔTSFC serves to confirm the basic assumption that load-induced seal rubs have a significant effect on short-term performance deterioration.

The analytical procedure provides for the detailed description of loads and deflections as they vary with time for arbitrary flight profiles and thereby permits the effects of individual loads to be isolated for evaluation. For the JT9D-7, studies of this kind indicated that air loads (inlet lift) are the dominant factor; maneuver loads (G's and gyros) are of secondary importance, and thrust loads do not alone contribute to performance losses after the production engine acceptance test.

Usefulness of the procedure as a diagnostics tool for understanding the major cause of early performance deterioration (rub-induced clearance changes) has been demonstrated. At the same time, potential usefulness of the procedure as a design tool which can be used to minimize these effects in the future (through improved structural design features such as new mounting concepts, cowl load sharing, and stiffening of the engine as well as active clearance control and optimum bearing placement) has also been inferred.

SECTION 7.0

PLANNED AND PROPOSED FOLLOW-ON EFFORTS

To this point, the loads and deflections which arise during flight have been idealized to be quasi-steady (slowly varying with time) in order that relatively simple structural analysis techniques could be employed. Recognizing that this assumption might be inadequate for gust and inertia loads, generalization of the structural model to include dynamic effects has been scheduled as part of the JT9D Jet Engine Diagnostics Program. In general terms, the effort will add mass and damping to the stiffness model and permit time-phased responses of seal components to be tracked. Relative gap closures will, in turn, be compared with previous quasi-steady results to provide updated load factors for use in the damage/deterioration calculation itself.

As seen in the main body of the report, predicted average rub damage and associated increases in TSFC were found to be in good agreement with JT9D-7/747 test and service experience. Predicted circumferential rub patterns for most stages, however, were not found to agree well with the limited rub measurements currently available. Since uncertainty exists about both the analytical and experimental results, the need for gathering additional data has become apparent. A follow-on project which addresses this issue and others of concern to the performance deterioration problem is fully compatible with the intent of the Diagnostics Program and is in the process of being proposed.

SECTION 8.0

REFERENCES

[1] Schrem, E, "ASKA, User's Reference Manual", ISD Report No. 73, Stuttgart, 1971.

[2] White, J. L. and Todd, E. S., "Normal Modes Vibration Analysis of the JT9D/747 Propulsion System", J. Aircraft, Vol. 15, No. 1, January 1978, pp. 28-32.

[3] Liepmann, H. W., and Roshko, A., "Elements of Gas Dynamics", John Wiley and Sons, Inc., New York, 1957, p. 139.

[4] Short-Term Performance Deterioration in JT9D-7A (SP) Engine 695743; JT9D Jet Engine Diagnostics Program, Contract NAS3-20632, NASA CR-135431, 1978.

TABLE I

CALCULATED CLOSURE DUE TO INLET AIR LOADS AT LIFT-OFF ROTATION FOR THE HIGH-PRESSURE TURBINE SECOND STAGE

Circum. Location (degrees)	Closure (mils)		
	Symmetric Component	Antisymmetric Component	Asymmetric Total*
0.	+12.	+ 0.	+12.
12.	+11.	- 4.	+ 7.
24.	+10.	- 8.	+ 2.
36.	+ 9.	- 12.	- 3.
48.	+ 7.	- 15.	- 8.
60.	+ 5.	- 16.	- 11.
72.	+ 2.	- 18.	- 16.
84.	+ 0.	- 17.	- 17.
96.	- 2.	- 16.	- 18.
108.	- 4.	- 15.	- 19.
120.	- 6.	- 13.	- 19.
132.	- 7.	- 11.	- 18.
144.	- 8.	- 8.	- 16.
156.	- 9.	- 6.	- 15.
168.	- 10.	- 3.	- 13.
180.	- 10.	+ 0.	- 10.
192.	- 10.	+ 3.	- 7.
204.	- 9.	+ 6.	- 3.
216.	- 8.	+ 8.	+ 0.
228.	- 7.	+ 11.	+ 4.
240.	- 6.	+ 13.	+ 7.
252.	- 4.	+ 15.	+11.
264.	- 2.	+ 16.	+14.
276.	+ 0.	+ 17.	+17.
288.	+ 2.	+ 18.	+20.
300.	+ 5.	+ 16.	+21.
312.	+ 7.	+ 15.	+22.
324.	+ 9.	+ 12.	+21.
336.	+10.	+ 8.	+18.
348.	+11.	+ 4.	+15.

(-) Closure
(+) Opening

*Symmetric Component + Antisymmetric Component = Asymmetric Total

TABLE II

SUMMARY OF SUBSTRUCTURES

Substructure	Grid Points	Elements				
		Spring[a]	Rod	Beam	Membrane	Plate
Inlet Cowl	320		86	249		321
Fan and LPC	359			285		319
HPC	464	130		134		252
Turbine	587	2	1	343		480
Tailcone	362	16		165		314
Strut	185			266	124	
Rotors	171	345		168		
Thrust yoke	5			4		
Totals	2453	493	87	1615	124	1686

Total freedoms $\approx$ 11,000 Total elements $\approx$ 4000

[a] Scalar spring elements used for modeling bolt flanges and gyroscopic stiffness.

TABLE III

FLIGHT PROFILE PARAMETERS FOR
AIRPLANE ACCEPTANCE TEST

Altitude (ft)	Gross weight (lbs)	Airspeed (kts)	Net thrust	M_n	Flight condition	Description
0	500,000	110	36,000	0.186	100	Takeoff roll
0	500,000	126	36,000	0.214	101	Takeoff rotation
3,000	497,000	251	24,000	0.401	102	Early climb
17,500	494,000	291	16,500	0.617	103	Mid climb
35,000	486,000	276	7,000	0.860	104	High Mach cruise
35,000	467,000	246	9,000	0.770	105	Low Mach cruise
32,000	466,000	317	10,000	0.920	106	Maximum Mach
27,500	466,000	276	7,000	0.720	107	In-flight shutdown
20,000	466,000	372	15,600	0.830	108	Maximum q
17,000	457,000	161	18,500	0.340	109	1.3 V_S, 0° flaps
17,000	454,000	161	18,500	0.340	110	1.3 V_S, 10° flaps
17,000	450,000	161	18,500	0.340	111	1.3 V_S, 30° flaps
17,000	449,000	161	2,000	0.340	116	Early descent
3,000	449,000	153	2,000	0.240	113	Approach, 20° flaps
0	448,000	160	2,000	0.271	114	Touchdown
0	448,000	160	-10,628	—	115	Thrust reverse

TABLE IV

AVAILABLE FLIGHT TESTS

Flight Test	Instrumented Engine Location	Inlet Type
100-4	–	BID
101-3	Inboard	BID
101-5	Inboard	BID
102-1	Inboard	BID
90-6	Outboard	Fixed Lip
91-2	Inboard	Fixed Lip
92-3	–	Fixed Lip
92-4	Inboard	Fixed Lip
106-3	Inboard	Fixed Lip

TABLE V

BASIC LOAD CASES

- Steady State Aerodynamic Loads
  - Inlet Airloads at Flight Condition 101
  - Inlet Airloads at Flight Condition 102
  - Inlet Airloads at Flight Condition 103
  - Inlet Airloads at Flight Condition 104
  - Inlet Airloads at Flight Condition 105
  - Inlet Airloads at Flight Condition 106
  - Inlet Airloads at Flight Condition 107
  - Inlet Airloads at Flight Condition 108
  - Inlet Airloads at Flight Condition 109
  - Inlet Airloads at Flight Condition 110
  - Inlet Airloads at Flight Condition 111
  - Inlet Airloads at Flight Condition 112
  - Inlet Airloads at Flight Condition 113
- Steady State Maneuver Loads
  - 1G Aft
  - 1G Down
  - 1G Outboard
  - .2 Radian/sec right turn
  - .2 Radian/sec pitch (down)
- Internal Engine Loads
  - 45K lbs thrust
- Engine Thrust Reverse
  - Fan thrust reverse

TABLE VI

FLIGHT ACCEPTANCE TEST INLET PRESSURE LOAD RESULTANTS

ID	Flight Condition	F_x	F_y	F_z	M_x	M_y	M_z	h	V_e	M_n	"X" Gust (Included)
100	Take-off roll	–	–	–	–	–	–	0	110	–	–
101	Take-off rotation	4,479.9	2,586.5	−2,378.	186,500	−323,027		0	126	.214	–
102	Early climb	3,492.5	1,977.5	53.8	89,855	−167,621	−9,777	3,000	151	.401	12. fps
103	Mid climb	2,531.7	914.4	−1,589.1	30,213	−65,447	−5,347	17,500	291	.617	9
104	High Mach cruise	2,028.5	760.8	−1,929.6	33,083	−63,847	−3,899	35,000	275.8	.860	8.6
105	Low Mach cruise	3,194.5	1,405.3	−1.858.1	55,119	−110,188	−74,061	35,000	246.9	.770	10.
106	Max. Mach	1,878.7	483.0	−1,866.7	13,915	−31,105	−3,450	32,000	316.5	.920	5.
107	In-flight shut-down/restart	3,210.	1,205.	−1,702	43,632	−93,040	−6,636	27,500	276.	.72	--
108	Max. q	−2,605.0	−2,337.4	−4,955.0	−104,032	+167,061	10,608	20,000	372.3	.830	6.5
109	1.3 V_{stall}, 0° flaps	6,627.6	3,816.4	−2,449.6	185,150	−354,644	17,800	17,000	161.2	.340	10.5
110	1.3 V_{stall}, 10° flaps	3,251.6	2,140.8	−1,109.2	149,980	−292,453	−6,556	17,000	161.2	.340	10.5
111	1.3 V_{stall}, 30° flaps	2,797.5	1,517.8	−322.5	70,486	−132,388	−7,441	17,000	161.2	.340	10.5
112	Early descent	2,932.	1,504.	−385.	61,736	−111,882	−7,840	17,000	161.	.340	–
113	Approach, 20° flaps	3,712.8	2,119.2	−457.7	93,053	−170,076	−11,308	3,000	153.0	.240	12.
114	Touchdown	–	–	–	–	–	–	0	160.	–	–
115	Thrust reverse	–	–	–	–	–	–	0	160.	–	–

TABLE VII

INERTIA AND MANEUVER LOAD VALUES (INBOARD AND OUTBOARD ENGINES)

		Inboard Engine						Outboard				
ID	Flight Condition	Fn	±gx	±gy	gz	$\dot{\theta}$ Pitch*	$\dot{\phi}$ Yaw	±gx	±gy	gz	$\dot{\theta}$ Pitch*	$\dot{\phi}$ Yaw
100	Take-off roll	36,000	1.43	.0	0.	0.	0.	1.77	.00	0.	0.	0.
101	Take-off rotation	36,000	1.0	.0	0.	.052	.052	1.00	.00	0.	.052	.052
102	Early climb	24,000	1.3	.042	0.	.016	.016	1.55	.13	0.	.016	.016
103	Mid climb	16,500	1.24	.064	0.	.010	.010	1.54	.17	0.	.010	.010
104	High Mach cruise	7,000	1.76	.137	0.	.035	.035	2.39	.19	0.	.035	.035
105	Low Mach cruise	9,000	1.76	.15	0.	.023	.023	2.39	.196	0.	.023	.023
106	Max. Mach	10,000	1.22	.074	0.	.005	.005	1.40	.12	0.	.005	.005
107	Inflight shutdown	7,000	1.042	.042	0.	.005	.005	1.12	.13	0.	.005	.005
108	Max. q	15,600	1.3	.096	0.	.008	.008	1.56	.16	0.	.008	.008
109	1.3 Vs, 0^{o} flaps	18,500	1.62	.043	0.	.040	.040	2.14	.12	0.	.040	.040
110	1.3 Vs, 10^{o} flaps	18,500	1.64	.043	0.	.041	.041	2.18	.12	0.	.041	.041
111	1.3 Vs, 30^{o} flaps	18,500	1.63	.043	0.	.041	.041	2.17	.12	0.	.041	.041
112	Early descent	2,000	1.2	.042	0.	.054	.054	1.58	.13	0.	.054	.054
113	Approach, 20^{o} flaps	2,000	1.64	.028	0.	.054	.054	2.18	.08	0.	.054	.054
114	Touchdown	2,000	1.45	.0	0.	0.	0.	1.67	.00	0.	0.	0.
115	Thrust reverse	−41,120	1.0	.0	−.30	0.	0.	1.00	.00	−.30	0.	0.

*Rigid body values used for both inboard and outboard engines.

TABLE VIII

CLOSURE MAP FOR FLIGHT CONDITION 102; SYMMETRIC LOADING

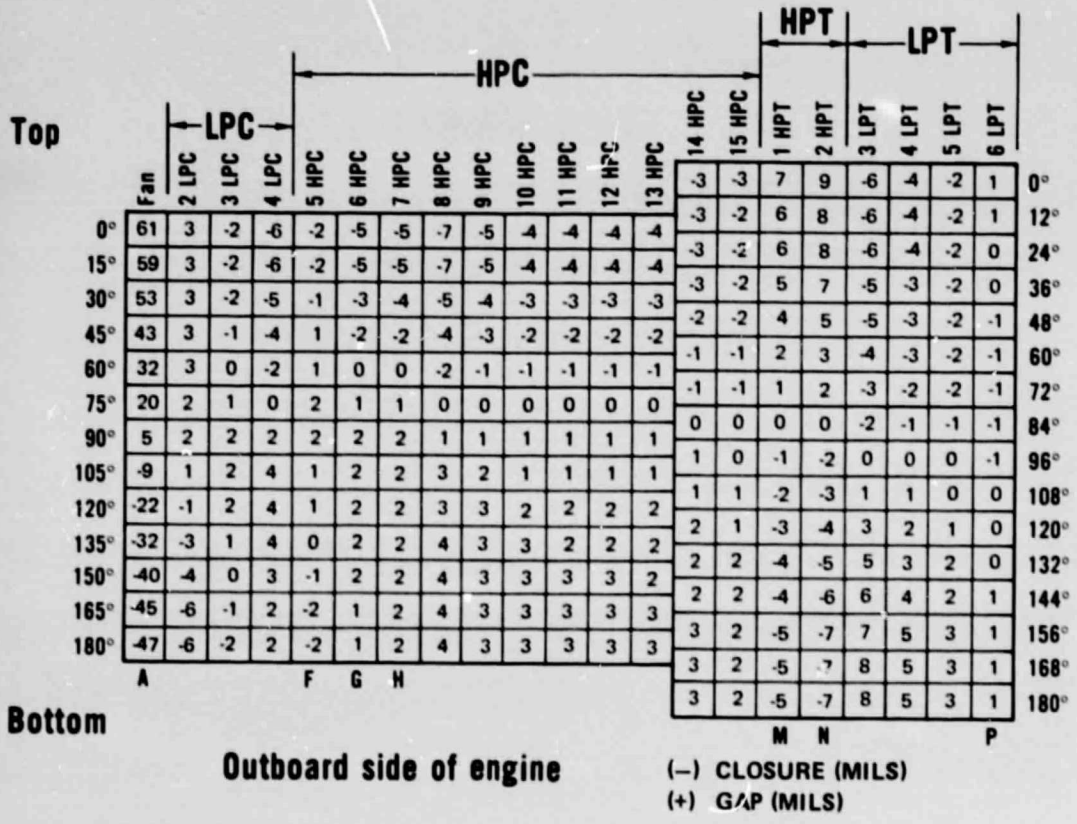

TABLE IX

CLOSURE MAP FOR "1G" DOWN; SYMMETRIC LOADING

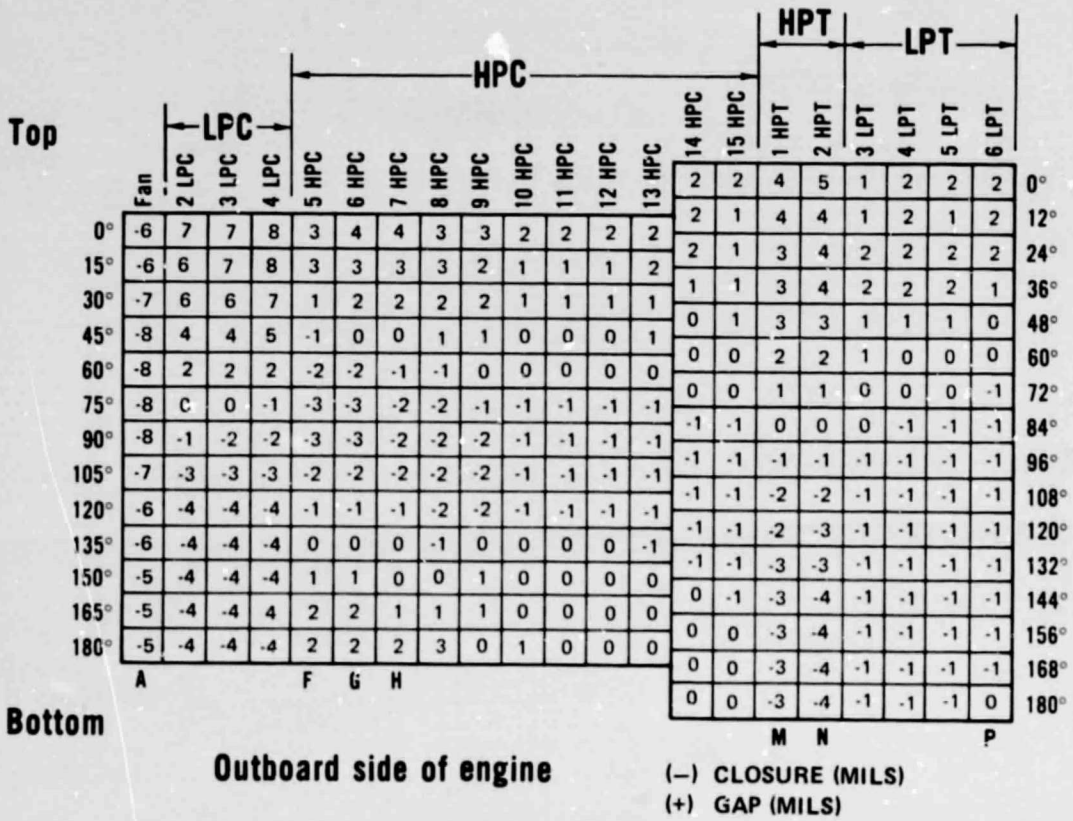

TABLE X

CLOSURE MAP FOR 0.2 RAD/SEC YAW LEFT; SYMMETRIC LOADING

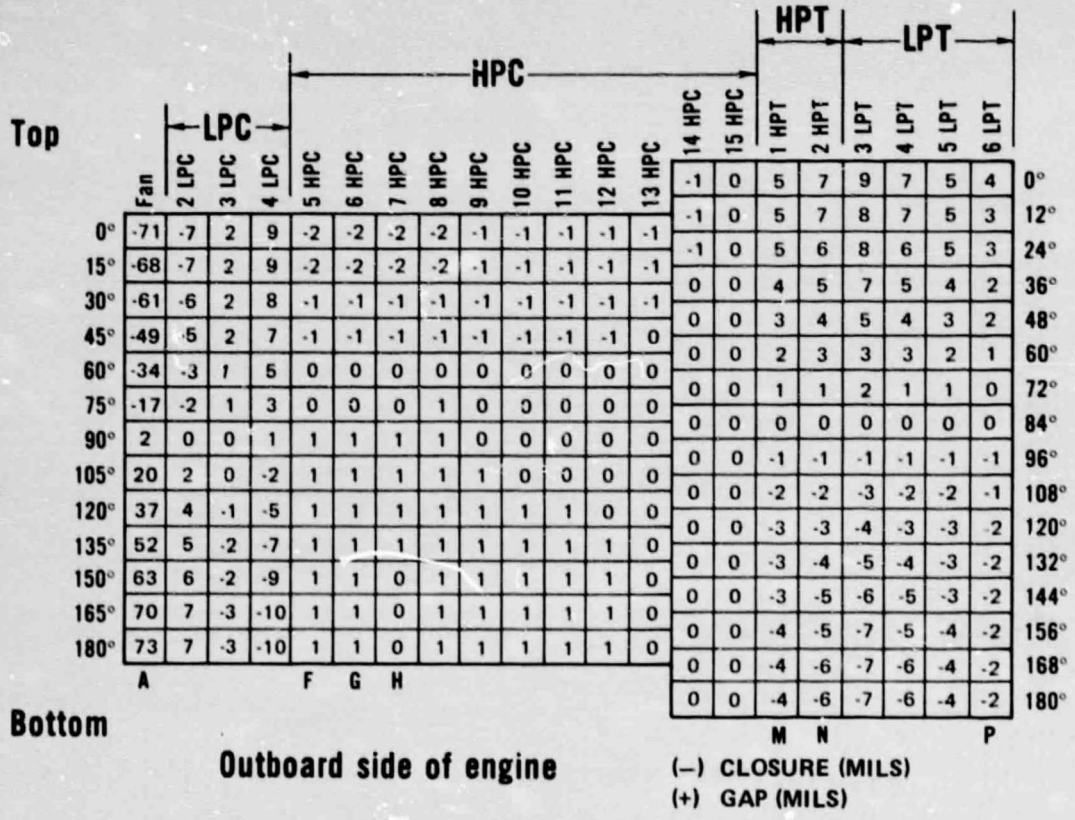

TABLE XI

CLOSURE MAP FOR 45K POUNDS THRUST; SYMMETRIC LOADING

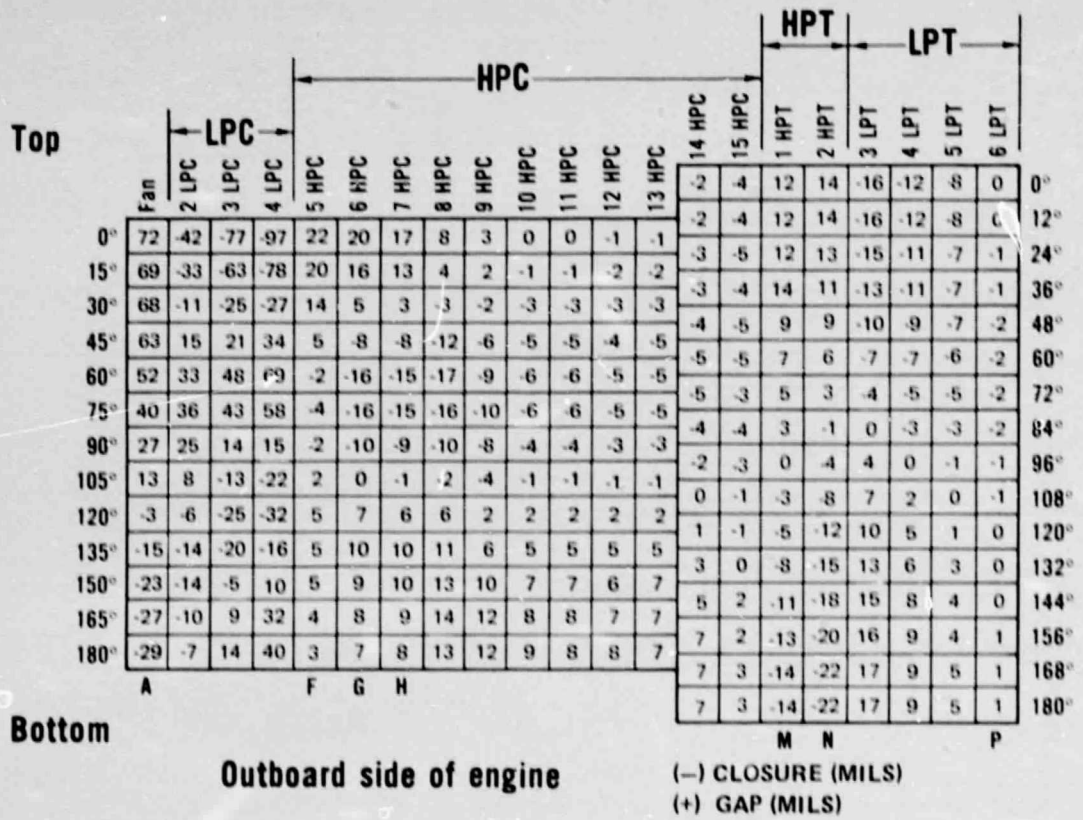

TABLE XII

SYMMETRIC LOAD CASE COMBINATIONS

Load description	Flight condition															
	100	101	102	103	104	105	106	107	108	109	110	111	112	113	114	115
1g down	1.77	1	1.55	1.54	2.39	2.39	1.4	1.12	1.56	2.14	2.18	2.17	1.58	2.18	1.67	1.4
1g aft																-0.3
0.2 rad/sec (right)	—	-.260	±0.08	-0.05	-0.175	±0.115	±0.205	±0.205	±0.04	±0.2	±0.205	±0.205	±0.27	±0.27	—	—
45K lbs thrust	0.8	0.8	0.5345	0.3302	0.1126	0.1587	0.1807	0.1933	0.2365	0.3566	0.5864	0.4039	0.0456	0.0324	0.0444	0
Inlet airload #101		1														
Inlet airload #102			1										0.9078			
Inlet airload #103				1												
Inlet airload #104					1											
Inlet airload #105						1										
Inlet airload #106							1									
Inlet airload #107								1								
Inlet airload #108									1							
Inlet airload #109										1						
Inlet airload #110											1					
Inlet airload #111												1				
Inlet airload #112													1			
Inlet airload #113														1		
Axial component thrust reverse																2
Radial component thrust reverse																0.9456
Pitch moment thrust reverse																0.3862
Turbine droop	1	1	1	1	1	1	1	1	1	1	1	1	1	1	1	1

TABLE XIII

ANTISYMMETRIC LOAD CASE COMBINATIONS

Load description	Flight condition															
	100	101	102	103	104	105	106	107	108	109	110	111	112	113	114	115
1g side (outb'd)			0.13	0.17	0.17	0.21	0.13	0.13	0.16	0.12	0.12	0.12	0.13	0.08		
Inlet airloads #101		1														
Inlet airloads #102			1										0.9078			
Inlet airloads #103				1												
Inlet airloads #104					1											
Inlet airloads #105						1										
Inlet airloads #106							1									
Inlet airloads #107								1								
Inlet airloads #108									1							
Inlet airloads #109										1						
Inlet airloads #110											1					
Inlet airloads #111												1				
Inlet airloads #112													1			
Inlet airloads #113														1		
0.2 rd/sec pitch			±.08	±.05	±.175	±.115	±.025	±.025	+.04	+.2	+.205	+.205	±.27	±.27		

TABLE XIV

BASE-LINE CLEARANCES (INCH); AXISYMMETRIC LOADING

	Flight Condition															
Stage	100	101	102	103	104	105	106	107	108	109	110	111	112	113	114	115
Fan	.057	.006	.008	.001	.011	.015	0.	.057	0.	.010	.008	.005	.004	.010	.013	.013
2 LPC	.067	.024	.027	.022	.030	.033	.023	.061	.023	.044	.031	.013	.061	.062	.062	.033
3 LPC	.028	.008	.009	.007	.011	.012	.007	.025	.007	.017	.011	.003	.029	.025	.025	.012
4 LPC	.036	.009	.002	.009	.005	.008	.000	.031	.000	.016	.006	.000	.031	.032	.022	.008
5 HPC	.017	.015	.008	.008	.013	.015	.011	.040	.007	.009	.011	.011	.009	.027	.011	.013
6 HPC	.013	.017	.011	.012	.016	.018	.014	.042	.010	.012	.015	.015	.013	.030	.013	.012
7 HPC	.036	.035	.028	.029	.033	.035	.031	.050	.027	.028	.032	.032	.030	.045	.036	.037
8 HPC	.022	.020	.015	.016	.021	.022	.018	.045	.015	.016	.019	.019	.017	.034	.023	.023
9 HPC	.020	.030	.020	.014	.020	.021	.017	.037	.014	.016	.018	.018	.016	.030	.016	.022
10 HPC	.013	.017	.013	.016	.020	.022	.016	.042	.017	.018	.019	.019	.017	.030	.013	.015
11 HPC	.005	.015	.010	.013	.014	.015	.013	.025	.010	.012	.013	.013	.013	.018	.002	.008
12 HPC	.010	.030	.027	.028	.025	.025	.026	.018	.025	.025	.026	.026	.027	.024	.014	.015
13 HPC	.017	.033	.021	.023	.025	.026	.026	.020	.021	.022	.024	.024	.025	.028	.019	.020
14 HPC	.010	.013	.020	.019	.023	.023	.022	.015	.018	.021	.022	.022	.020	.025	.013	.081
15 HPC	.018	.025	.019	.020	.023	.023	.023	.018	.019	.018	.021	.021	.021	.025	.021	.019
1 HPT	.020	.036	.037	.030	.038	.041	.028	.045	.035	.035	.032	.035	.032	.046	.031	.023
2 HPT	.000	.005	.015	.025	.037	.037	.015	.030	.016	.032	.035	.035	.025	.040	.005	.002
3 LPT	.035	.085	.077	.045	.035	.033	.065	.003	.055	.040	.040	.040	.020	.045	.035	.030
4 LPT	.045	.085	.077	.046	.041	.042	.057	.005	.065	.047	.042	.040	.025	.060	.051	.047
5 LPT	.031	.071	.063	.036	.041	.043	.051	.006	.061	.051	.041	.037	.041	.066	.041	.041
6 LPT	.017	.052	.047	.024	.028	.033	.017	.002	.042	.037	.029	.028	.007	.057	.030	.027

TABLE XV

JT9D-7 BUILD CLEARANCES (INCH)

Stage	Nominal	Tolerance
Fan	.105	±.01
2 LPC	.0705	±.0145
3 LPC	.0295	±.0135
4 LPC	.0455	±.0145
5 HPC	.0425	±.008
6 HPC	.05	±.008
7 HPC	.061	±.008
8 HPC	.052	±.007
9 HPC	.046	±.006
10 HPC	.041	±.0085
11 HPC	.026	±.006
12 HPC	.0236	±.006
13 HPC	.0284	±.0066
14 HPC	.0245	±.0035
15 HPC	.036	±.005
1 HPT	.073	±.006
2 HPT	.038	±.008
3 LPT	.036	±.0058
4 LPT	.033	±.0088
5 LPT	.065	±.0088
6 LPT	.052	±.0094

TABLE XVI

JT9D-7 AIR SEAL ABRADABILITY FACTORS

Stage	D_B/δ	D_R/δ
Fan	0	1
2 LPC	0	1
3 LPC	0	1
4 LPC	0	1
5 HPC	0	1
6 HPC	0	1
7 HPC	0	1
8 HPC	0	1
9 HPC	0	1
10 HPC	0	1
11 HPC	0	1
12 HPC	0	1
13 HPC	0	1
14 HPC	0	1
15 HPC	0	1
1 HPT	0.4	0.6
2 HPT	0.2	0.8
3 LPT	0.4	0.6
4 LPT	0.4	0.6
5 LPT	0.4	0.6
6 LPT	0.4	0.6

TABLE XVII

PERFORMANCE INFLUENCE COEFFICIENTS

Stage		Average clearance change (mils)		% Δ TSFC		
				SSLTO		Cruise
Fan		100		0.46		0.89
2 LPC		10		0.116		0.12
3 LPC		10		0.116		0.12
4 LPC		10		0.116		0.12
5 HPC		10		0.059		0.031
6 HPC		10		0.059		0.031
7 HPC		10		0.059		0.031
8 HPC		10		0.059		0.031
9 HPC		10		0.059		0.031
10 HPC		10		0.059		0.031
11 HPC		10		0.059		0.031
12 HPC		10		0.059		0.031
13 HPC		10		0.059		0.031
14 HPC		10		0.059		0.031
15 HPC		10		0.059		0.031
1 HPT		10		0.45		0.24
2 HPT		10		0.27		0.13
3 LPT		10		0.11		0.10
4 LPT		10		0.08		0.08
5 LPT		10		0.05		0.05
6 LPT		10		0.03		0.04

TABLE XVIII

LOCAL DAMAGE MAP FOR AIRPLANE ACCEPTANCE TEST

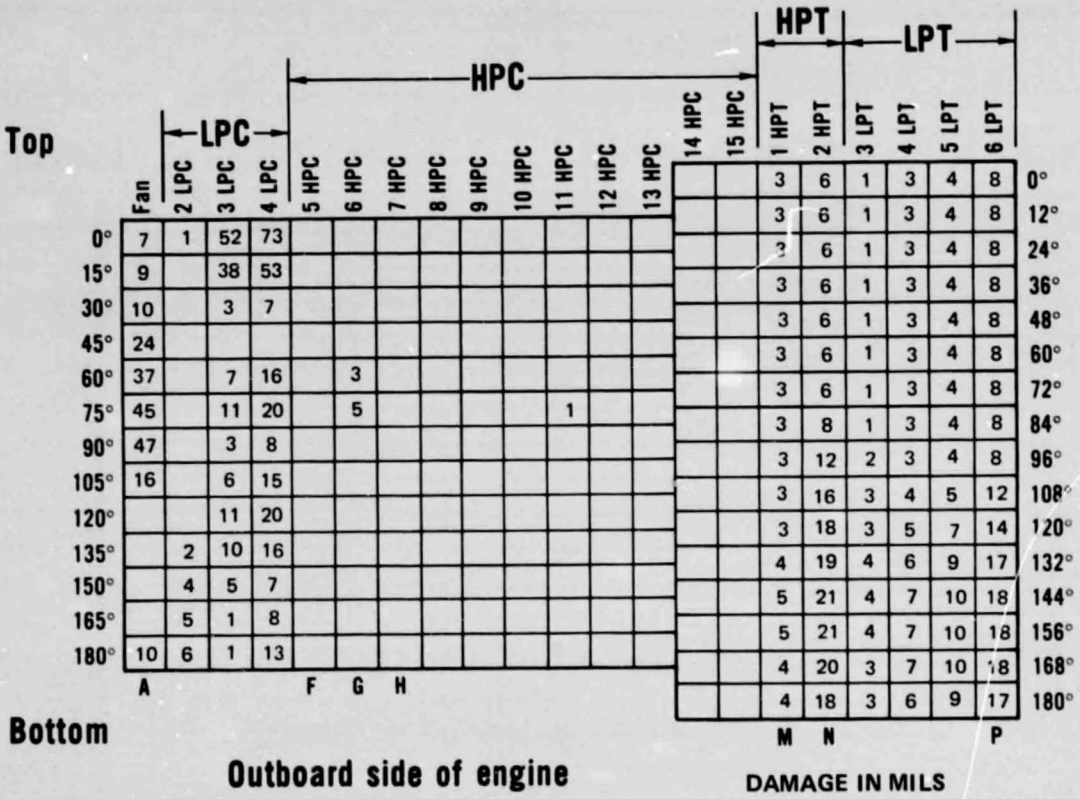

	Fan	2 LPC	3 LPC	4 LPC	5 HPC	6 HPC	7 HPC	8 HPC	9 HPC	10 HPC	11 HPC	12 HPC	13 HPC	14 HPC	15 HPC	1 HPT	2 HPT	3 LPT	4 LPT	5 LPT	6 LPT	
0°	7	1	52	73												3	6	1	3	4	8	0°
15°	9		38	53												3	6	1	3	4	8	12°
30°	10		3	7												3	6	1	3	4	8	24°
45°	24															3	6	1	3	4	8	36°
60°	37		7	16		3										3	6	1	3	4	8	48°
75°	45		11	20		5					1					3	6	1	3	4	8	60°
90°	47		3	8												3	6	1	3	4	8	72°
105°	16		6	15												3	8	1	3	4	8	84°
120°			11	20												3	12	2	3	4	8	96°
135°		2	10	16												3	16	3	4	5	12	108°
150°		4	5	7												3	18	3	5	7	14	120°
165°		5	1	8												4	19	4	6	9	17	132°
180°	10	6	1	13												5	21	4	7	10	18	144°
																5	21	4	7	10	18	156°
																4	20	3	7	10	18	168°
																4	18	3	6	9	17	180°
	A				F	G	H									M	N				P	

TABLE XIX

JT9D-7 AVERAGE DAMAGE VALUES AFTER FIRST FLIGHT

Stage	(mils)
FAN	10
2 LPC	2
3 LPC	14
4 LPC	21
3 LPT	1
4 LPT	4
5 LPT	5
6 LPT	10
5 HPC	–
6 HPC	–
7 HPC	–
8 HPC	–
9 HPC	–
10 HPC	–
11 HPC	–
12 HPC	–
13 HPC	–
14 HPC	–
15 HPC	–
1 HPT	3
2 HPT	10
% ΔTSFC (SSLTO)	1.13

TABLE XX

COMPARISON OF LOCAL AND AVERAGE OUTER AIR SEAL RUB DEPTHS NASTRAN VS. P-695743

Stage		Local Rub Depths, Inches* (0° is top dead center, viewed from the front)								Average Rub Depth, Inches
		0°	45°	90°	135°	180°	225°	270°	315°	
Fan	1	0.015/0.018	0.037/0.031	0.067/0.062	0.017/0.066	0.065/0.063	0.022/0.064	0.034/0.029	0.009/0.011	0.031/0.043
LPC	2	0.018/0.025	0.000/0.000	0.000/0.000	0.008/0.022	0.013/0.045	0.013/0.049	0.000/0.000	0.000/0.000	0.007/0.018
	3	0.075/0.009	0.000/0.000	0.005/0.000	0.018/0.011	0.005/0.015	0.025/0.015	0.005/0.000	0.000/0.001	0.019/0.006
	4	0.097/0.037	0.000/0.004	0.010/0.008	0.022/0.044	0.017/0.042	0.022/0.036	0.010/0.022	0.000/0.030	0.022/0.027
HPC	5	0.000/0.000	0.000/0.002	0.003/0.000	0.000/0.000	0.000/0.005	0.000/0.001	0.003/0.000	0.000/0.000	0.001/0.001
	6	0.000/0.000	0.000/0.004	0.004/0.001	0.000/0.000	0.000/0.000	0.000/0.000	0.004/0.000	0.001/0.000	0.001/0.001
	7	0.000/0.000	0.000/0.000	0.000/0.001	0.000/0.000	0.000/0.000	0.000/0.000	0.000/0.000	0.000/0.003	0.000/0.001
	8	0.000/0.006	0.000/0.002	0.000/0.008	0.000/0.000	0.000/0.000	0.000/0.000	0.000/0.000	0.000/0.010	0.000/0.003
	9	0.000/0.008	0.000/0.009	0.000/0.004	0.000/0.000	0.000/0.000	0.000/0.000	0.000/0.000	0.000/0.000	0.000/0.002
	10	0.000/0.016	0.000/0.010	0.000/0.018	0.000/0.009	0.000/0.006	0.000/0.006	0.000/0.015	0.000/0.029	0.000/0.014
	11	0.000/0.008	0.000/0.012	0.000/0.006	0.000/0.003	0.000/0.001	0.000/0.005	0.000/0.005	0.000/0.010	0.000/0.006
	12	0.000/0.018	0.000/0.018	0.000/0.015	0.000/0.028	0.000/0.020	0.000/0.012	0.000/0.012	0.000/0.022	0.000/0.018
	13	0.000/0.006	0.000/0.014	0.000/0.005	0.000/0.006	0.000/0.013	0.000/0.008	0.000/0.002	0.000/0.005	0.000/0.007
	14	0.000/0.017	0.000/0.019	0.000/0.018	0.000/0.019	0.000/0.025	0.000/0.017	0.000/0.013	0.000/0.021	0.000/0.019
	15	0.000/0.017	0.000/0.017	0.000/0.011	0.000/0.017	0.000/0.021	0.000/0.016	0.000/0.012	0.000/0.010	0.000/0.015
HPT	1	0.006/0.002	0.006/0.002	0.007/0.000	0.010/0.000	0.010/0.000	0.007/0.005	0.006/0.023	0.006/0.012	0.007/0.008
	2**	0.000/0.021	0.005/0.020	0.015.0.026	0.020/0.012	0.010/0.013	0.008/0.029	0.005/0.034	0.005/0.032	0.009/0.023
LPT	3**	0.001/0.004	0.001/0.000	0.001/0.004	0.001/0.005	0.001/0.006	0.002/0.015	0.002/0.015	0.001/0.012	0.001/0.007
	4**	0.002/0.004	0.002/0.000	0.004/0.002	0.005/0.000	0.004/0.000	0.003/0.004	0.002/0.005	0.002/0.011	0.003/0.003
	5**	0.004/0.000	0.004/0.020	0.004/0.000	0.009/0.000	0.008/0.000	0.004/0.000	0.004/0.013	0.004/0.004	0.005/0.003
	6**	0.008/0.000	0.008/0.005	0.008/0.003	0.010/0.000	0.017/0.008	0.010/0.033	0.010/0.010	0.008/0.000	0.010/0.005

* Presented as NASTRAN predicted/P-695743 measured values.

** Average of front and rear land rub depths at a given location.

TABLE XXI

AVERAGE DAMAGE (MILS) AND TSFC PREDICTIONS FOR 747 AIRPLANE SERVICE

Stage	50 flights	100 flights	150 flights	500 flights	1000 flights	3000 flights	5000 flights
Fan	18	25	31	41	51	58	67
2 LPC	3	3	4	5	6	6	6
3 LPC	15	15	15	16	17	17	17
4 LPC	22	23	23	24	25	25	25
3 LPT	1	1	1	1	1	1	1
4 LPT	3	3	3	3	3	3	3
5 LPT	5	5	5	5	5	5	5
6 LPT	10	10	10	11	11	11	11
5 HPC	–	–	–	1	1	1	1
6 HPC	–	–	–	2	2	2	2
7 HPC	–	–	–	–	–	–	–
8 HPC	–	–	–	–	–	–	–
9 HPC	–	–	–	–	–	–	–
10 HPC	–	–	–	–	–	–	–
11 HPC	–	–	–	–	1	1	1
12 HPC	–	–	–	–	–	–	–
13 HPC	–	–	–	–	–	–	–
14 HPC	–	–	–	–	–	–	–
15 HPC	–	–	–	–	–	–	–
1 HPT	5	6	7	7	8	8	8
2 HPT	12	13	14	15	16	16	16
%ΔTSFC (SSLTO)	1.36	1.54	1.65	1.78	1.86	2.09	2.12

TABLE XXII

AVERAGE DAMAGE (MILS) AND TSFC LOSS AT 150 FLIGHTS LOAD CONTRIBUTION

	Loading Condition*			
Stage	1	2	3	4
Fan	–	20	20	31
2 LPC	–	1	2	4
3 LPC	–	15	15	15
4 LPC	–	23	23	23
3 LPT	–	1	1	1
4 LPT	–	3	3	3
5 LPT	–	5	5	5
6 LPT	–	10	10	10
5 HPC	–	–	–	–
6 HPC	–	–	–	–
7 HPC	–	–	–	–
8 HPC	–	–	–	–
9 HPC	–	–	–	–
10 HPC	–	–	–	–
11 HPC	–	–	–	–
12 HPC	–	–	–	–
13 HPC	–	–	–	–
14 HPC	–	–	–	–
15 HPC	–	–	–	–
1 HPT	–	5	7	7
2 HPT	–	12	14	14
% ΔTSFC (SSLTO)	0	1.5	1.61	1.65

*Key:

1 Thrust only
2 Thrust + Airloads
3 Thrust + Airloads + G loadings
4 Thrust + Airloads + G loadings + gyro loadings

TABLE XXIII

AVERAGE DAMAGE (MILS) AND TSFC LOSS AT 500 FLIGHTS LOAD CONTRIBUTION

Stage	Loading Condition* 1	2	3	4
Fan	–	22	22	41
2 LPC	–	1	3	5
3 LPC	–	16	16	16
4 LPC	–	24	24	24
3 LPT	–	1	1	1
4 LPT	–	3	3	3
5 LPT	–	5	5	5
6 LPT	–	11	11	11
5 HPC	–	1	1	1
6 HPC	–	2	2	2
7 HPC	–	–	–	–
8 HPC	–	–	–	–
9 HPC	–	–	–	–
10 HPC	–	–	–	–
11 HPC	–	–	–	–
12 HPC	–	–	–	–
13 HPC	–	–	–	–
14 HPC	–	–	–	–
15 HPC	–	–	–	–
1 HPT	–	5	7	7
2 HPT	–	12	15	15
% ΔTSFC (SSLTO)	0	1.52	1.70	1.78

*Key:

1 Thrust only
2 Thrust + Airloads
3 Thrust + Airloads + G loadings
4 Thrust + Airloads + G loadings + gyro loadings

TABLE XXIV

AVERAGE DAMAGE (MILS) AND TSFC LOSS AT 1000 FLIGHTS LOAD CONTRIBUTION

	Loading Condition*			
Stage	1	2	3	4
Fan	–	24	24	51
2 LPC	–	4	4	6
3 LPC	–	17	17	17
4 LPC	–	25	25	25
3 LPT	–	1	1	1
4 LPT	–	3	3	3
5 LPT	–	5	5	5
6 LPT	–	11	11	11
5 HPC	–	1	1	1
6 HPC	–	2	2	2
7 HPC	–	–	–	–
8 HPC	–	–	–	–
9 HPC	–	–	–	–
10 HPC	–	–	–	–
11 HPC	–	1	1	1
12 HPC	–	–	–	–
13 HPC	–	–	–	–
14 HPC	–	–	–	–
15 HPC	–	–	–	–
1 HPT	–	5	8	8
2 HPT	–	13	16	16
% ΔTSFC (SSLTO)	0	1.65	1.77	1.86

*Key:

1 Thrust only
2 Thrust + Airloads
3 Thrust + Airloads + g loadings
4 Thrust + Airloads + g loadings + gyro loadings

TABLE XXV

AVERAGE DAMAGE (MILS) AND TSFC LOSS AT 5000 FLIGHTS LOAD CONTRIBUTION

	Loading Condition*			
Stage	1	2	3	4
Fan	–	24	24	67
2 LPC	–	4	4	6
3 LPC	–	17	17	17
4 LPC	–	25	25	25
3 LPT	–	1	1	1
4 LPT	–	3	3	3
5 LPT	–	5	5	5
6 LPT	–	11	11	11
5 HPC	–	1	1	1
6 HPC	–	2	2	2
7 HPC	–	–	–	–
8 HPC	–	–	–	–
9 HPC	–	–	–	–
10 HPC	–	–	–	–
11 HPC	–	1	1	1
12 HPC	–	–	–	–
13 HPC	–	–	–	–
14 HPC	–	–	–	–
15 HPC	–	–	–	–
1 HPT	–	5	8	8
2 HPT	–	13	16	16
% ΔTSFC (SSLTO)	0	1.8	1.98	2.12

*Key:

1 Thrust only
2 Thrust + Airloads
3 Thrust + Airloads + g loadings
4 Thrust + Airloads + g loadings + gyro loadings

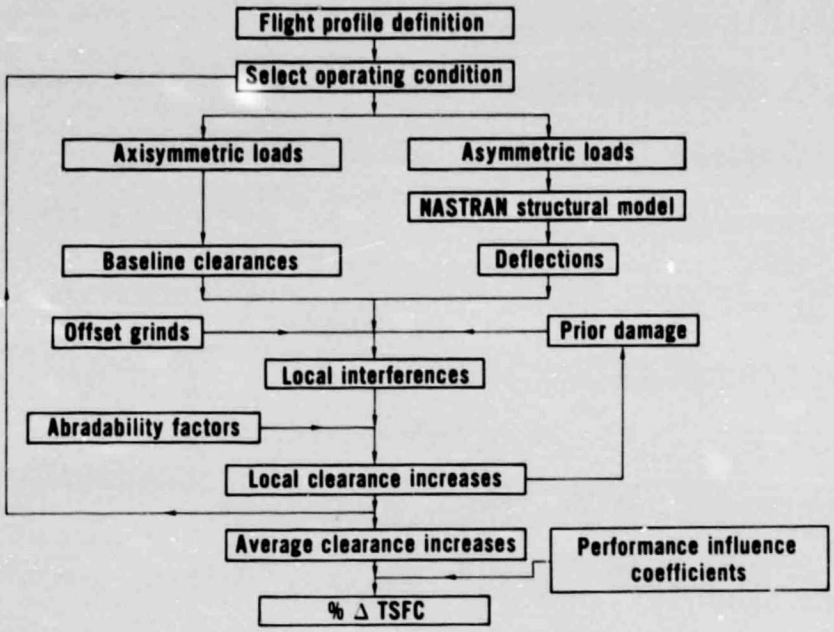

Figure 1 Flow Chart for the Analytical Model (J18750-4)

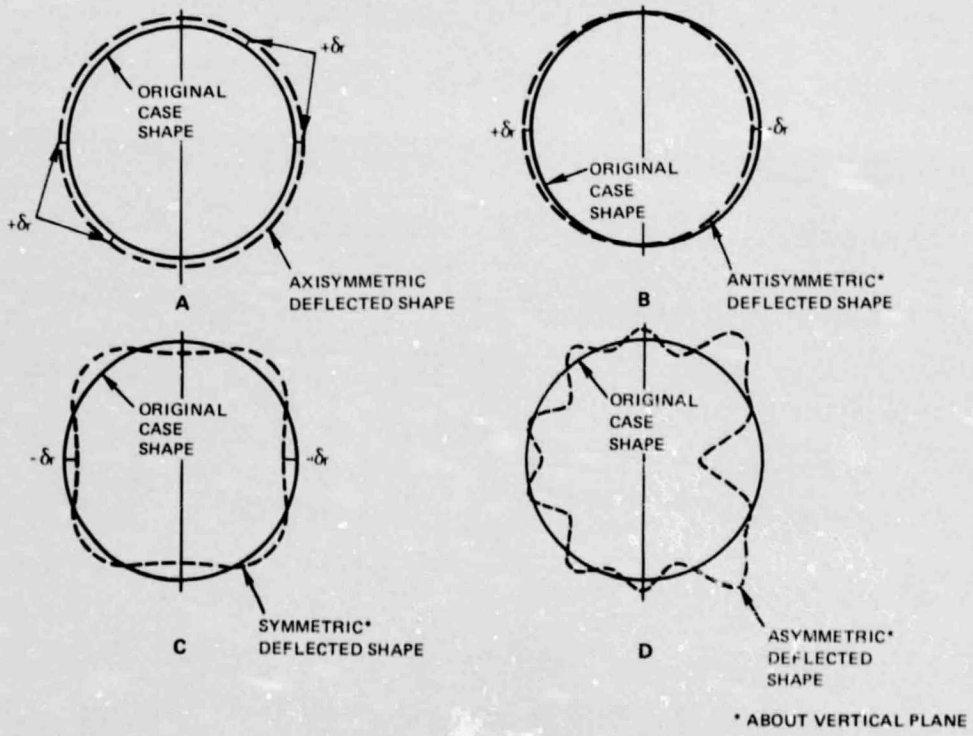

Figure 2 Illustrative Case Deflections and Their Characterization As (A) Axisymmetric, (B) Antisymmetric, (C) Symmetric, and (D) Asymmetric.

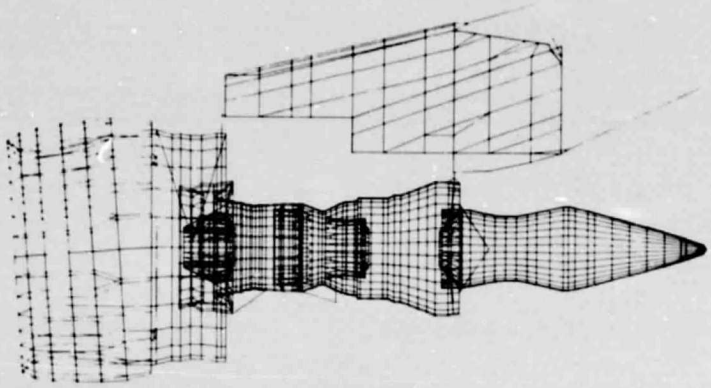

Figure 3 JT9D-7/747 Integrated NASTRAN Structural Model (J17825-9)

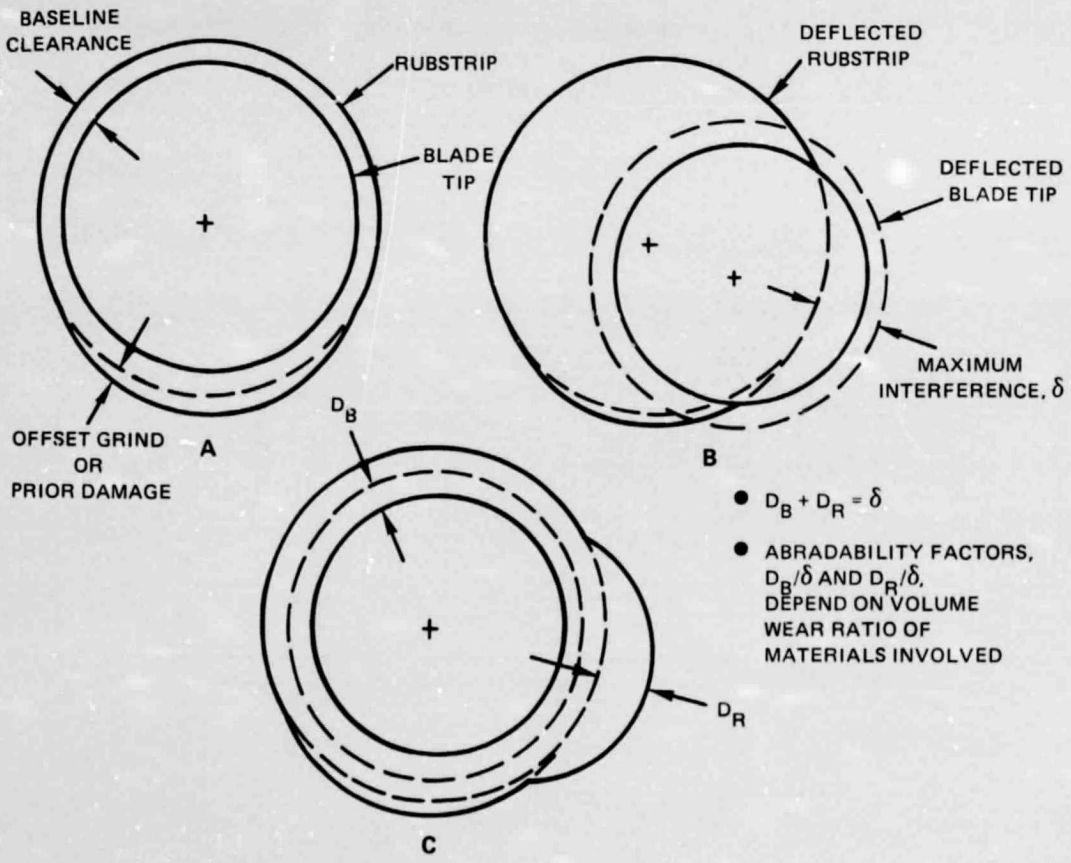

Figure 4 Schematic of Blade-Tip/Rub-Strip Damage Calculation (J17825-13)

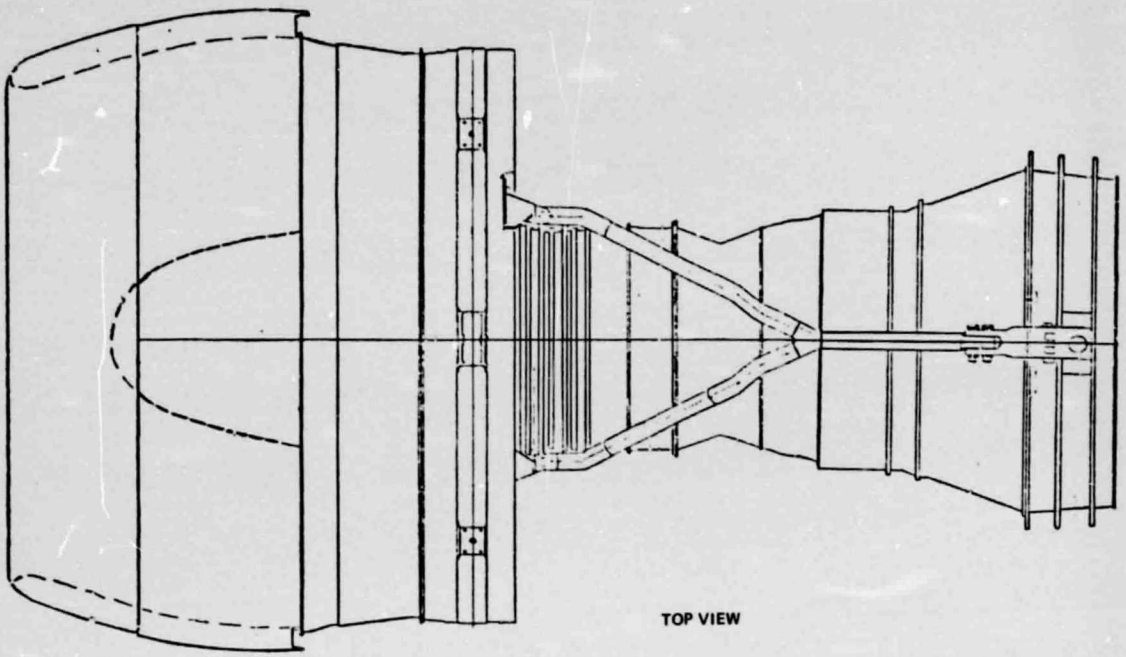

TOP VIEW

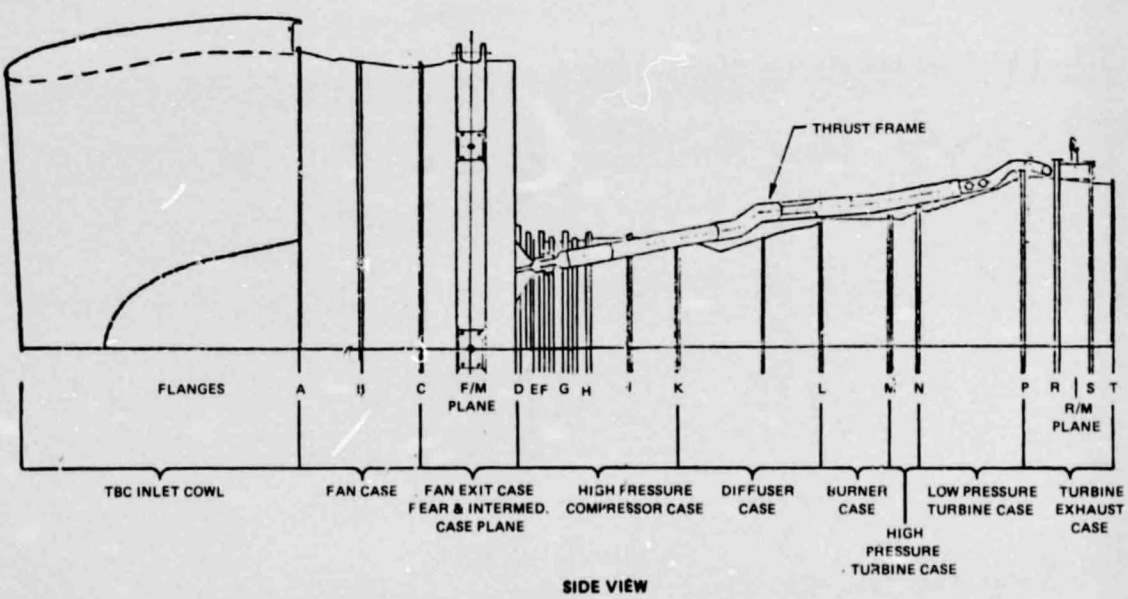

SIDE VIEW

Figure 5 JT9D-7 Engine With Thrust Frame Mounts

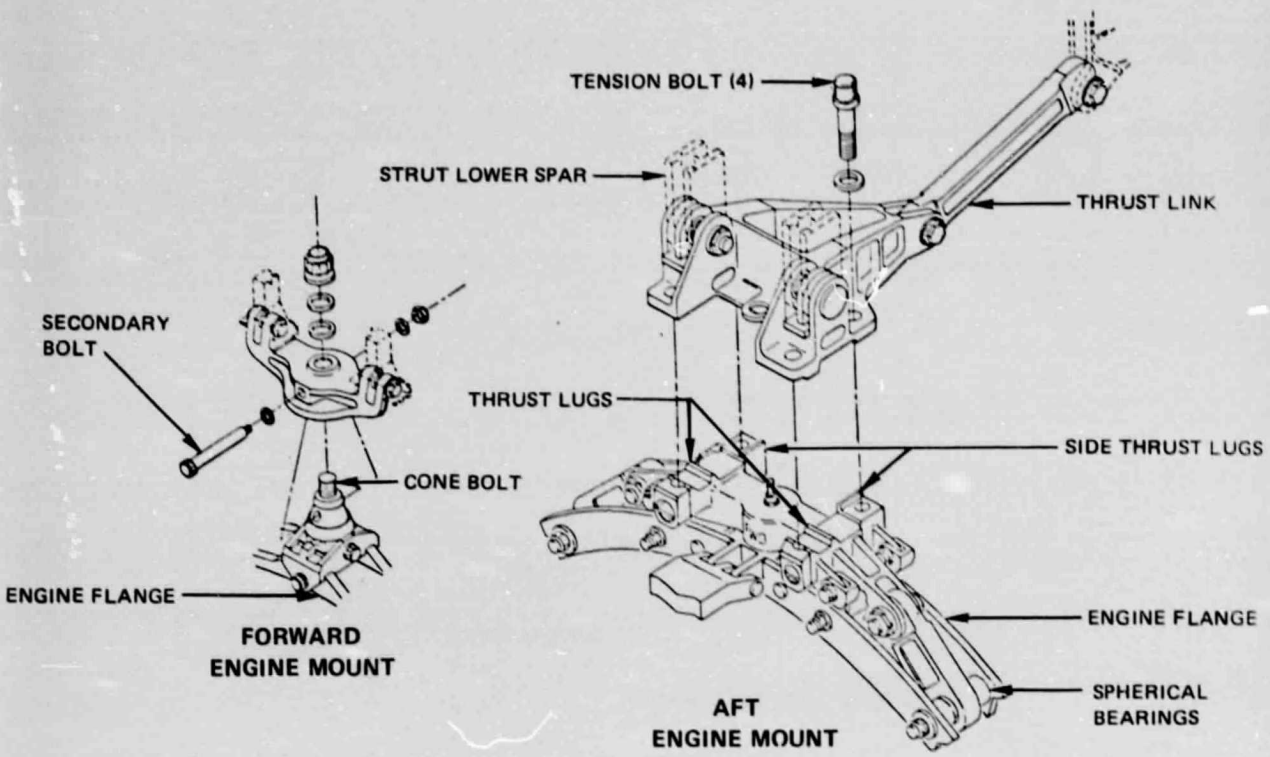

Figure 6 JT9D Engine Mounts

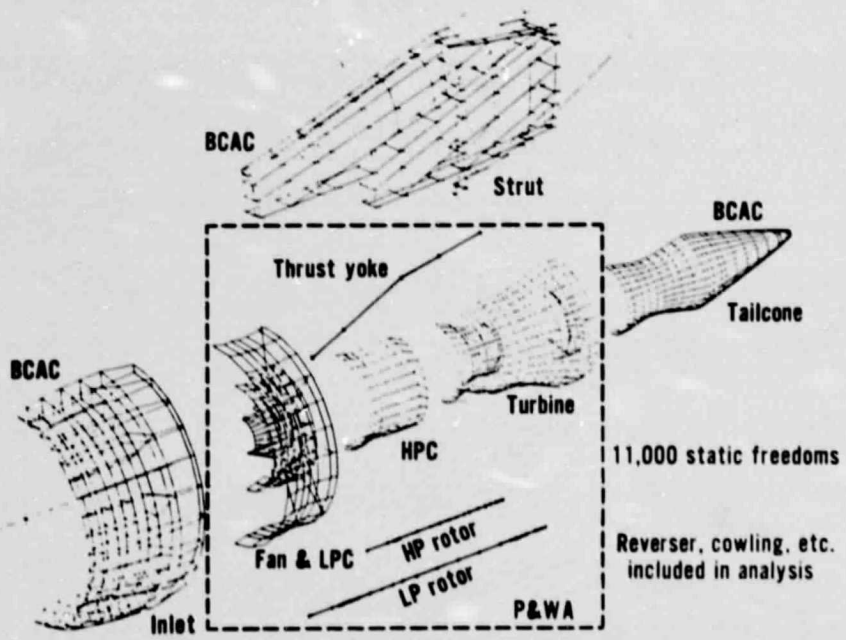

Figure 7 JT9D-7/747 Propulsion System Substructures and Responsibilities (J18750-5)

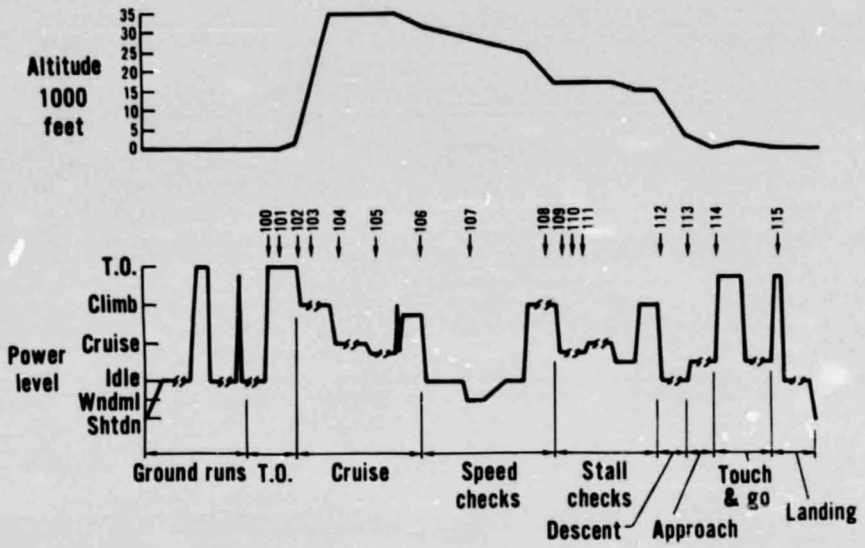

Figure 8 Airplane Acceptance Test Flight Profile (J18750-7)

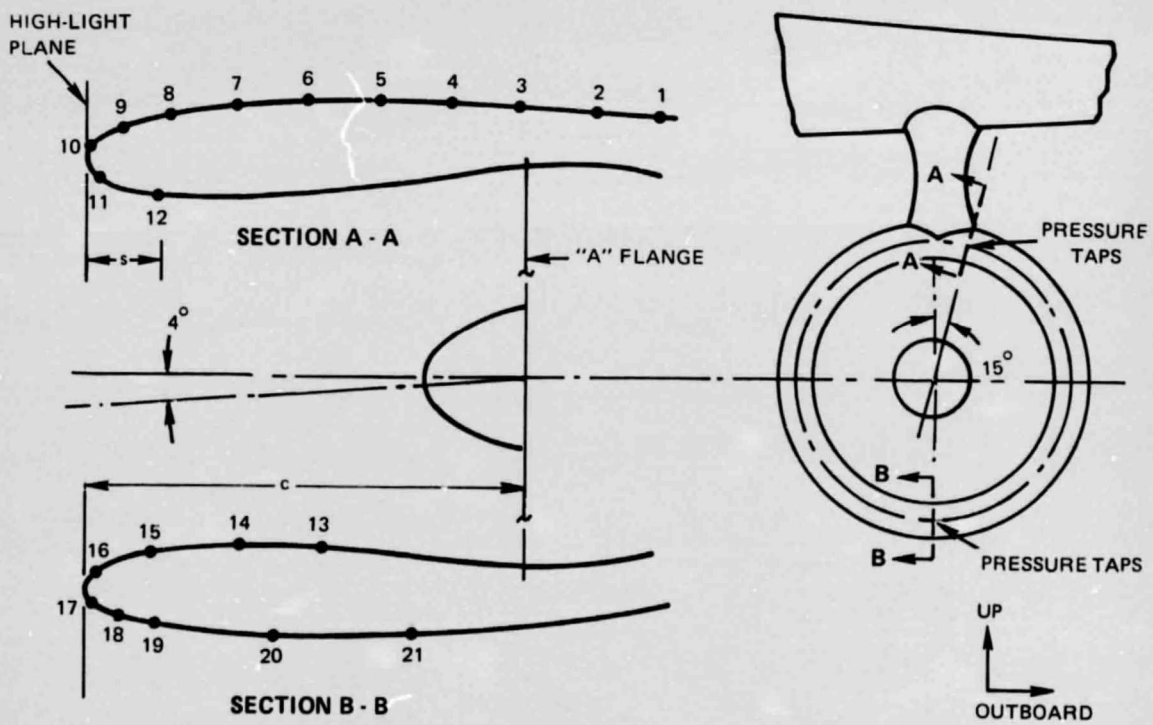

Figure 9 Flight Test Static Pressure Taps

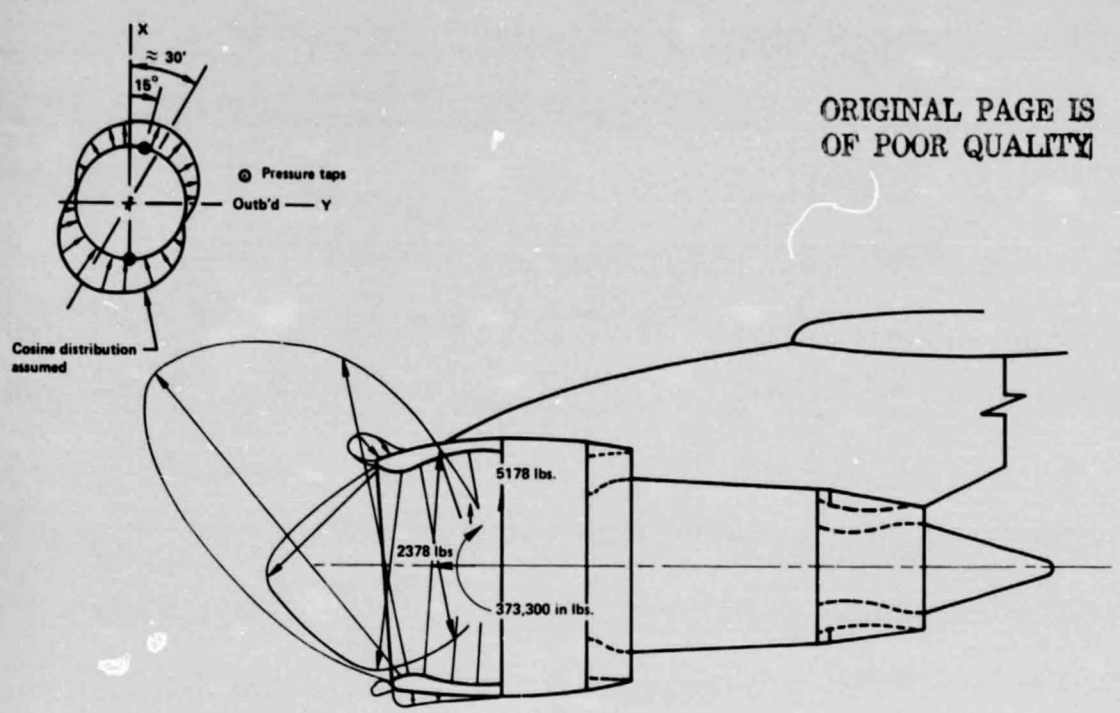

Figure 10 JT9D-7 Asymmetric Pressure Loads; Flight Test Condition 101 (Max. Take-Off) (J18204-2)

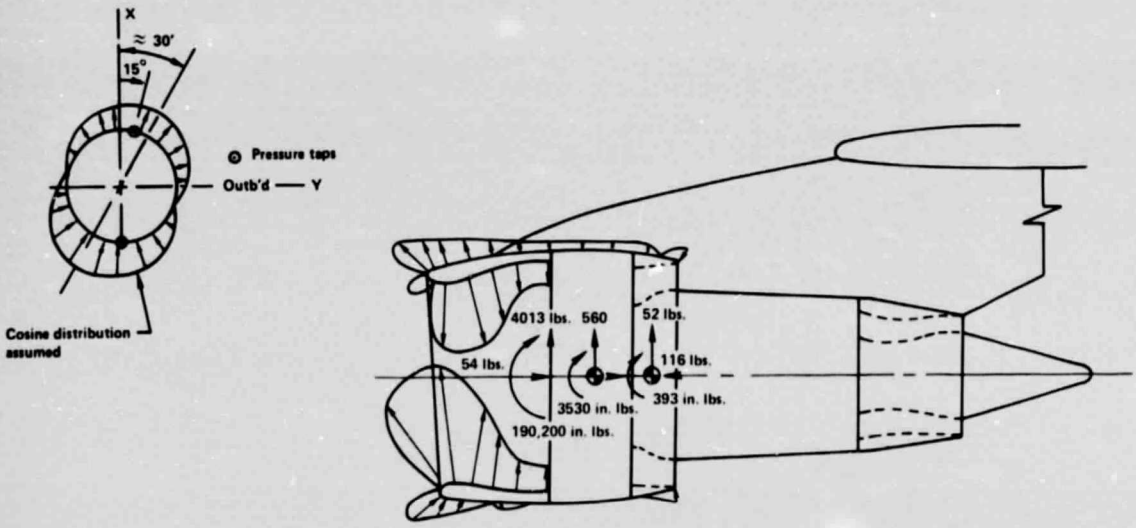

Figure 11 JT9D-7 Asymmetric Pressure Loads; Flight Test Condition 102 (Low Climb) (J18204-1)

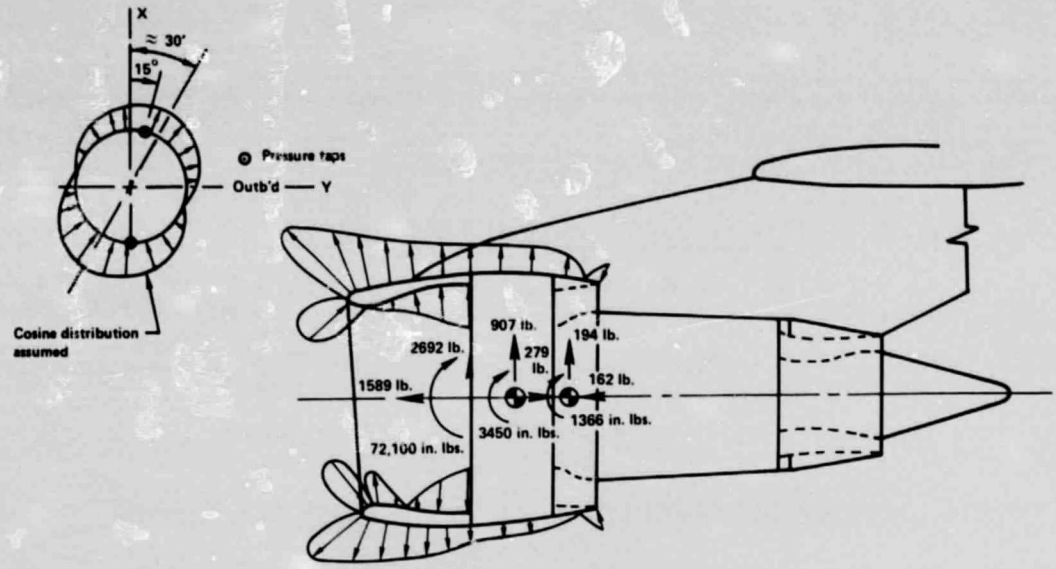

Figure 12 JT9D-7 Asymmetric Pressure Loads; Flight Test Condition 103 (Mid-Climb) (J18204-3)

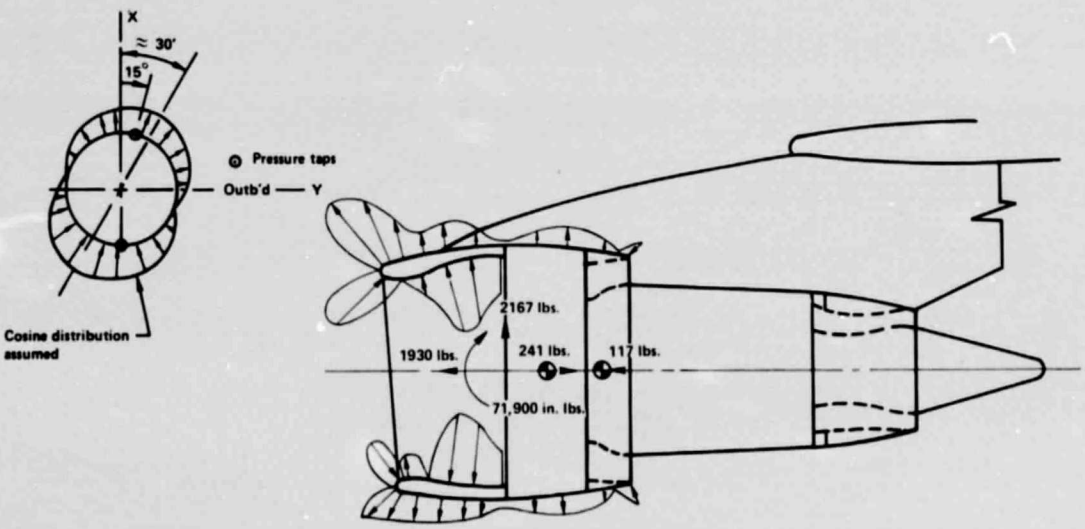

Figure 13 JT9D-7 Asymmetric Pressure Loads; Flight Test Condition 104 (High Mach Cruise) (J18204-4)

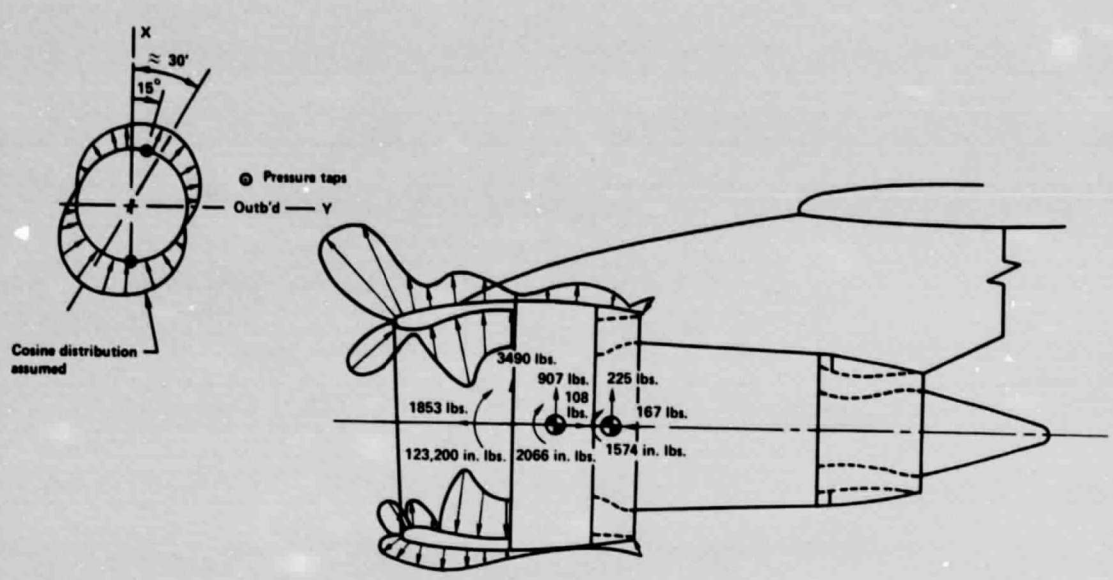

Figure 14 JT9D-7 Asymmetric Pressure Loads; Flight Test Condition 105 (Low Mach Cruise) (J18204-5)

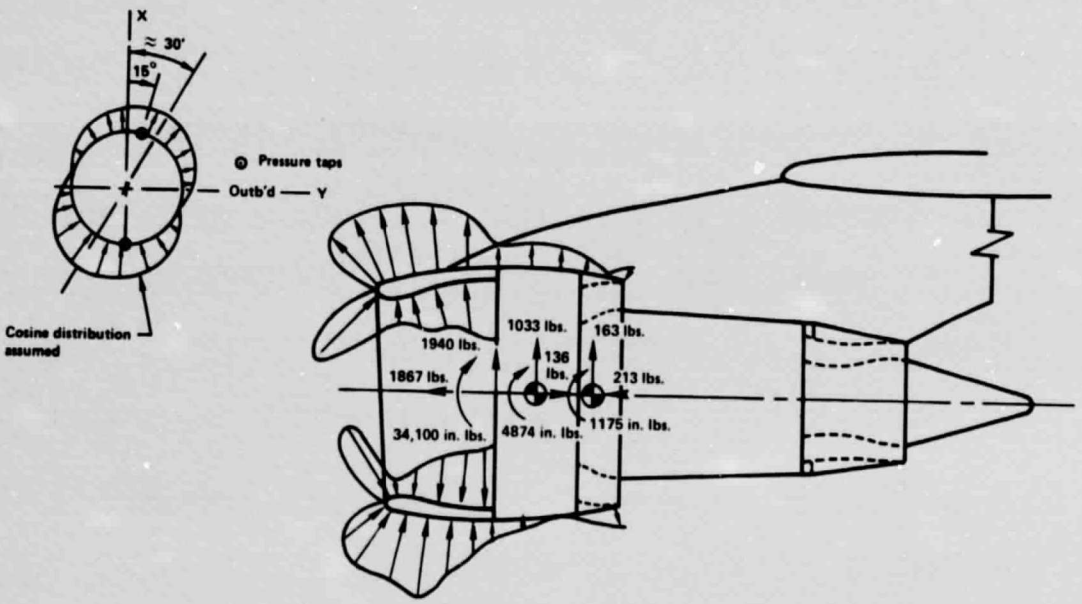

Figure 15 JT9D-7 Axymmetric Pressure Loads; Flight Test Condition 106 (Max. Mach) (J18204-6)

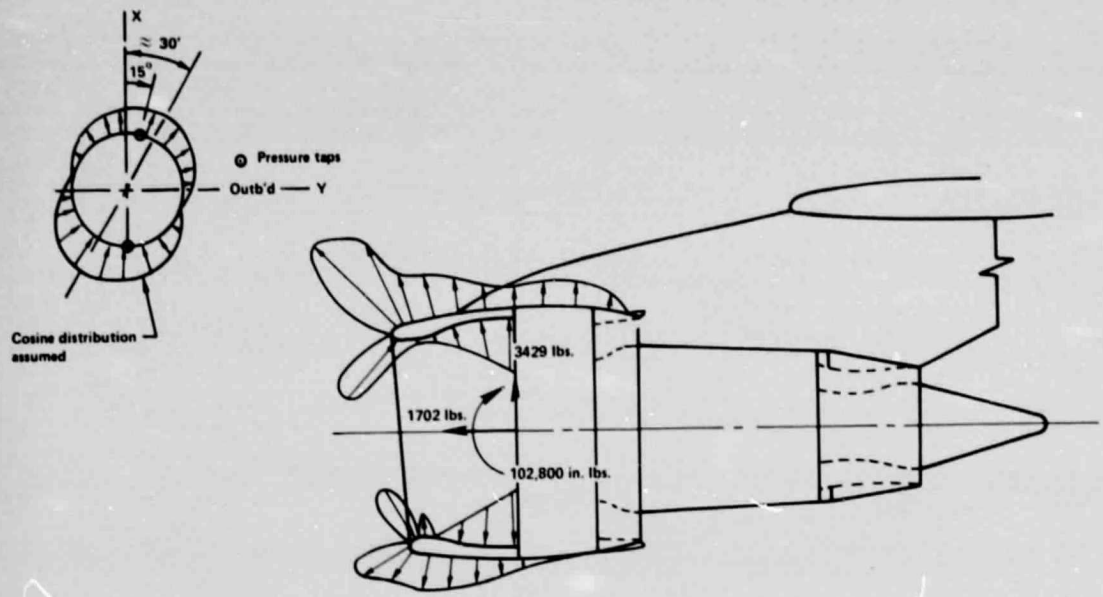

Figure 16 JT9D-7 Asymmetric Pressure Loads; Flight Test Condition 107 (Descent to Max. q) (J18204-7)

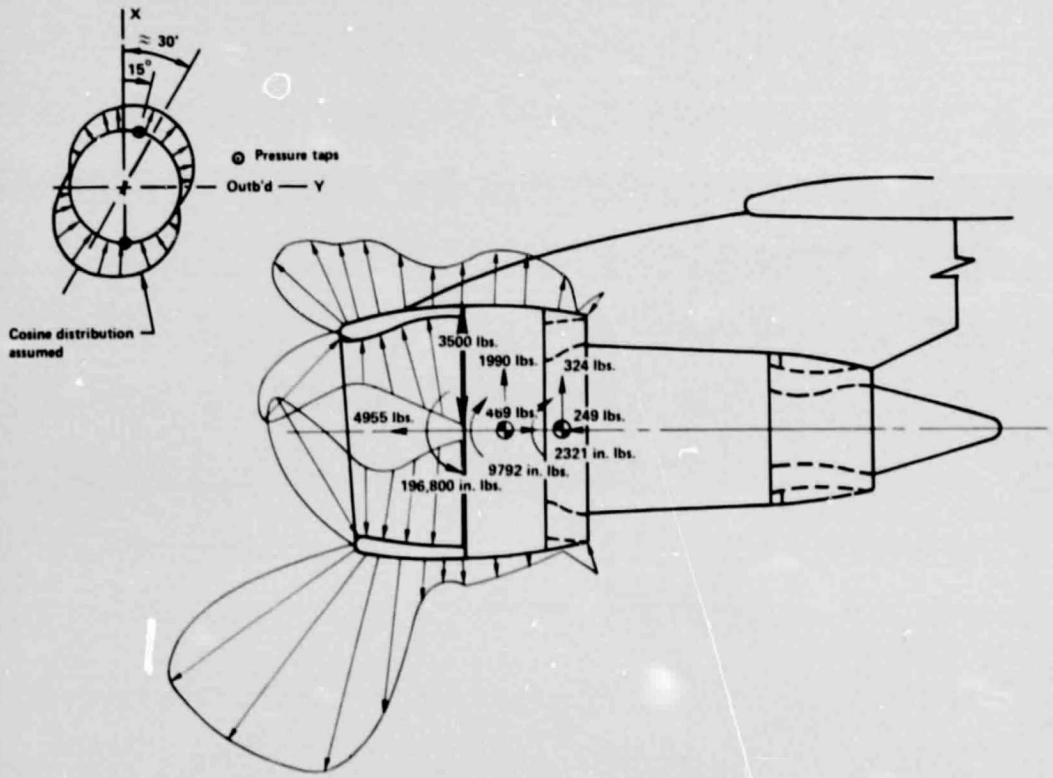

Figure 17 JT9D-7 Asymmetric Pressure Loads; Flight Test Condition 108 (Max. q) (J18204-8)

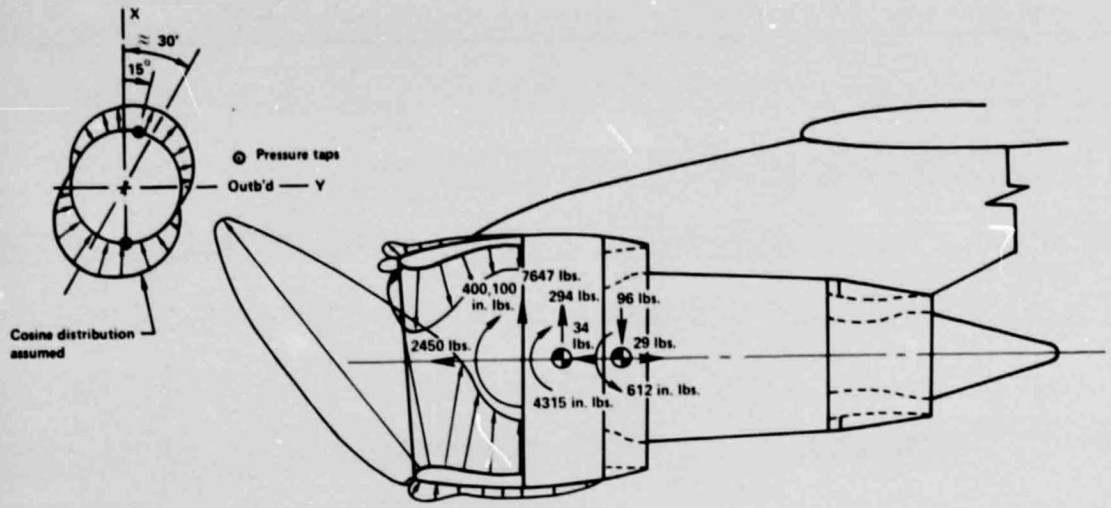

Figure 18 JT9D-7 Asymmetric Pressure Loads; Flight Test Condition 109 (1.3 V_S, 0-degree Flaps)
(J18204-9)

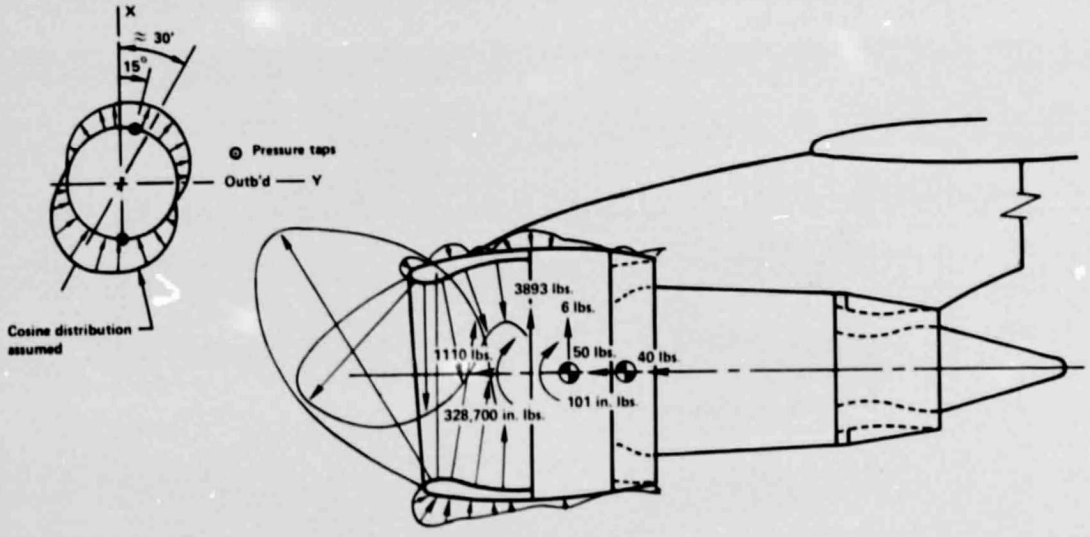

Figure 19 JT9D-7 Asymmetric Pressure Loads; Flight Test Condition 110 (1.3 V_S, 10-degree Flaps)
(J18204-10)

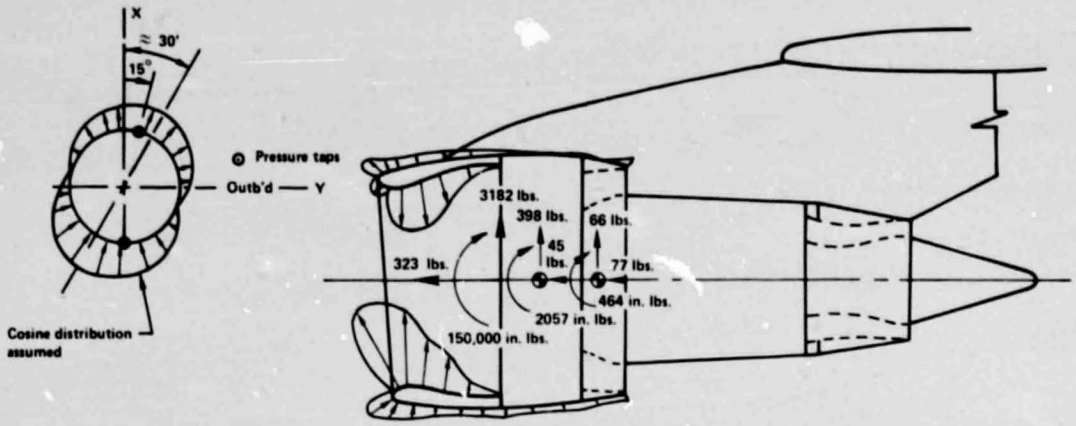

Figure 20 JT9D-7 Asymmetric Pressure Loads; Flight Test Condition 111 (1.3 V_S, 30-degree Flaps)
(J18204-11)

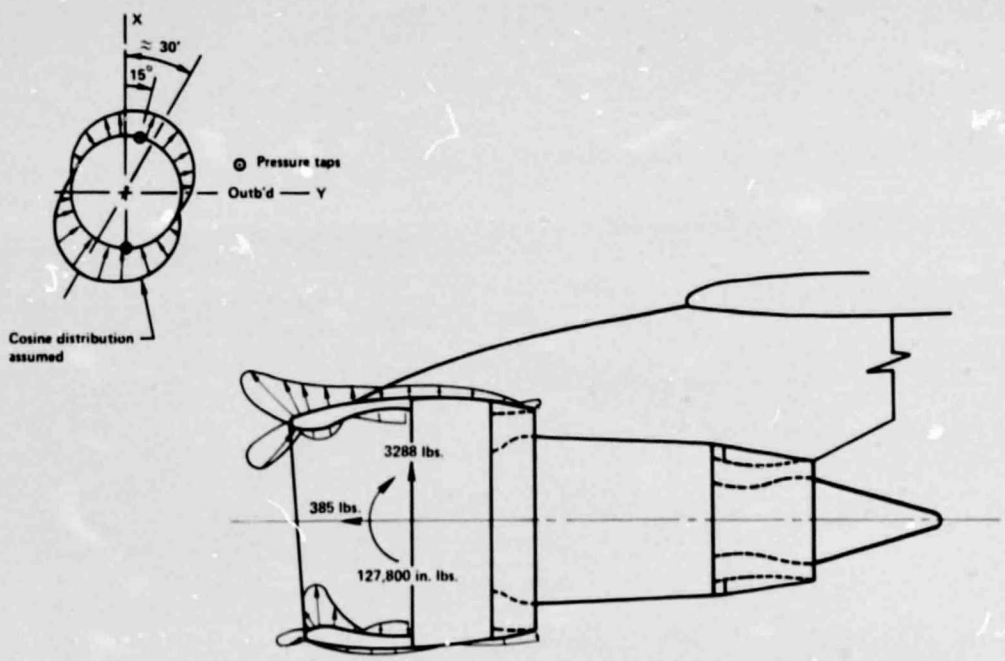

Figure 21 JT9D-7 Asymmetric Pressure Loads; Flight Test Condition 112 (Descent to Approach)
(J18204-12)

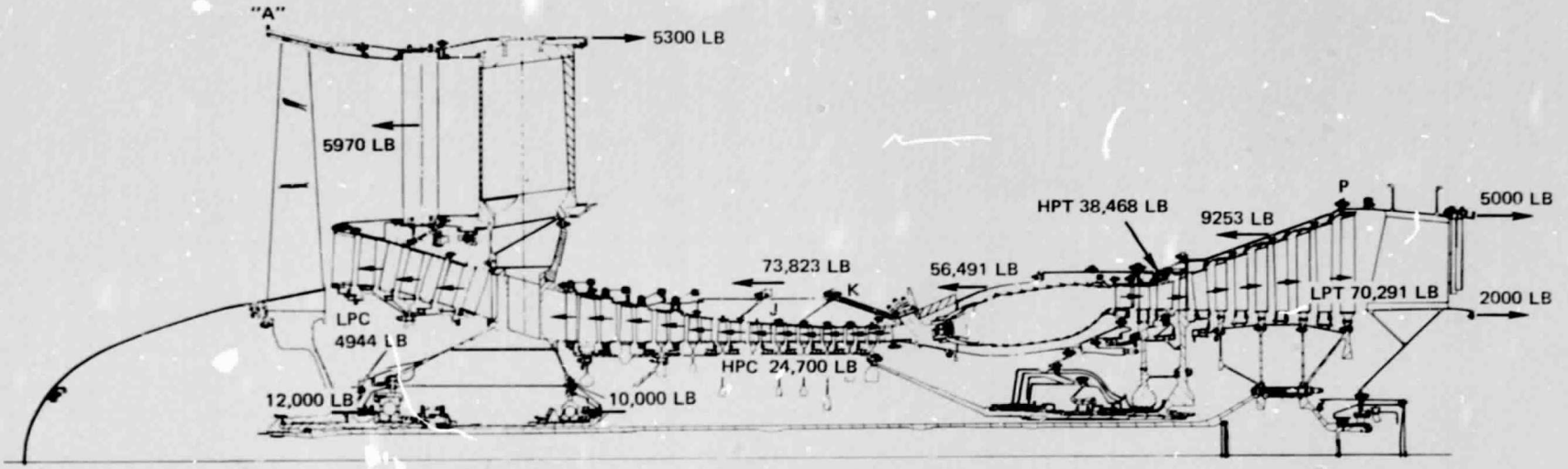

Figure 22 JT9D-7 Distributed Thrust Load Map

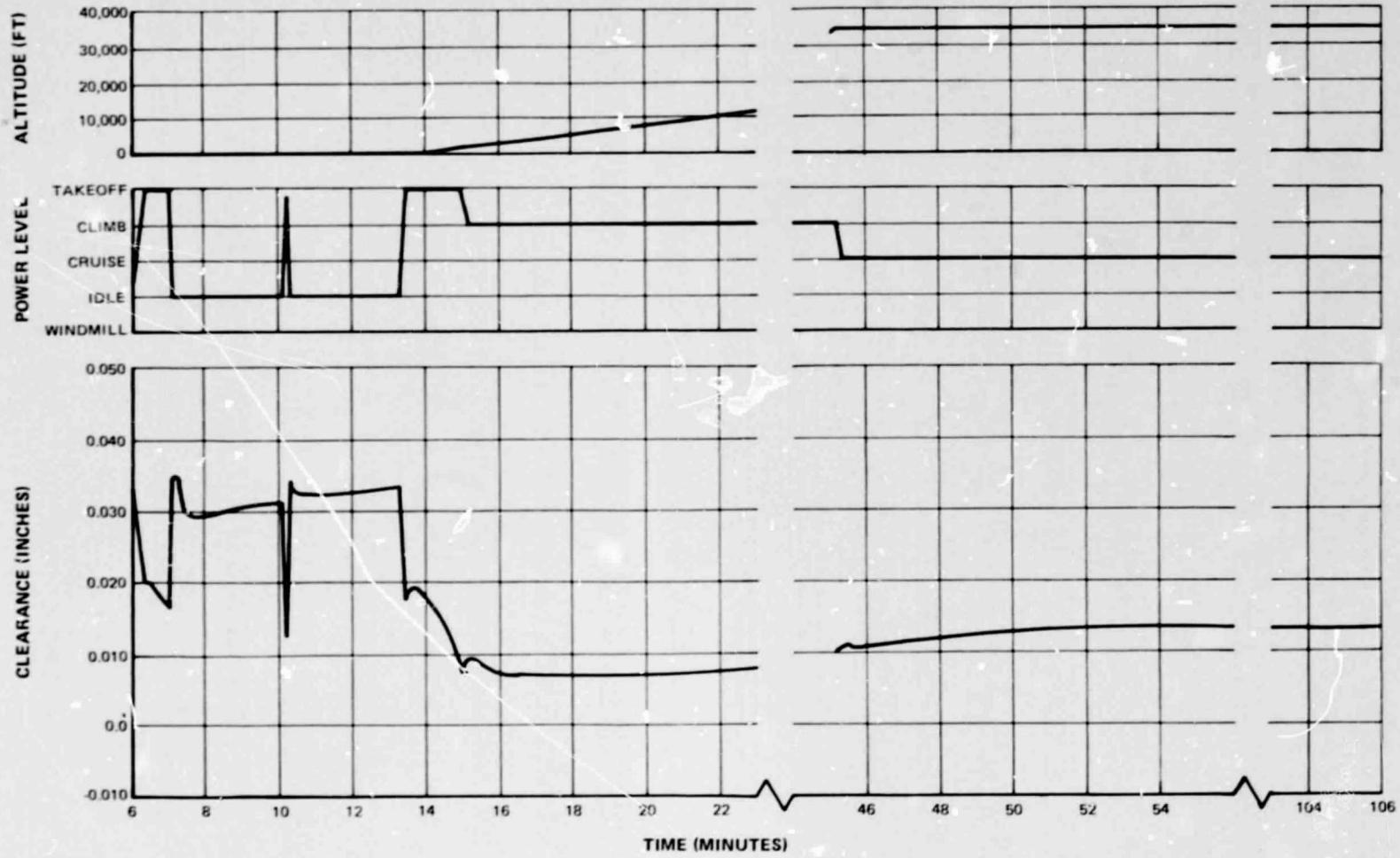

Figure 23a High-Pressure Compressor Fifth-Stage Blade Tip Radial Clearance; 747 Flight Acceptance Test Profile

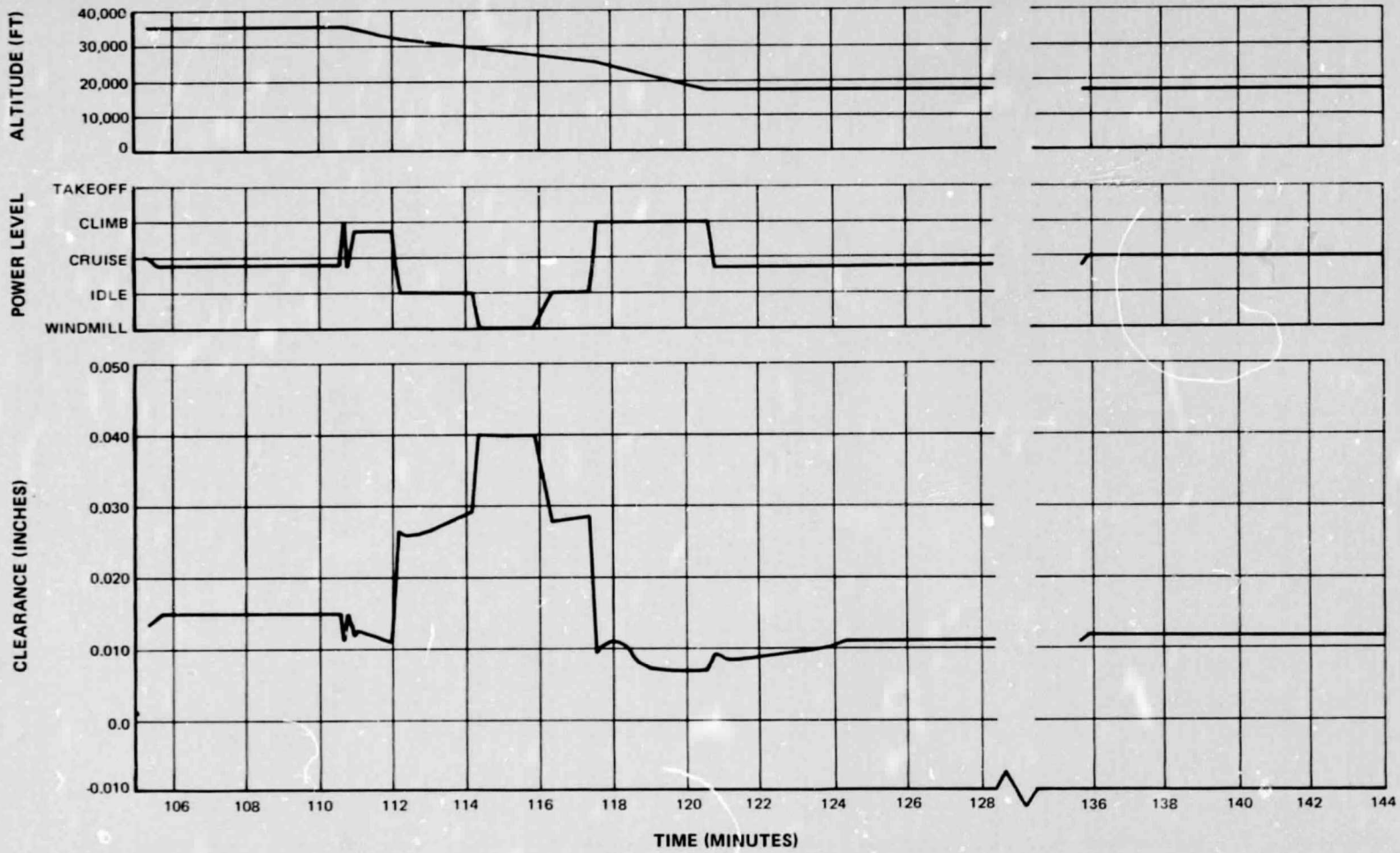

Figure 23b High-Pressure Compressor Fifth-Stage Blade Tip Radial Clearance; 747 Flight Acceptance Test Profile (Cont'd.)

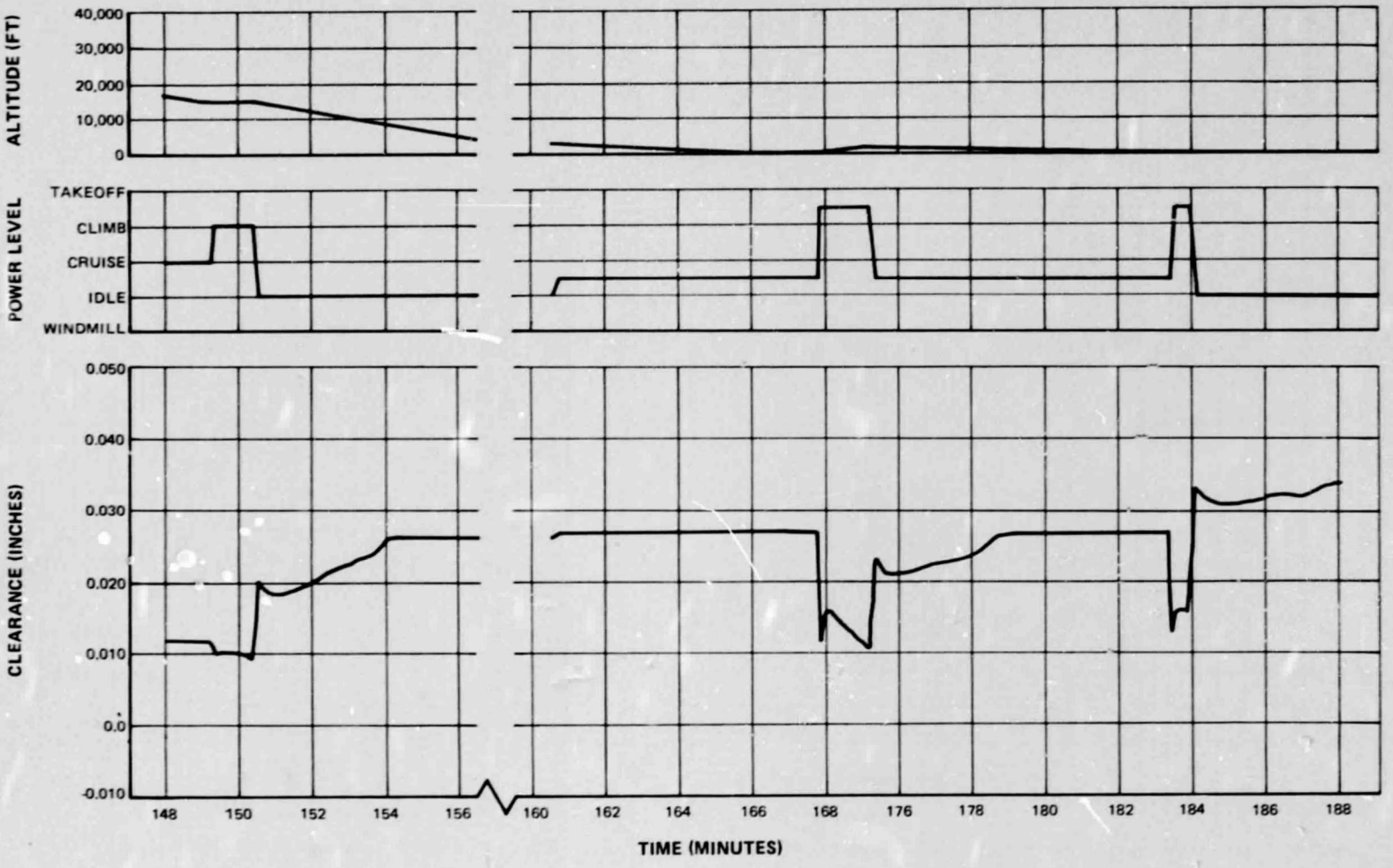

Figure 23c High-Pressure Compressor Fifth-Stage Blade Tip Radial Clearance; 747 Flight Acceptance Test Profile (Cont'd.)

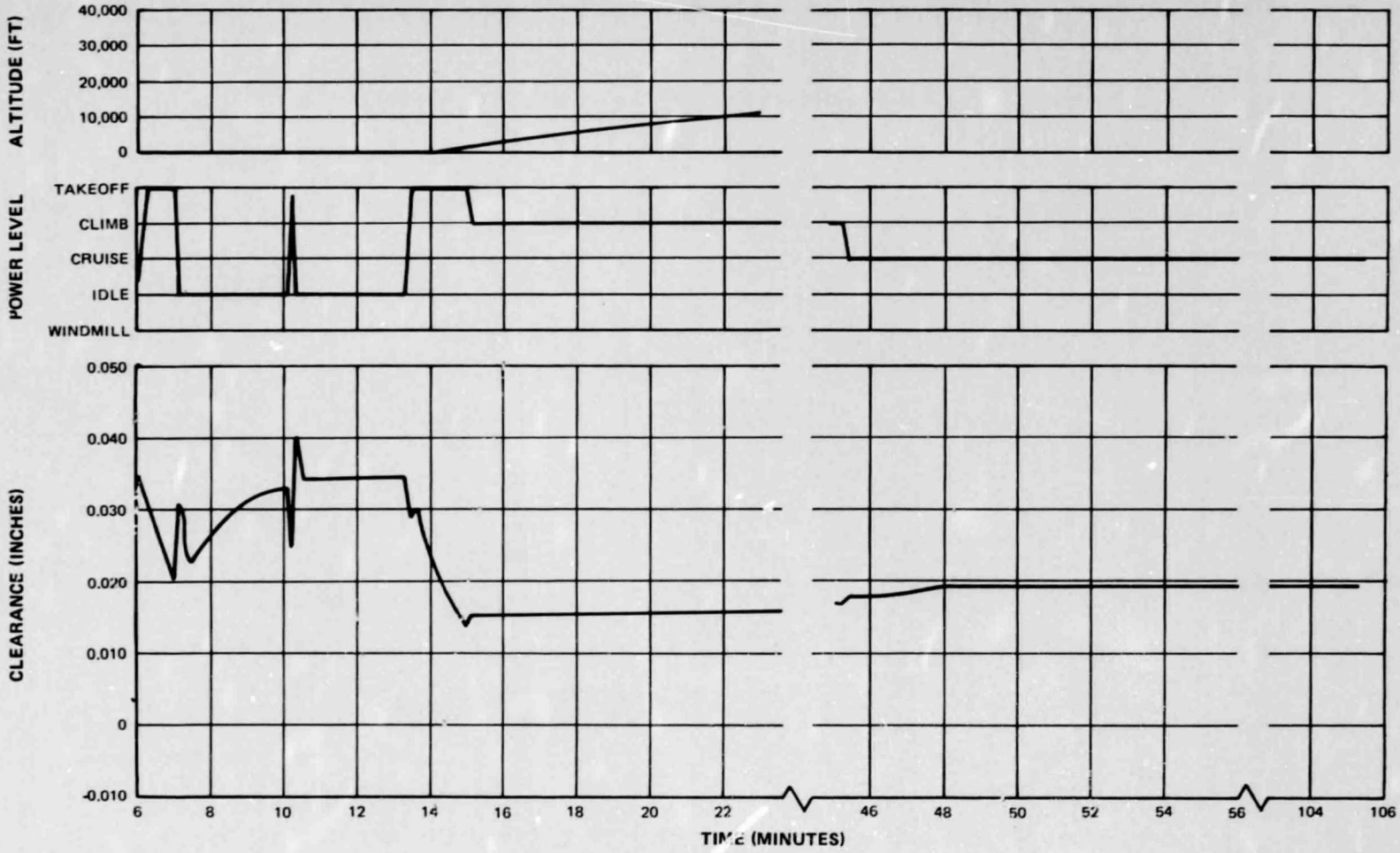

Figure 24a High-Pressure Compressor Ninth-Stage Blade Tip Radial Clearance; 747 Flight Acceptance Test Profile

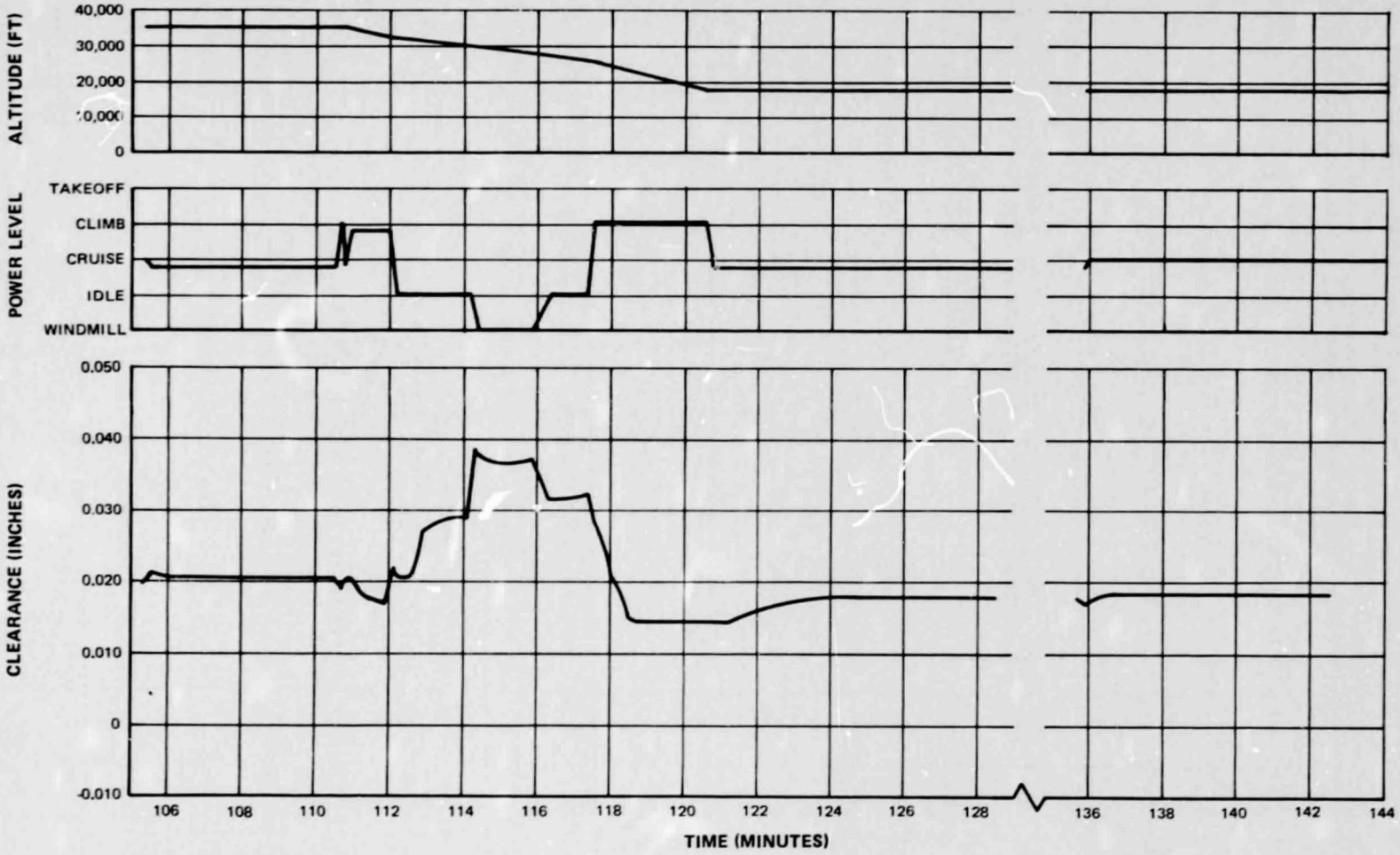

Figure 24b High-Pressure Compressor Ninth-Stage Blade Tip Radial Clearance; 747 Flight Acceptance Test Profile (Cont'd.)

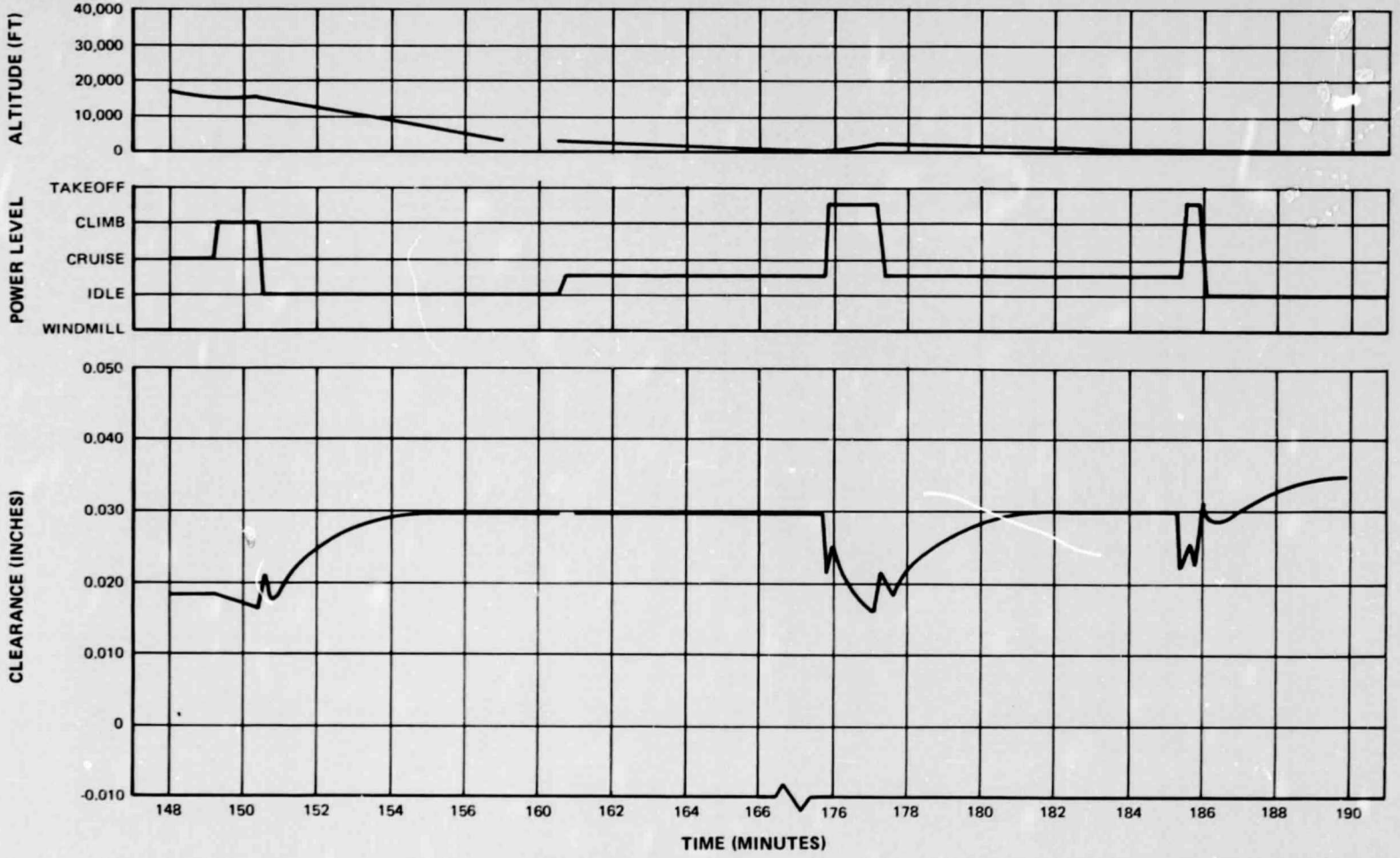

Figure 24c High-Pressure Compressor Ninth-Stage Blade Tip Radial Clearance; 747 Flight Acceptance Test Profile (Cont'd.)

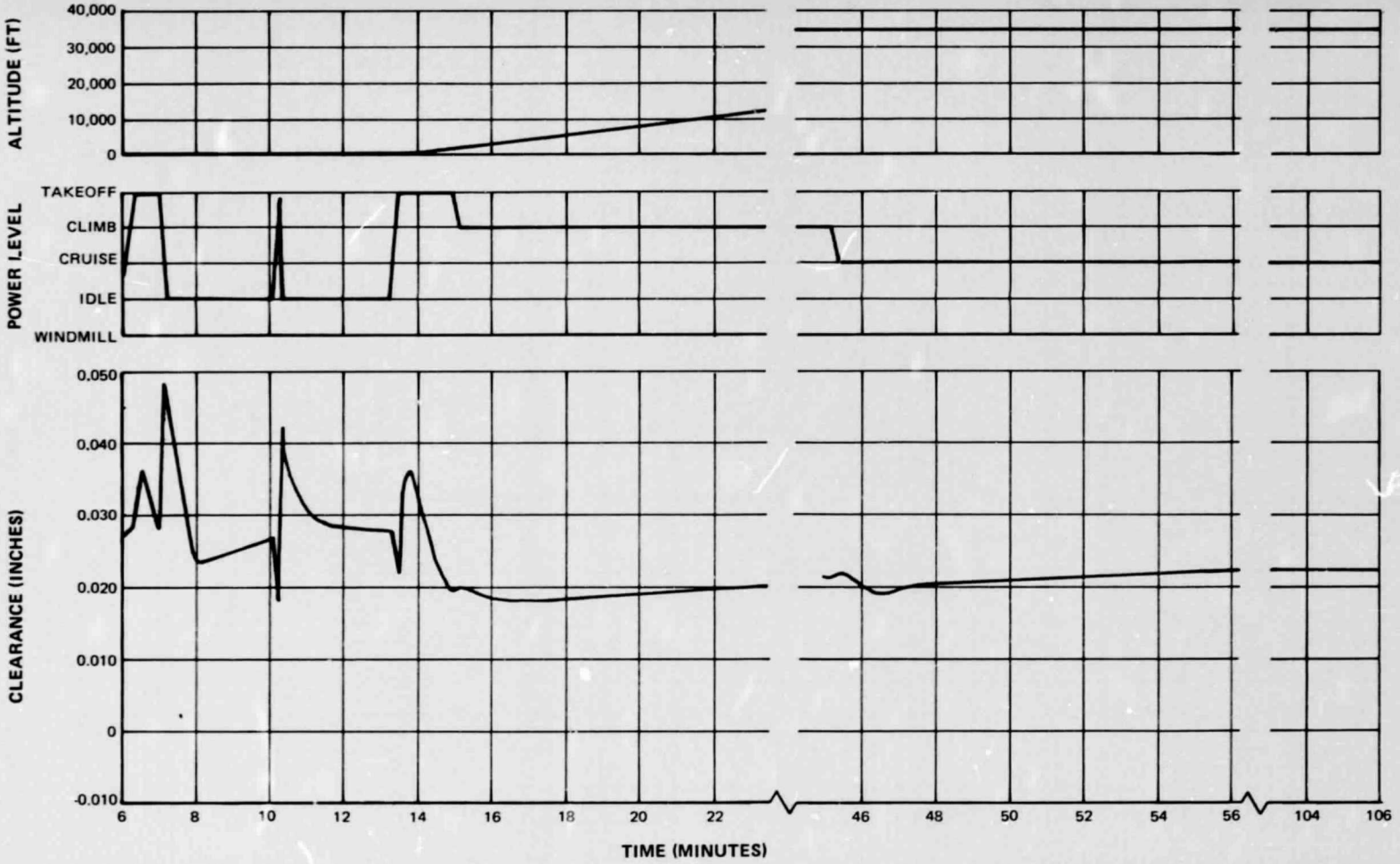

Figure 25a High-Pressure Compressor 15th-Stage Blade Tip Radial Clearance; 747 Flight Acceptance Test Profile

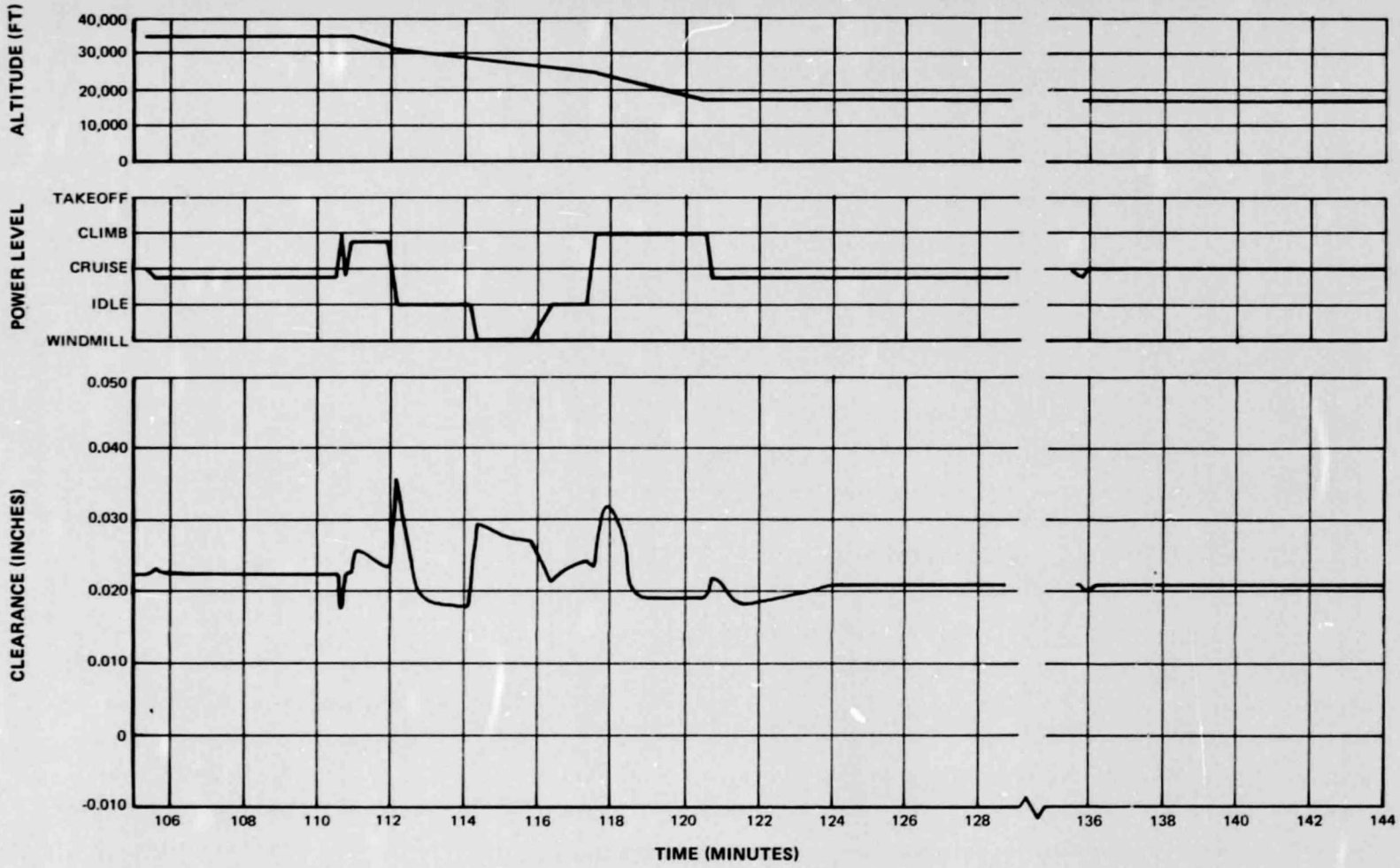

Figure 25b High-Pressure Compressor 15th-Stage Blade Tip Radial Clearance; 747 Flight Acceptance Test Profile (Cont'd.)

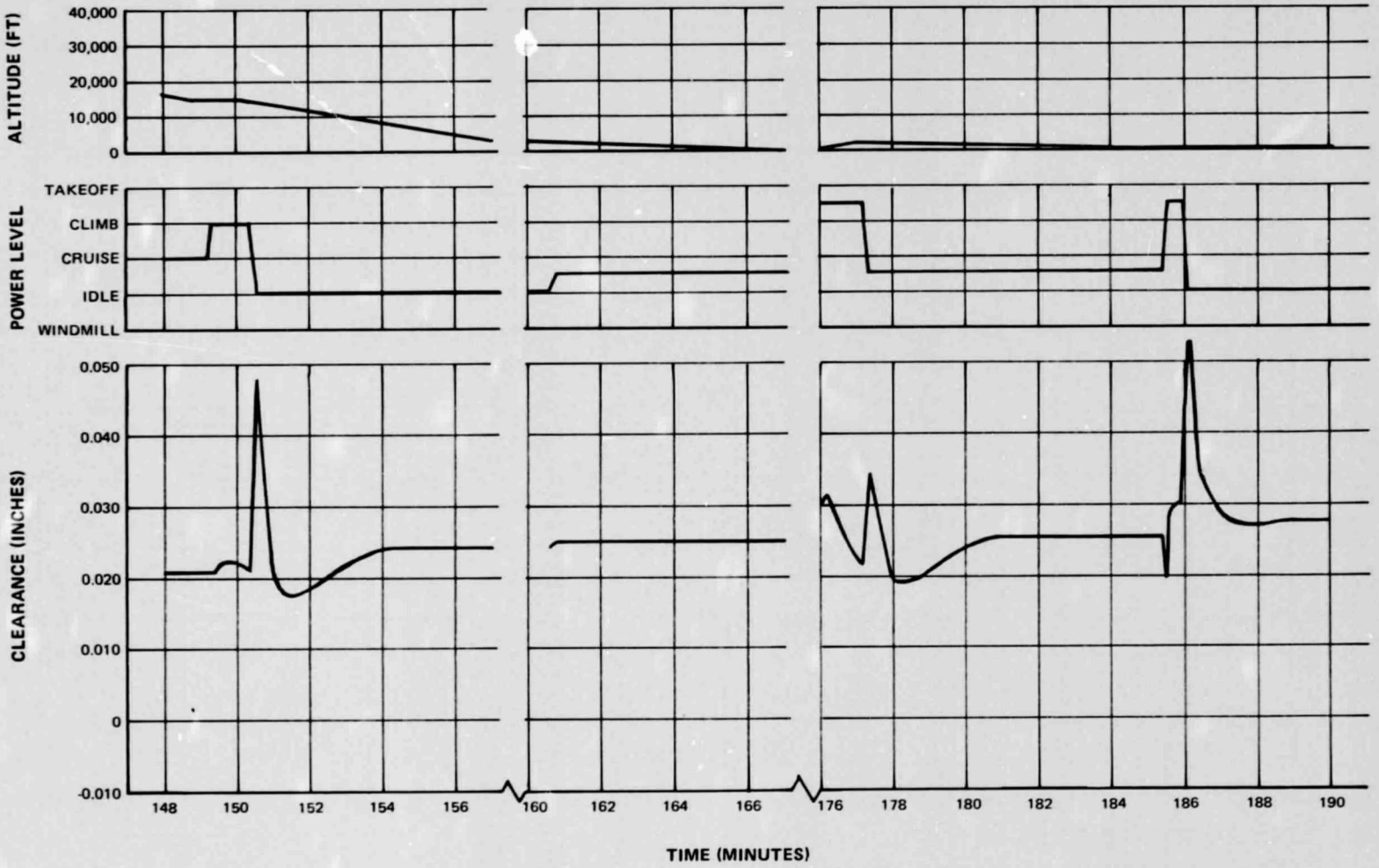

Figure 25c High-Pressure Compressor 15th-Stage Blade Tip Radial Clearance; 747 Flight Acceptance Test Profile (Cont'd.)

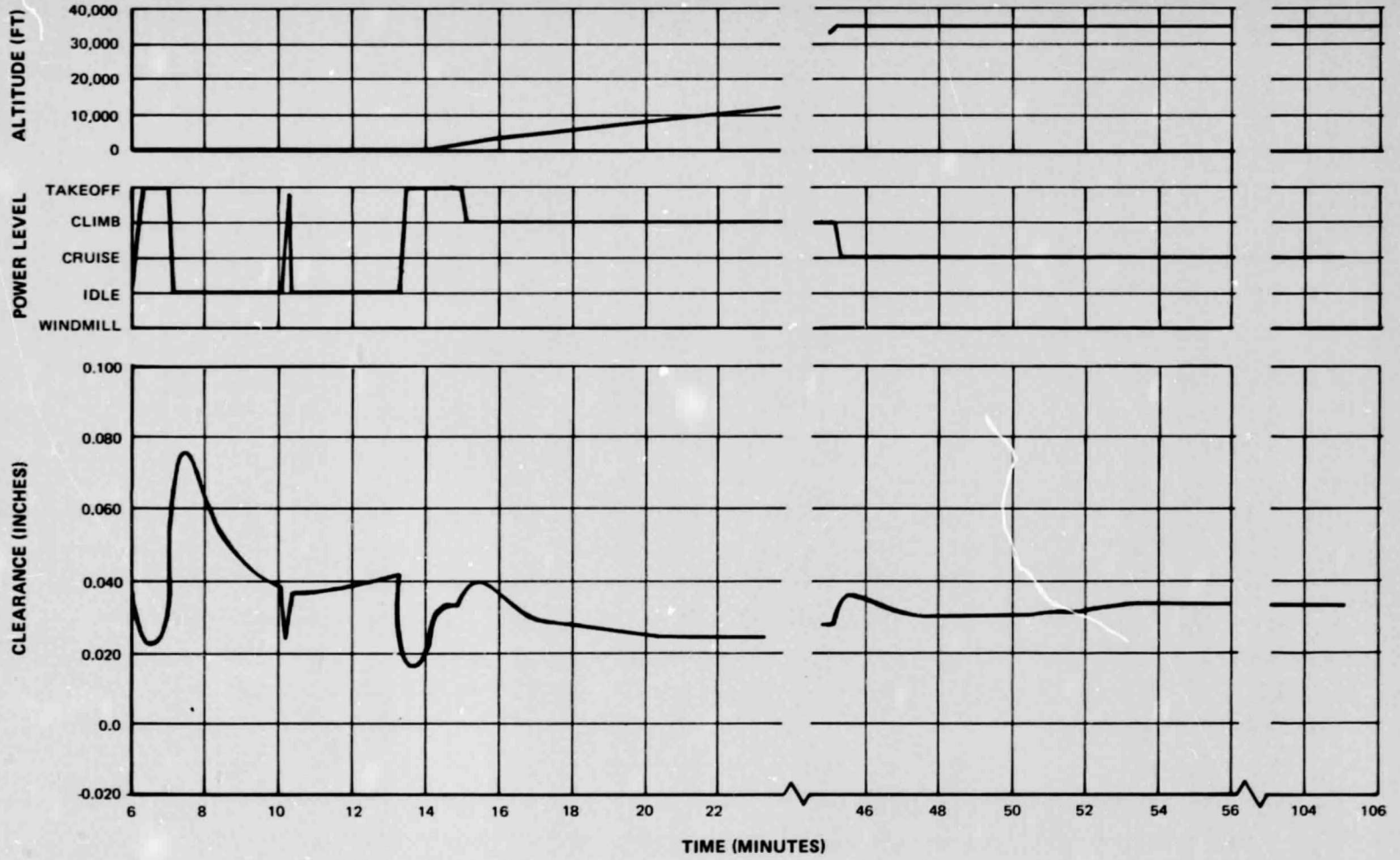

Figure 26a High-Pressure Turbine First-Stage Blade Tip Radial Clearance; 747 Flight Acceptance Test Profile

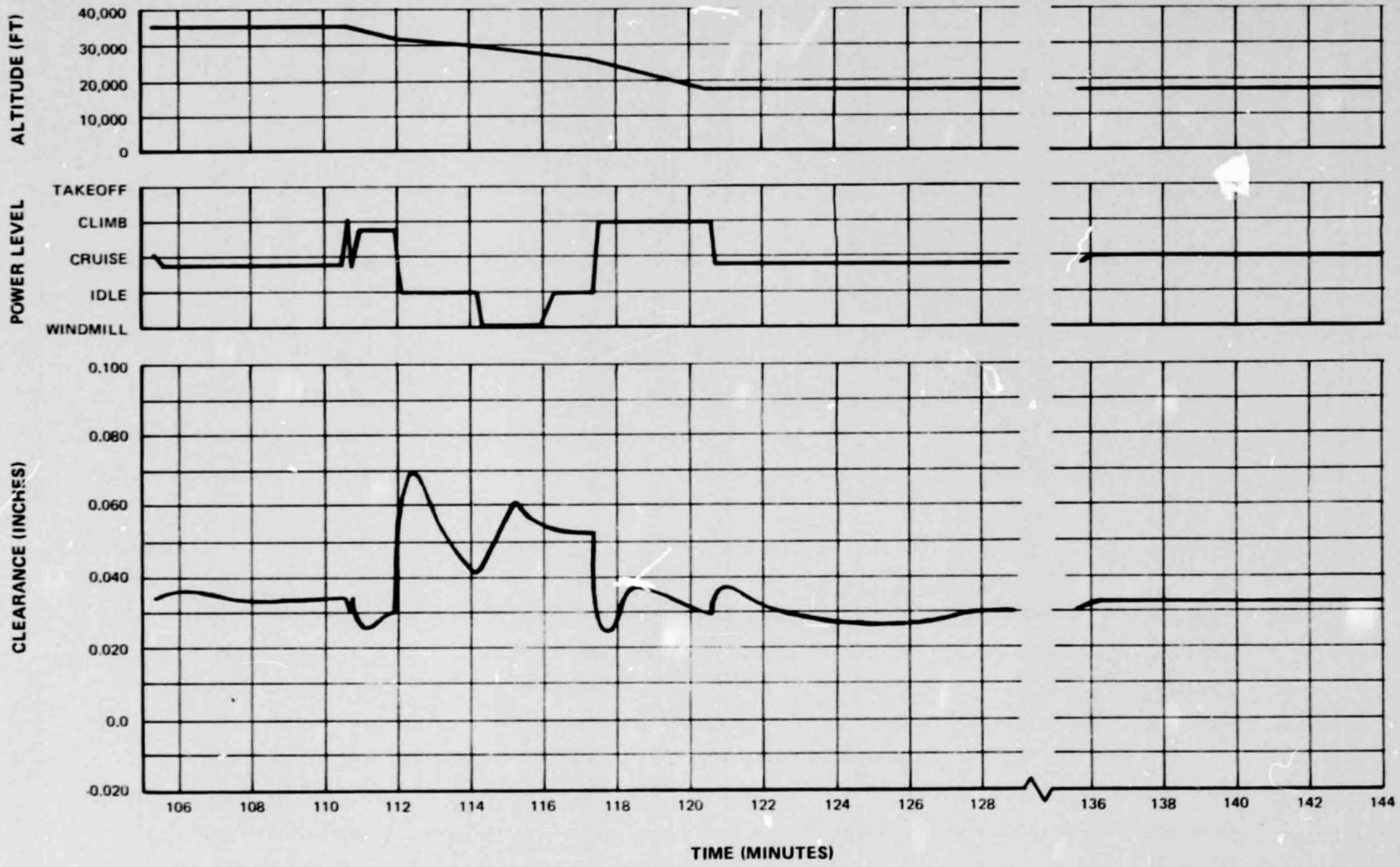

Figure 26b High-Pressure Turbine First-Stage Blade Tip Radial Clearance; 747 Flight Acceptance Test Profile (Cont'd.)

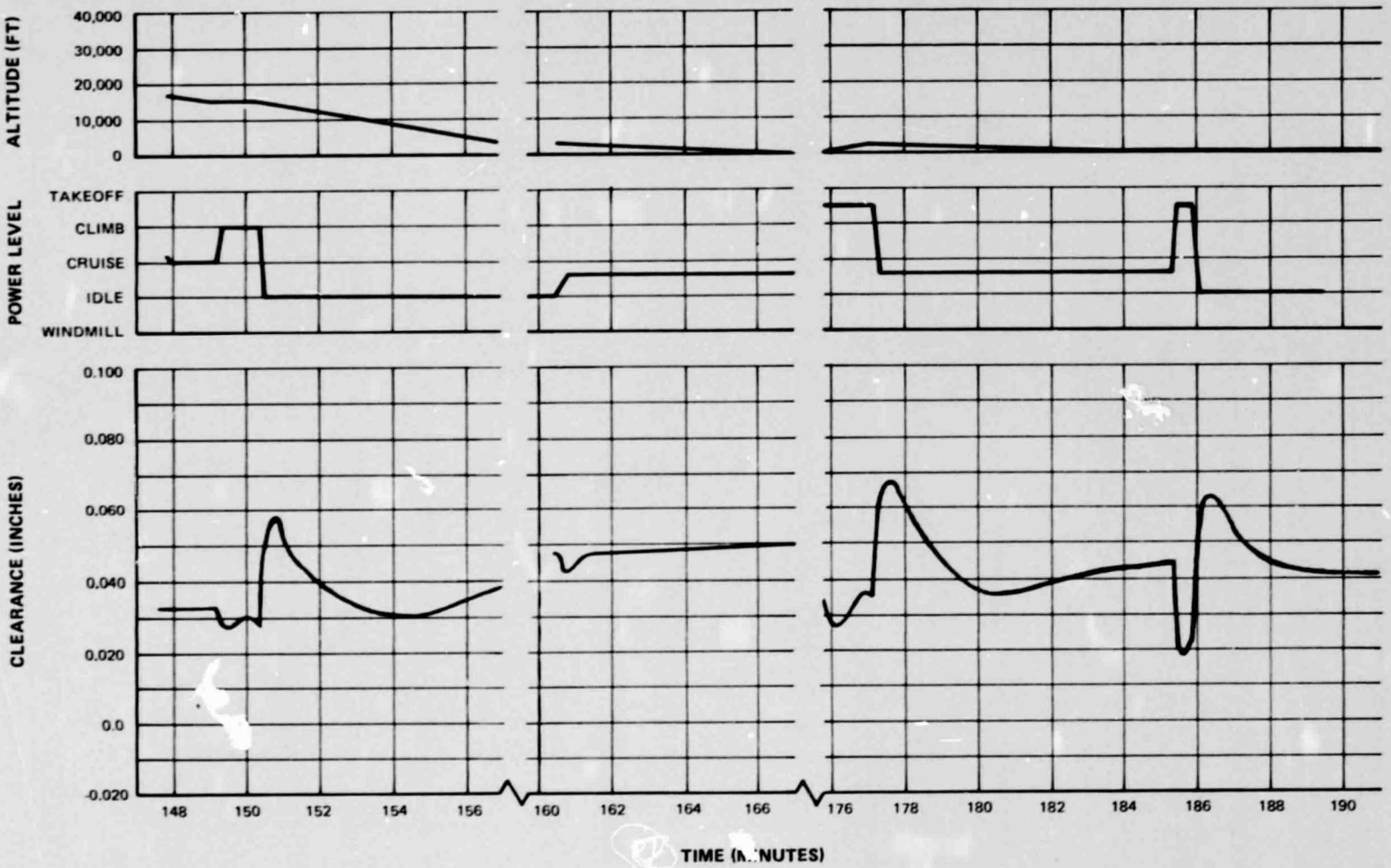

Figure 26c High-Pressure Turbine First-Stage Blade Tip Radial Clearance; 747 Flight Acceptance Test Profile (Cont'd.)

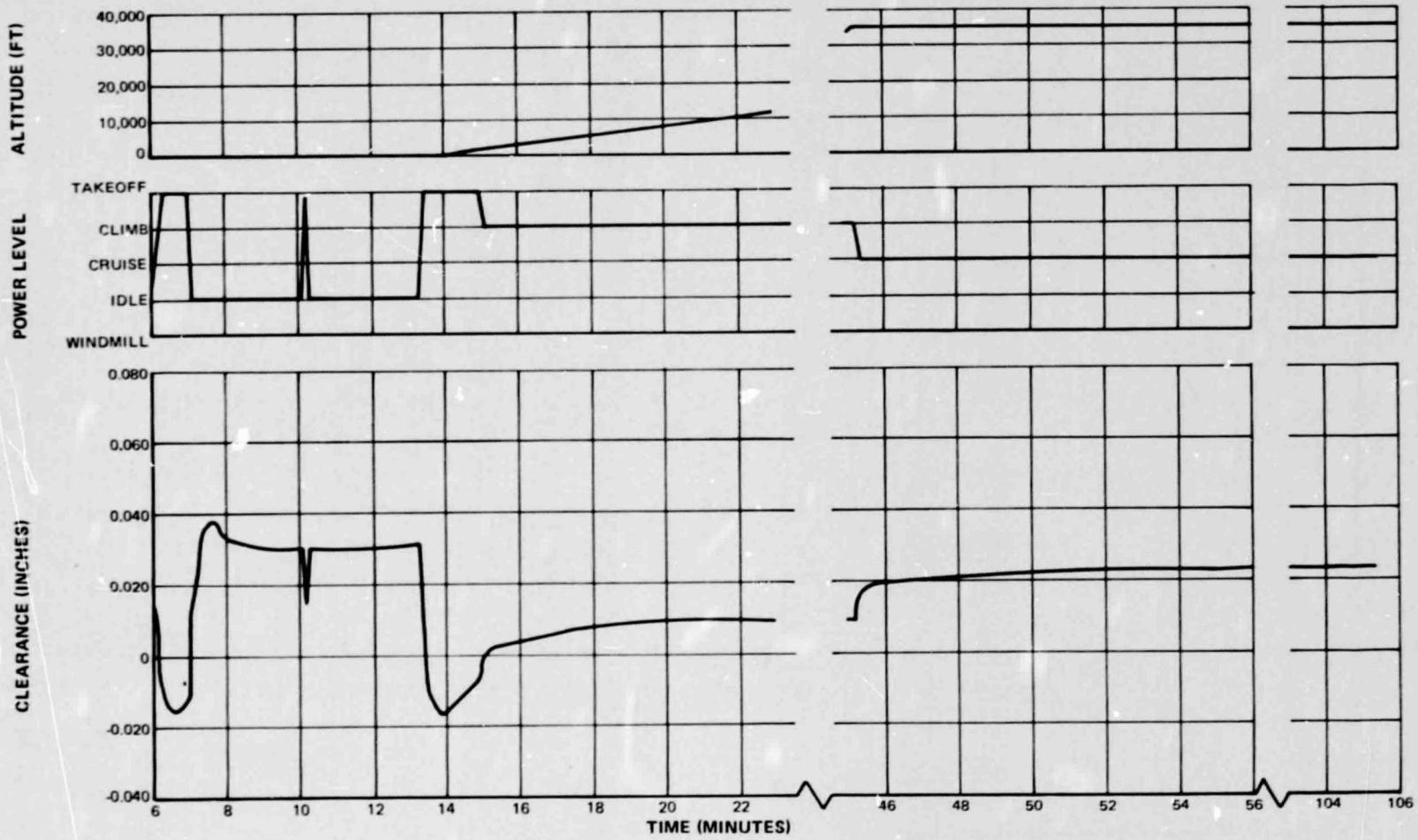

Figure 27a High-Pressure Turbine Second-Stage Blade Tip Radial Clearance; 747 Flight Acceptance Test Profile

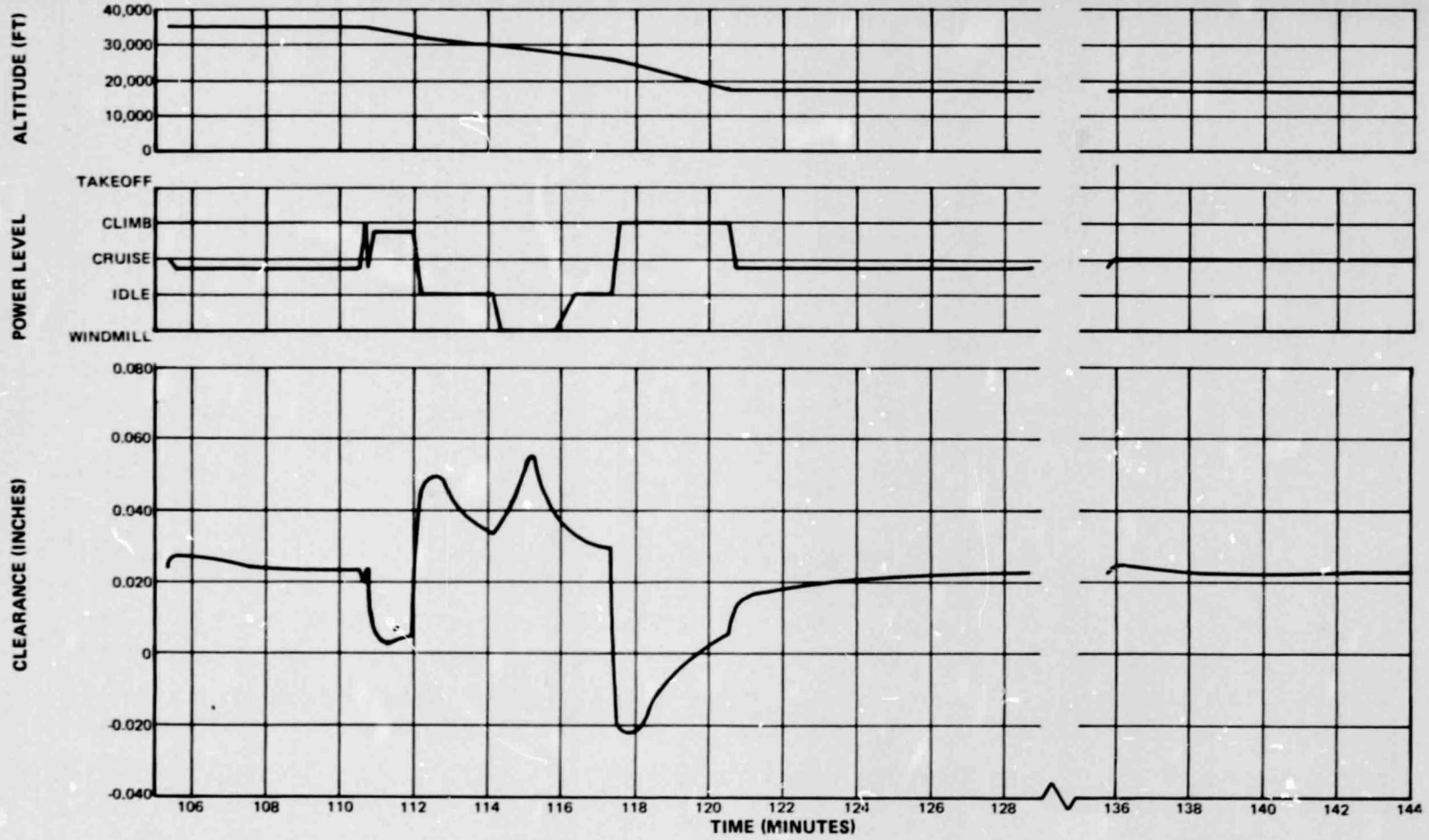

Figure 27b High-Pressure Turbine Second-Stage Blade Tip Radial Clearance; 747 Flight Acceptance Test Profile (Cont'd.)

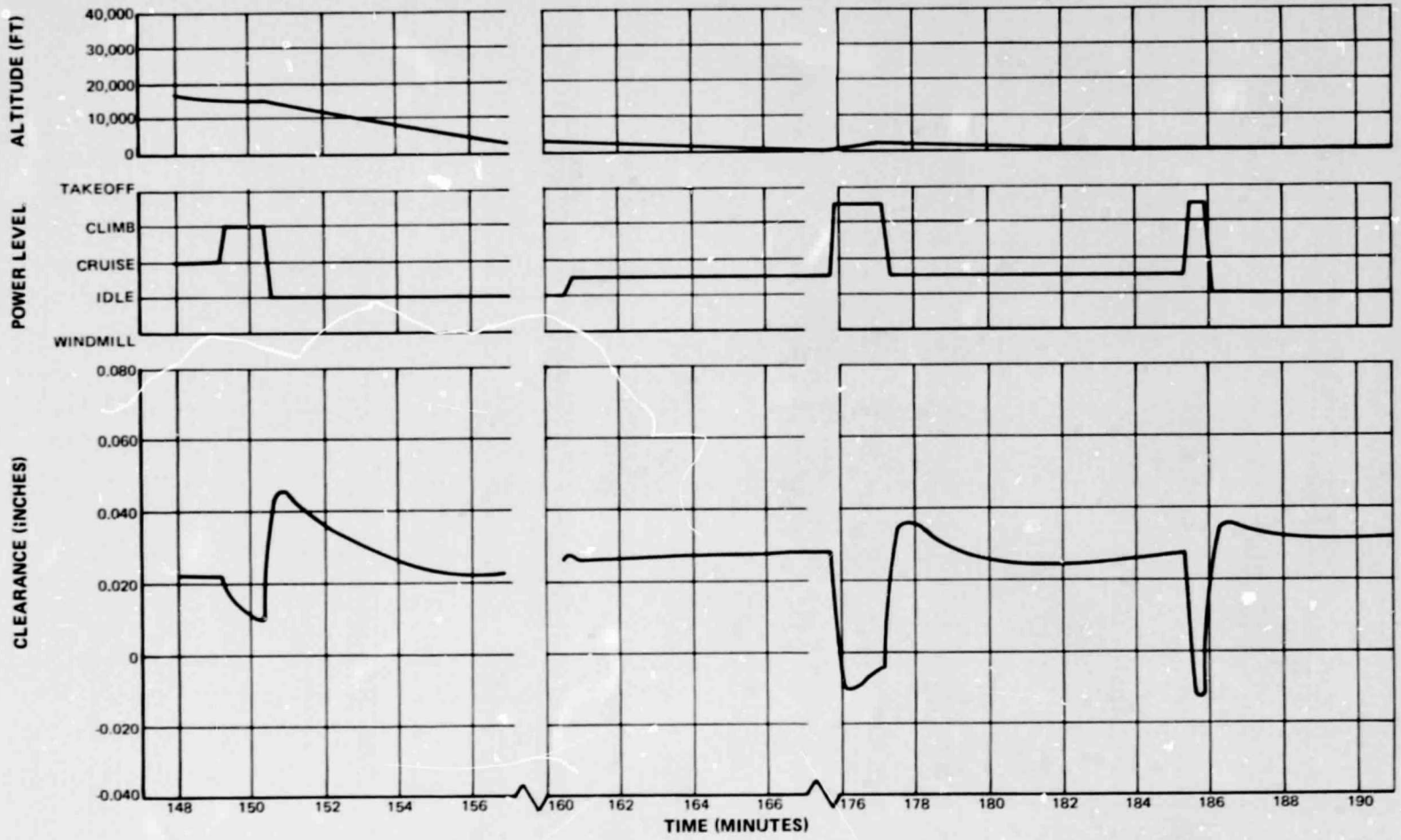

Figure 27c. High-Pressure Turbine Second-Stage Blade Tip Radial Clearance; 747 Flight Acceptance Test Profile (Cont'd.)

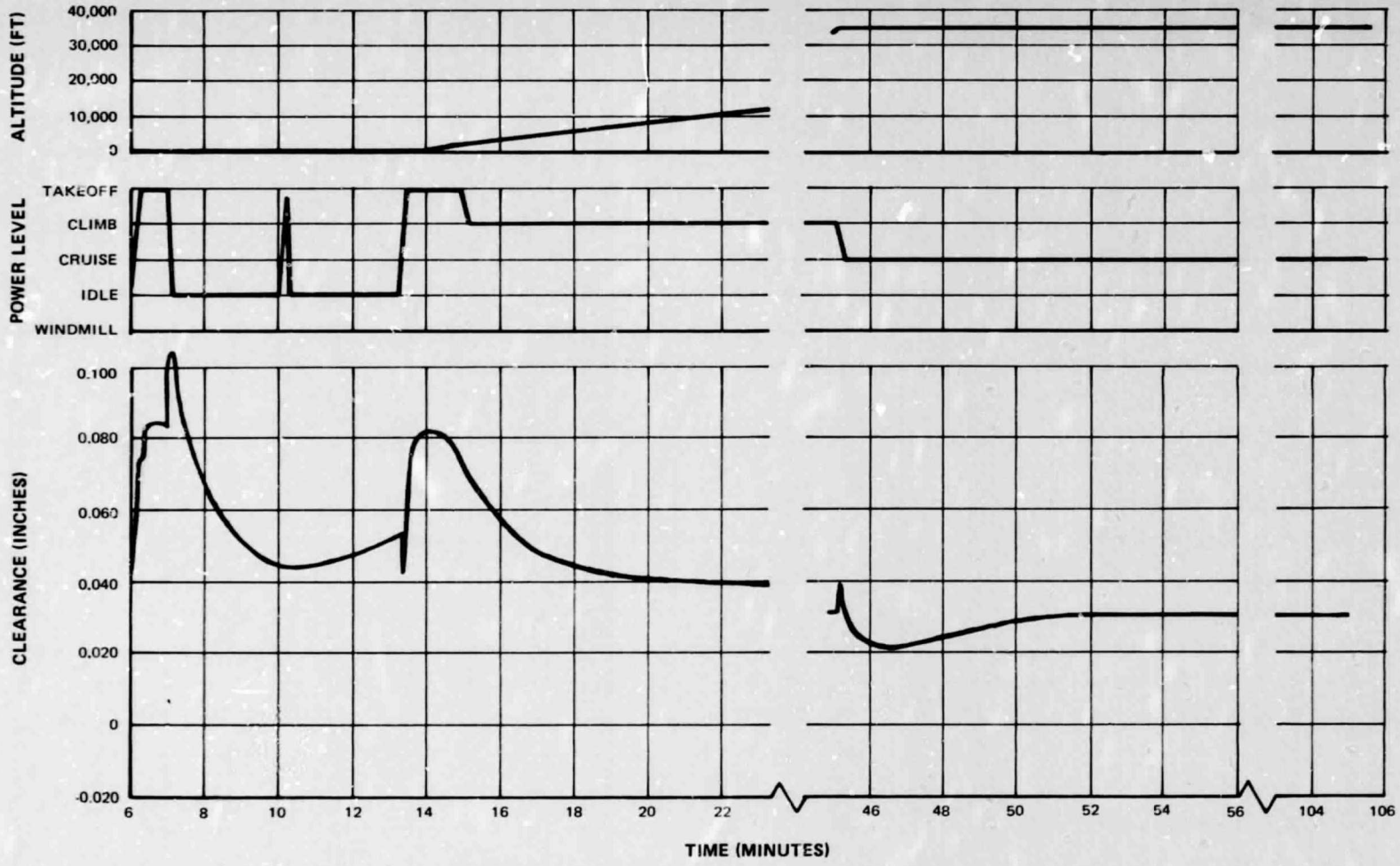

Figure 28a Low-Pressure Turbine Third-Stage Blade Tip Radial Clearance; 747 Flight Acceptance Test Profile

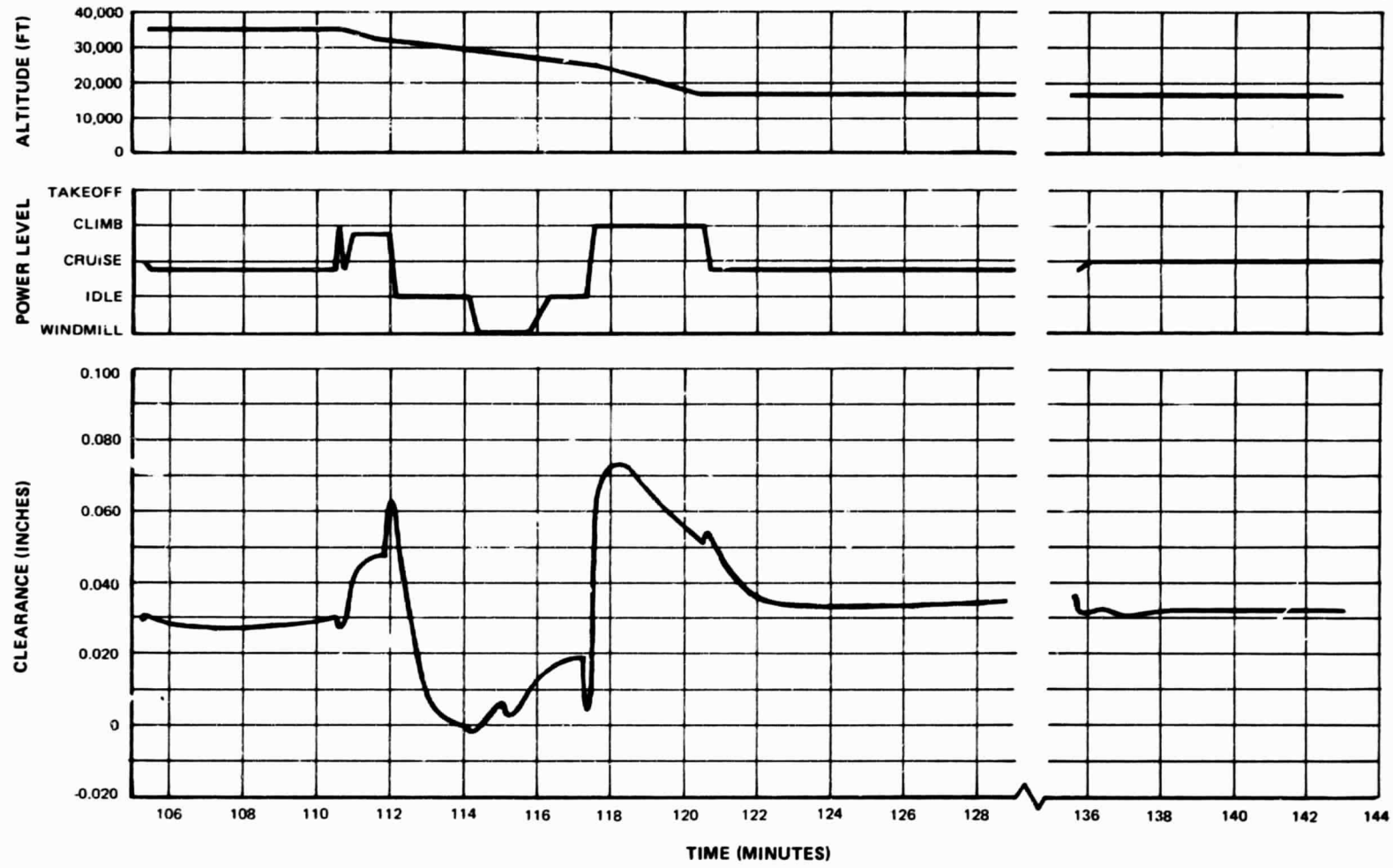

Figure 28b Low-Pressure Turbine Third-Stage Blade Tip Radial Clearance; 747 Flight Acceptance Test Profile (Cont'd.)

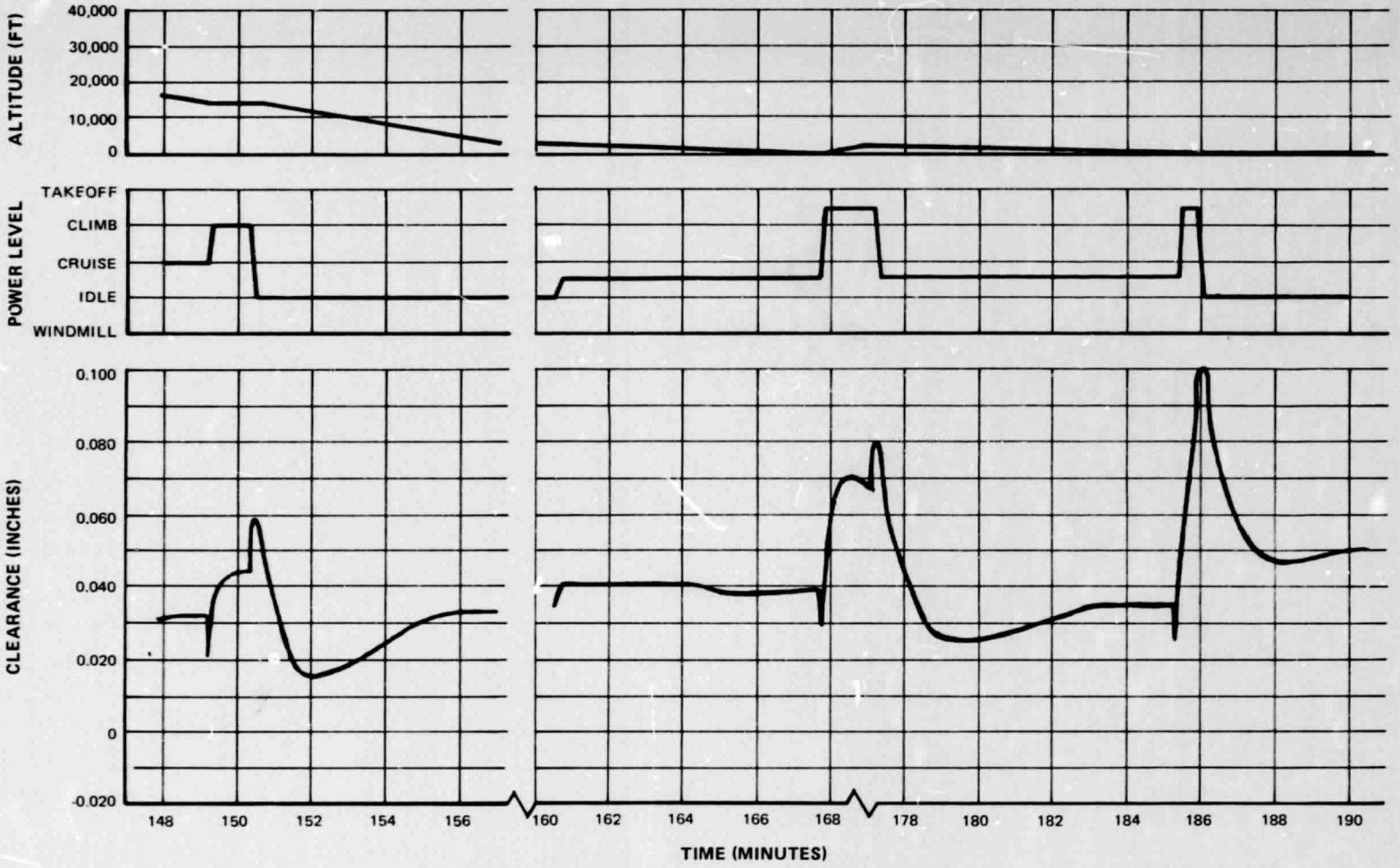

Figure 28c Low-Pressure Turbine Third-Stage Blade Tip Radial Clearance; 747 Flight Acceptance Test Profile (Cont'd.)

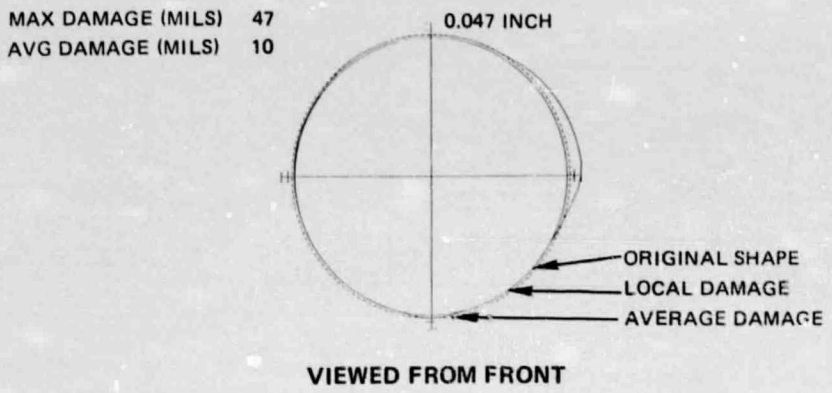

Figure 29 Fan Damage; 747 Flight Acceptance Test

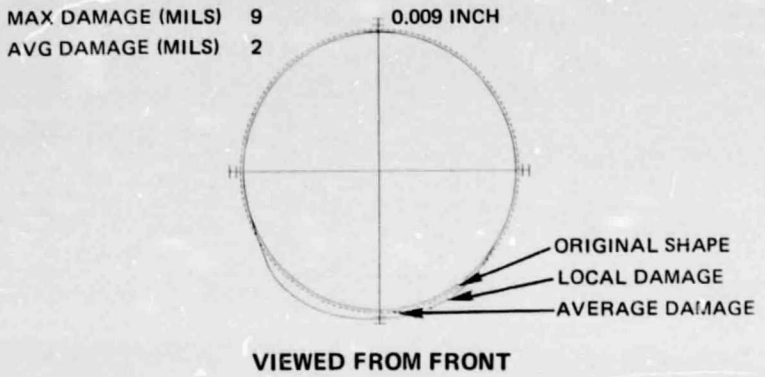

Figure 30 Low-Pressure Compressor Second-Stage Damage; 747 Flight Acceptance Test

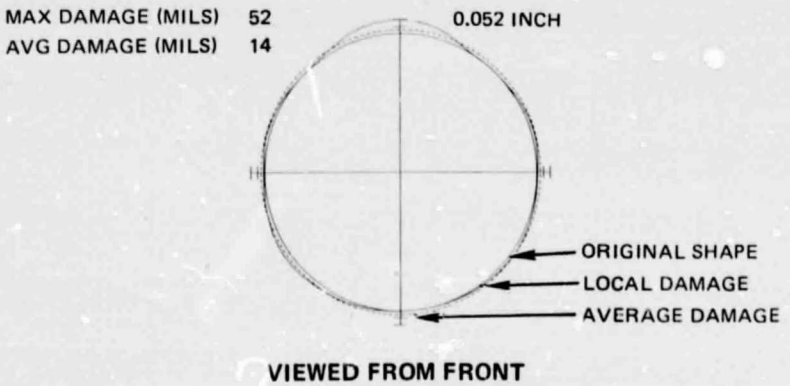

Figure 31 Low-Pressure Compressor Third-Stage Damage; 747 Flight Acceptance Test

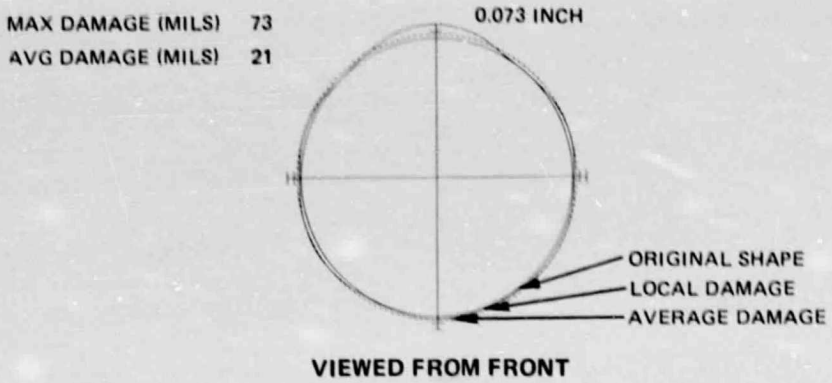

Figure 32 Low-Pressure Compressor Fourth-Stage Damage; 747 Flight Acceptance Test

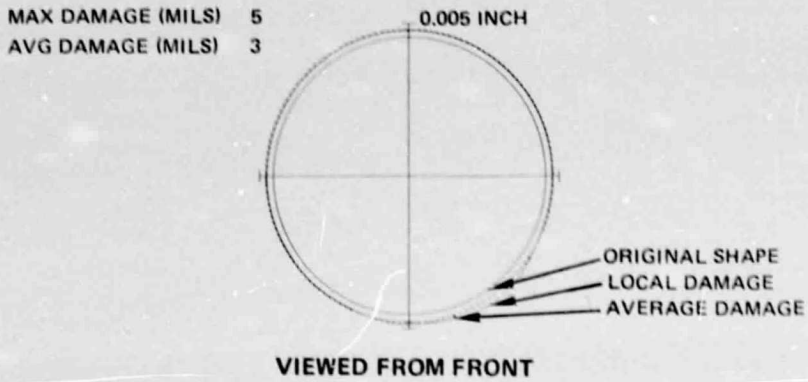

Figure 33 High-Pressure Turbine First-Stage Damage; 747 Flight Acceptance Test

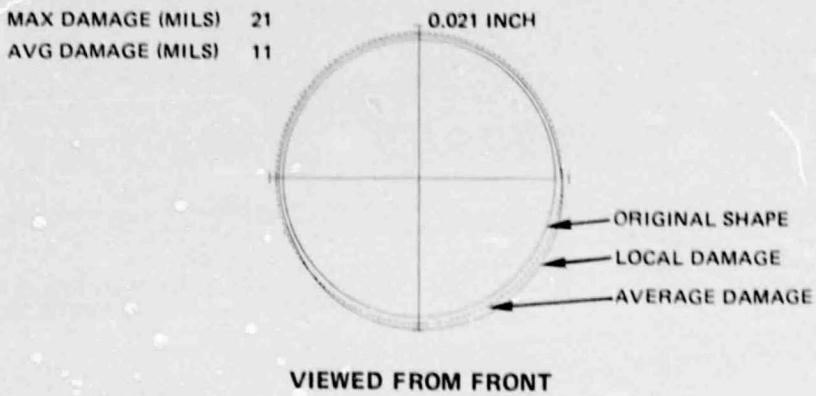

Figure 34 High-Pressure Turbine Second-Stage Damage; 747 Flight Acceptance Test

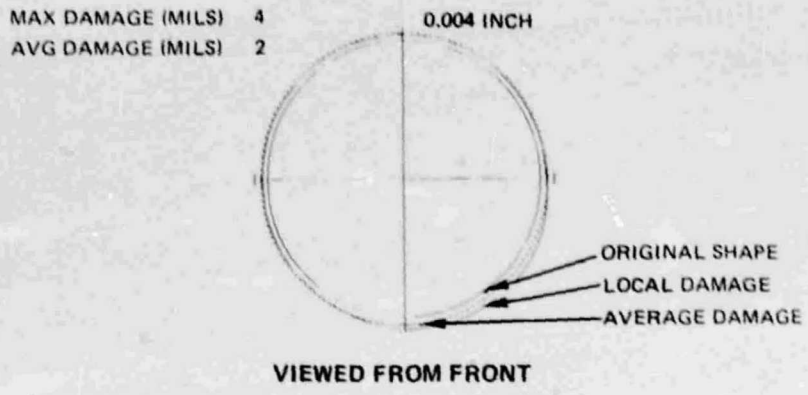

Figure 35 Low-Pressure Turbine Third-Stage Damage; 747 Flight Acceptance Test

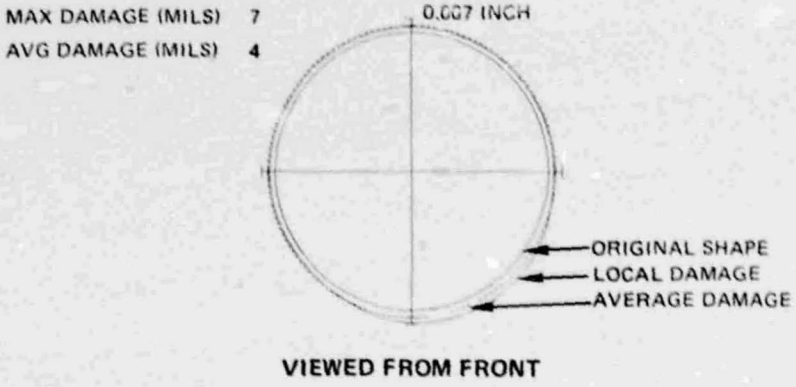

Figure 36 Low-Pressure Turbine Fourth-Stage Damage; 747 Flight Acceptance Test

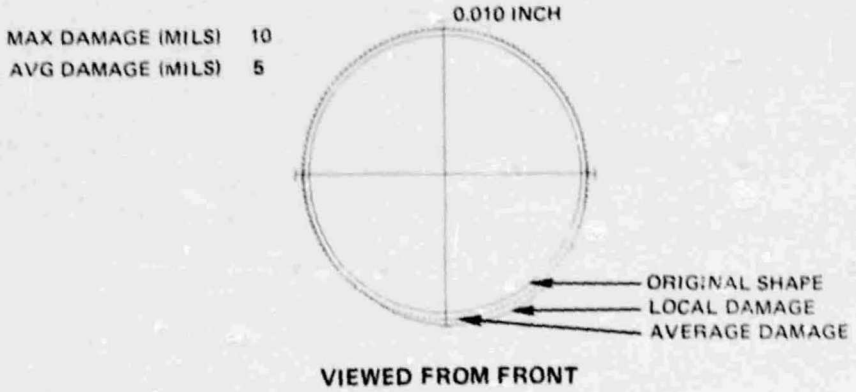

Figure 37 Low-Pressure Turbine Fifth-Stage Damage; 747 Flight Acceptance Test

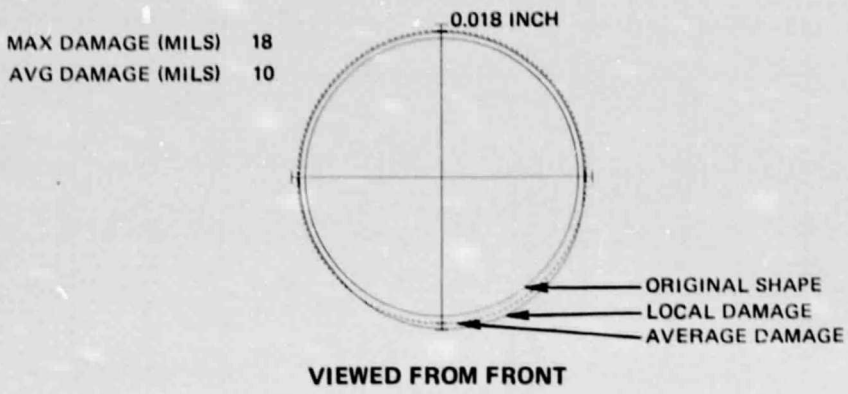

Figure 38 Low-Pressure Turbine Sixth-Stage Damage; 747 Flight Acceptance Test

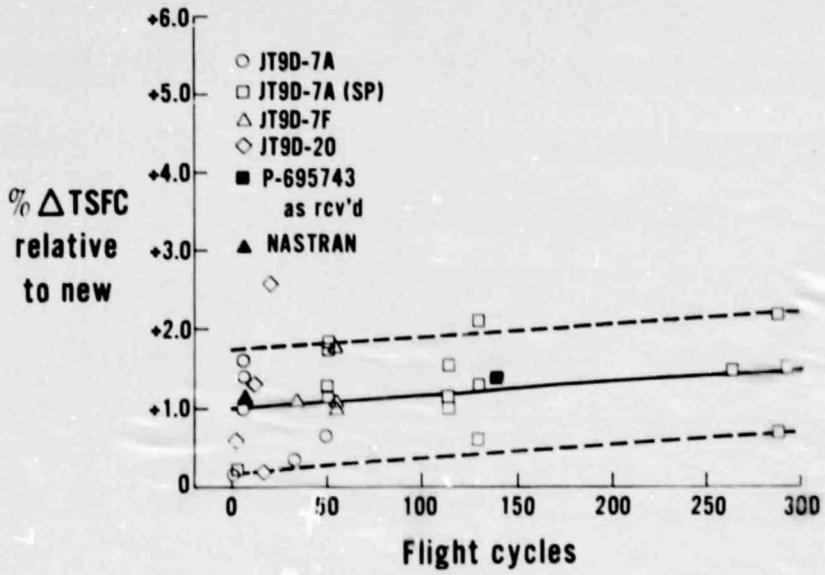

Figure 39 Comparison of Measured Short-Term Performance Deterioration, Based On Three-Hour Flight Cycle, With NASTRAN Results for the First Flight

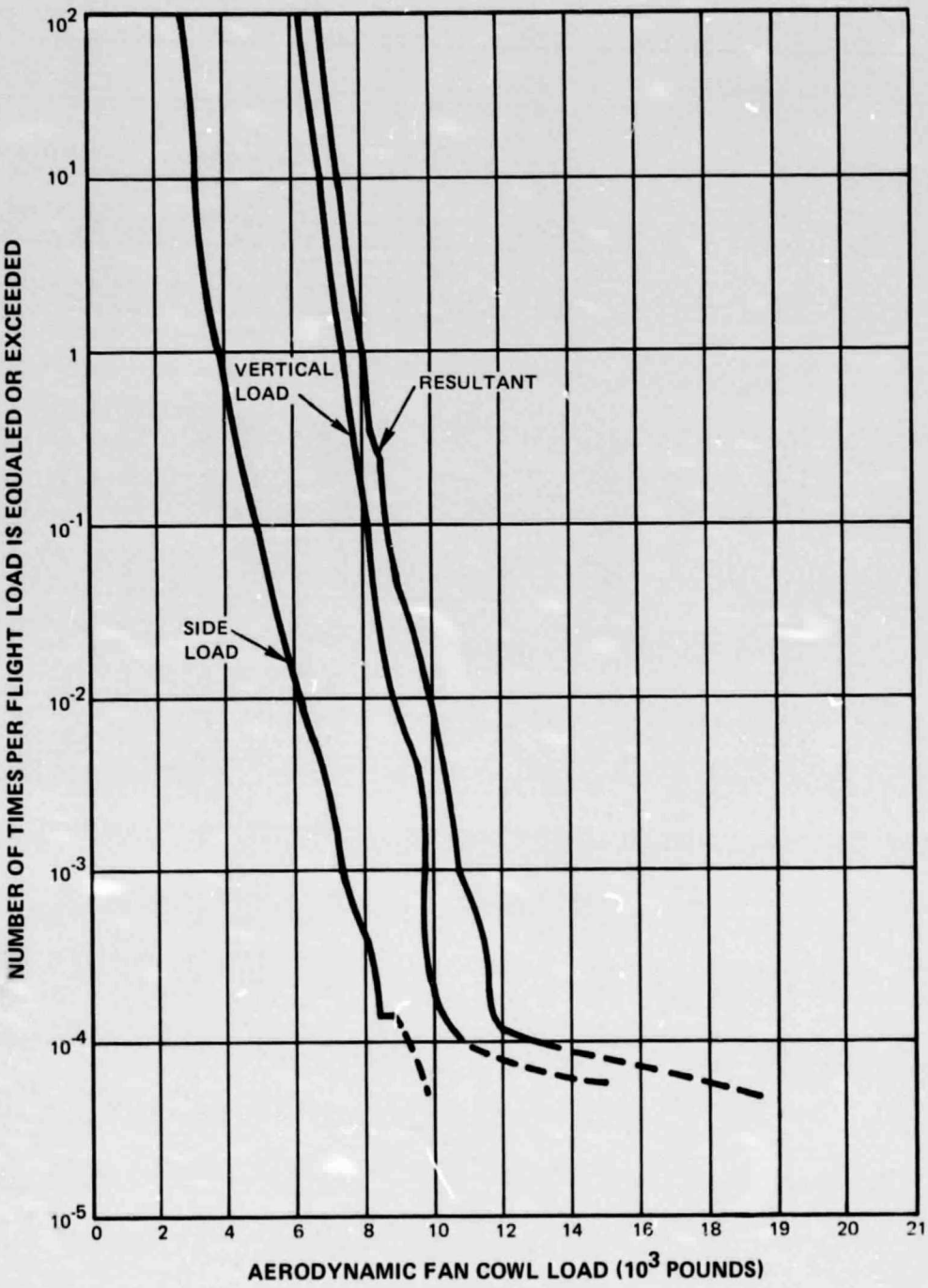

Figure 40 Exceedance Curves for JT9D-7/747 Aerodynamic Fan-Cowl Loads With a Fixed Geometry Inlet, Based On a Three-Hour Flight Cycle

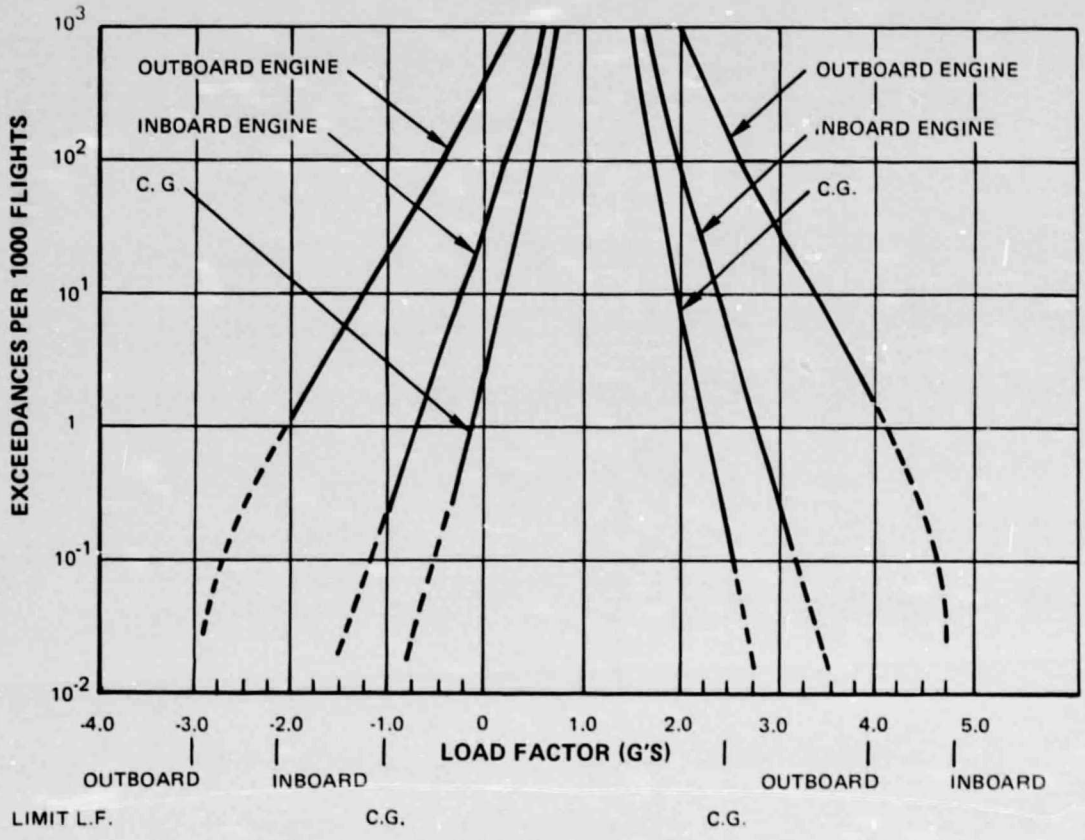

Figure 41 Exceedance Curves for JT9D-7/747 Gravitational (G) Loads, Based On a Three-Hour Flight Cycle

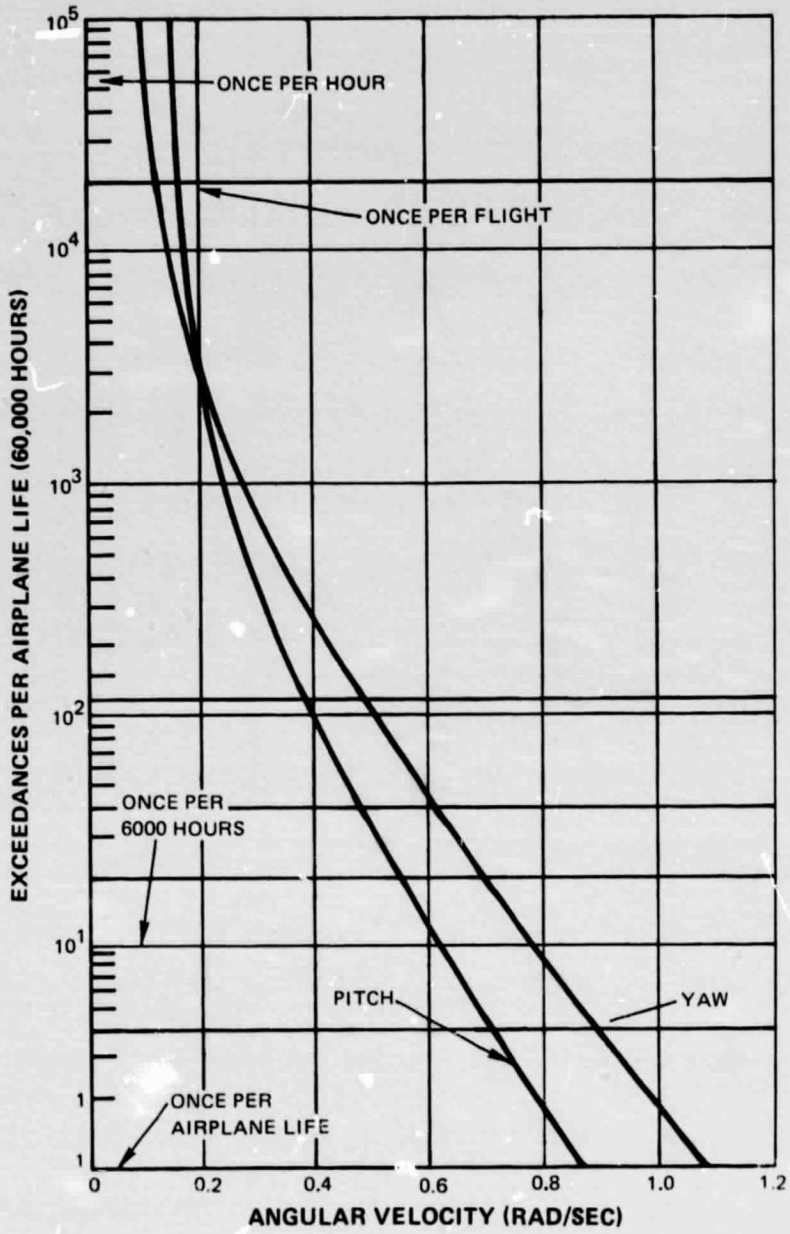

Figure 42 Exceedance Curves for JT9D-7/747 Gyroscopic Loads, Based On a Three-Hour Flight Cycle

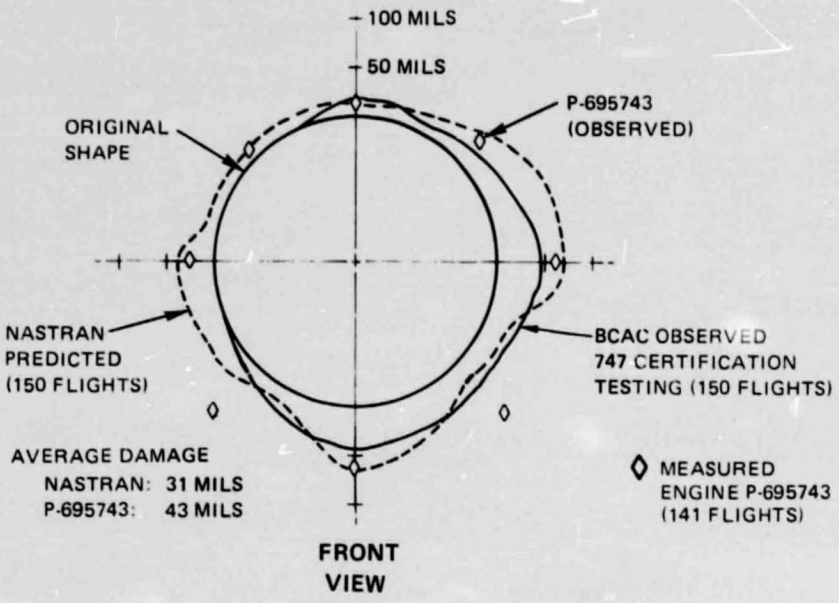

Figure 43 Comparison of Predicted and Measured Fan Rub Patterns

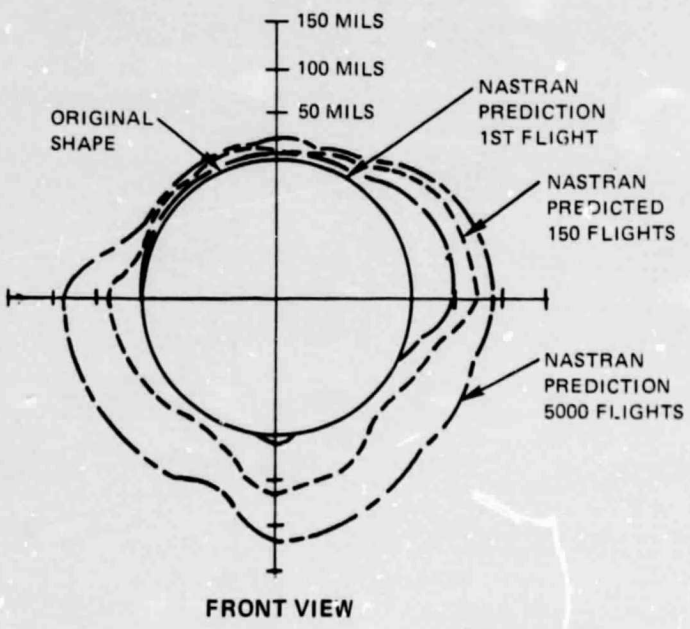

Figure 44 Comparison of Predicted Fan Rub Patterns as a Function of Number of Flights

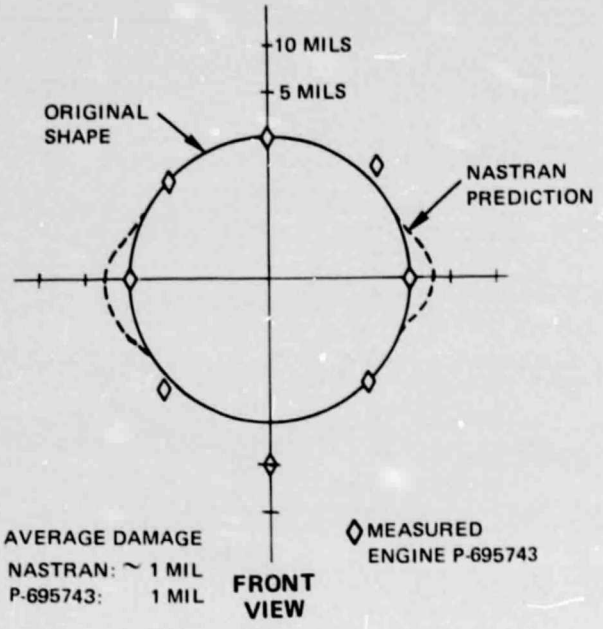

Figure 45 Comparison of Predicted and Measured High-Pressure Compressor Fifth-Stage Rub Patterns

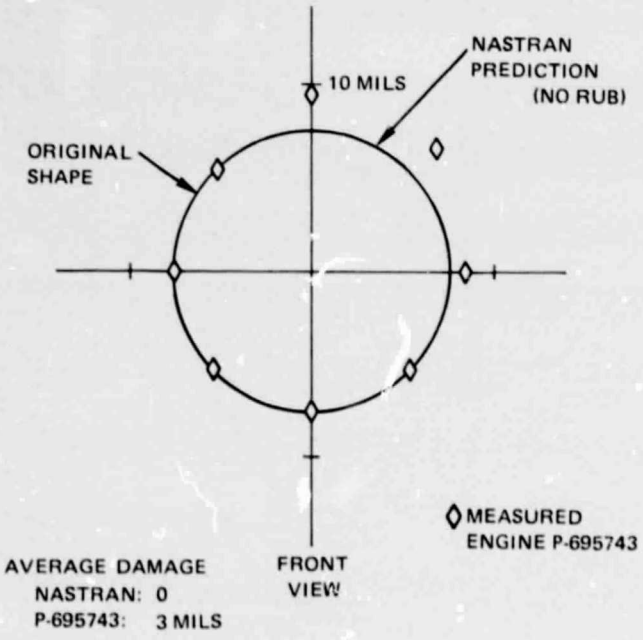

Figure 46 Comparison of Predicted and Measured High-Pressure Compressor Ninth-Stage Rub Patterns

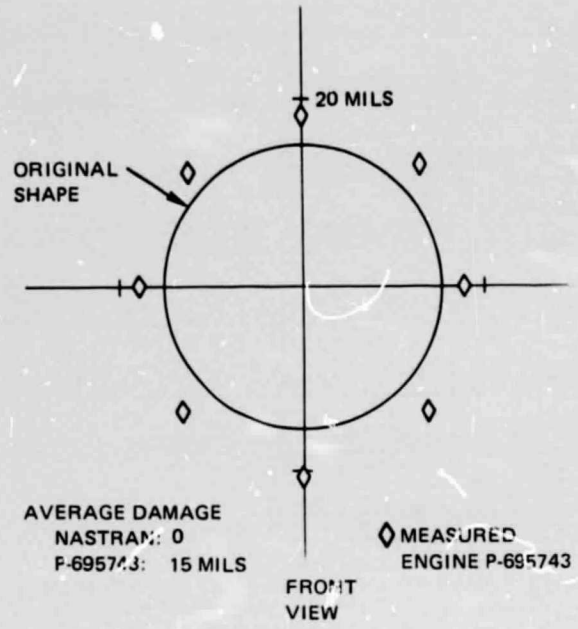

Figure 47 Comparison of Predicted and Measured High-Pressure Compressor 15th-Stage Rub Patterns

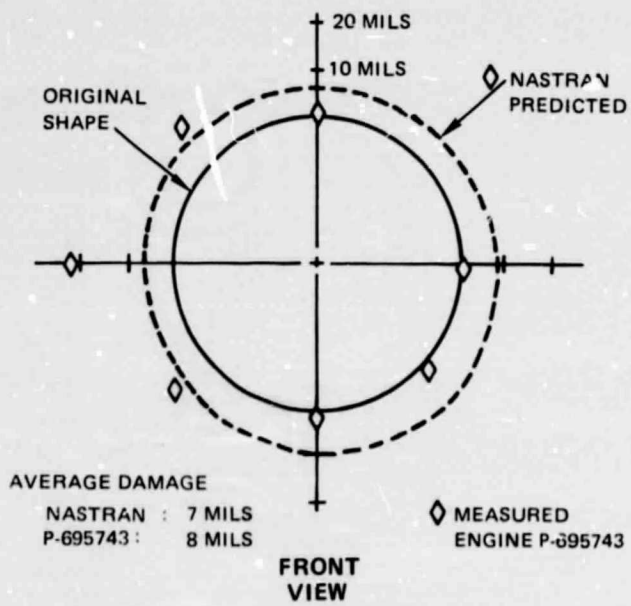

Figure 48 Comparison of Predicted and Measured High-Pressure Turbine First-Stage Rub Patterns

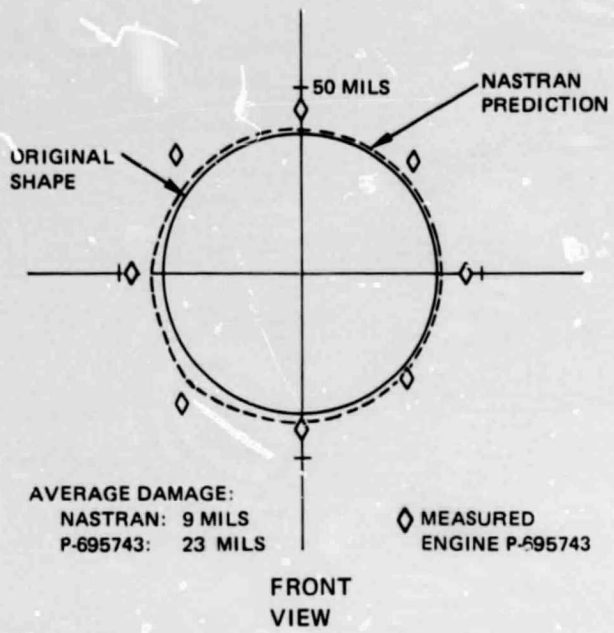

Figure 49 Comparison of Predicted and Measured High-Pressure Turbine Second-Stage Rub Patterns

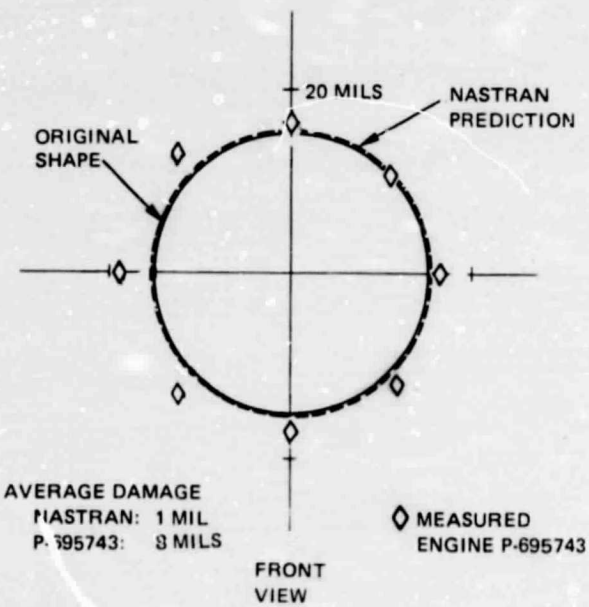

Figure 50 Comparison of Predicted and Measured Low-Pressure Turbine Third-Stage Rub Patterns

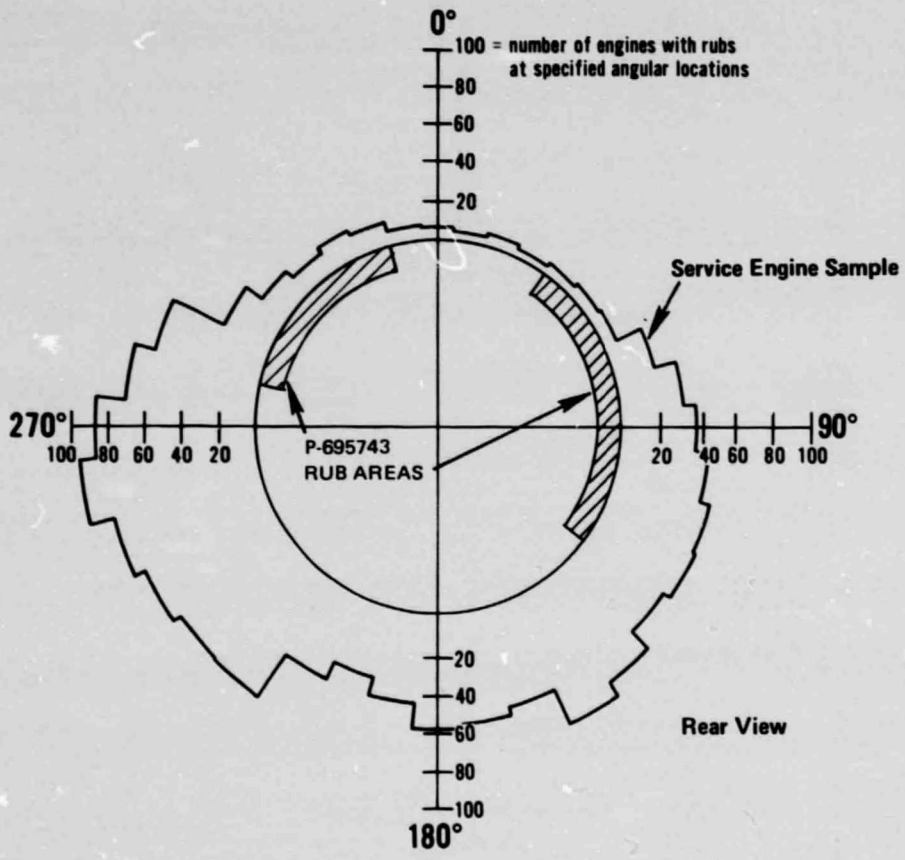

Figure 51 JT9D First-Stage High-Pressure Turbine Outer Air Seal Rub Patterns

C-2

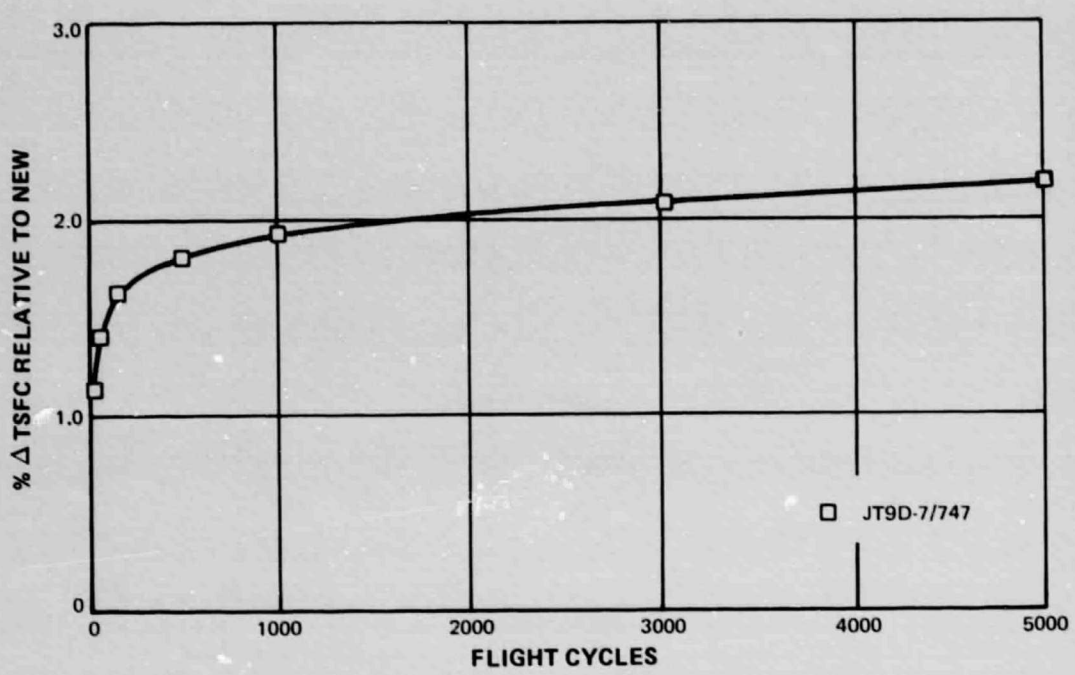

Figure 52 Predicted Engine Performance Deterioration

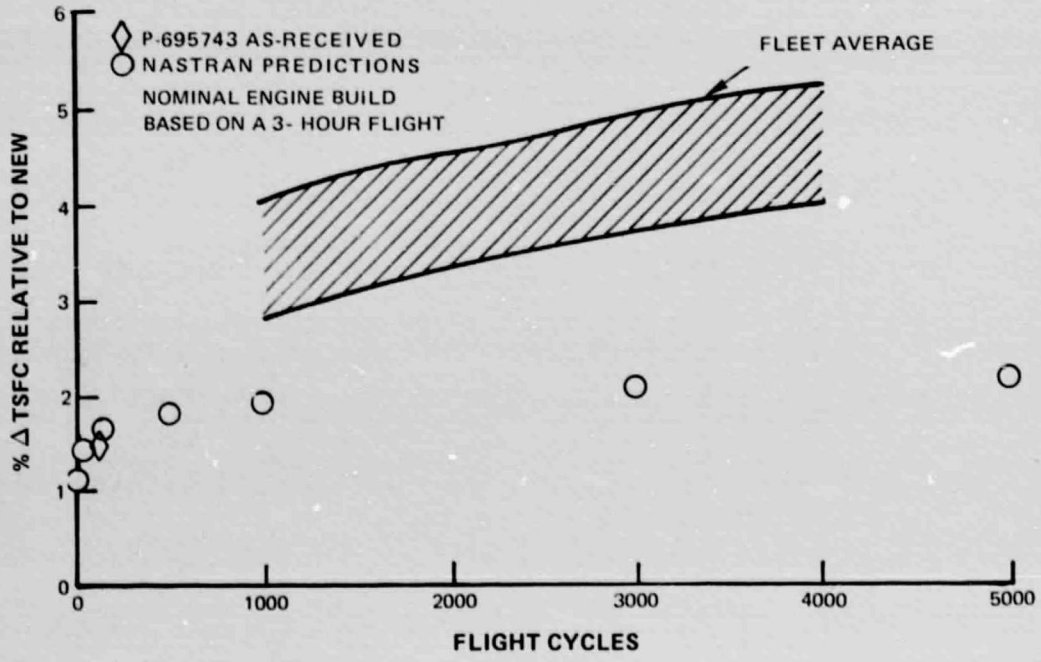

Figure 53 Predicted Performance Deterioration Over a Range of Flight Cycles Compared to "Fleet Average" Prerepair Performance Deterioration At Constant Thrust, Relative to New

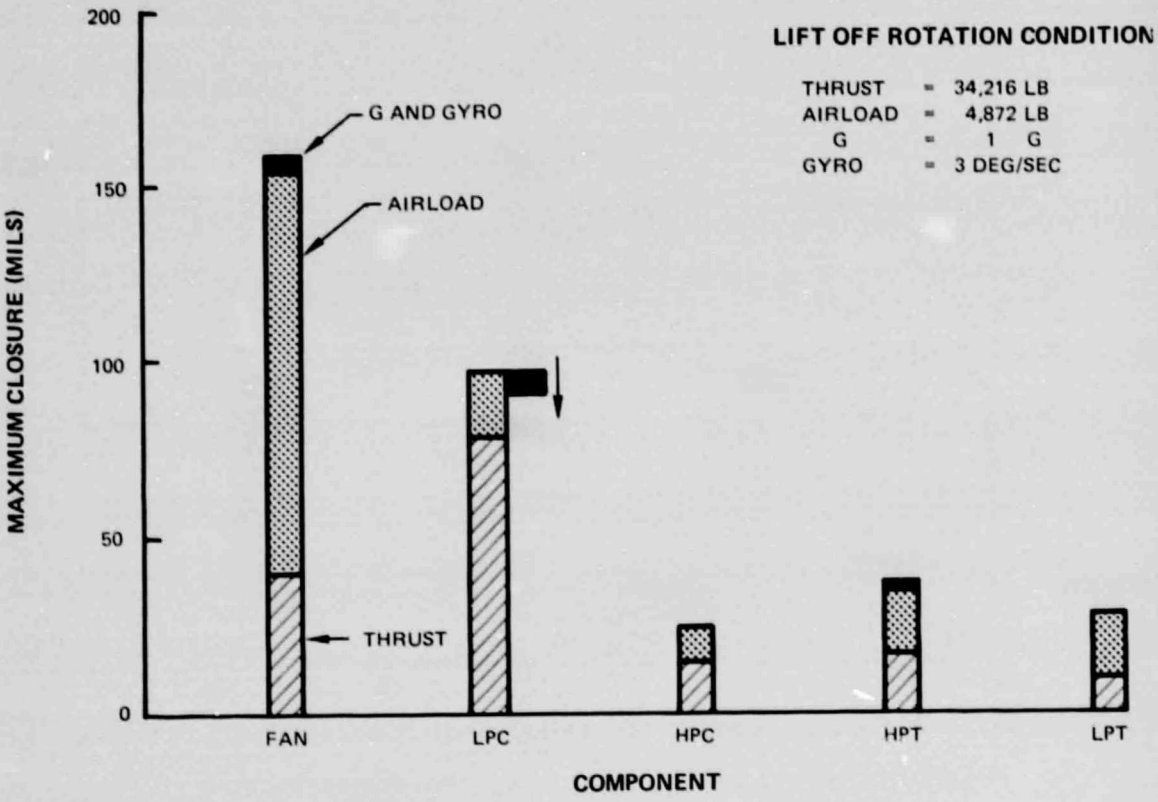

Figure 54 Static Analysis of Closures At Lift-Off Rotation

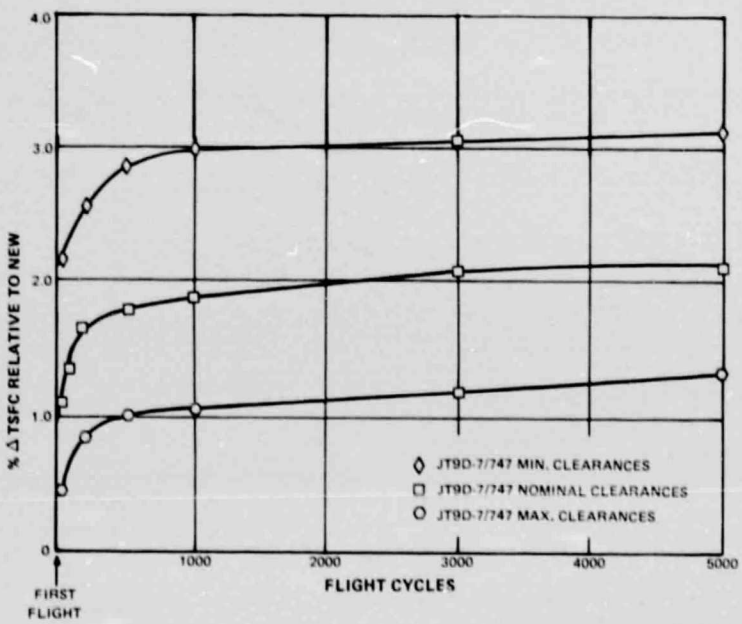

Figure 55 Effect of Variations In Build Clearances On Engine Performance Deterioration

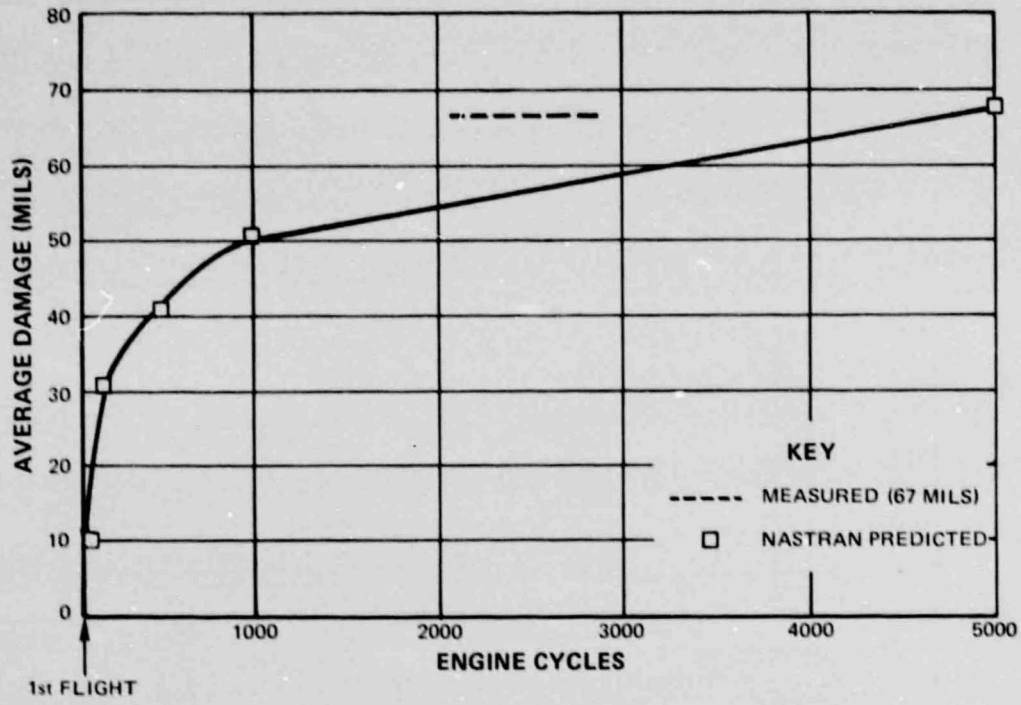

Figure 56 Comparison of Predicted Average Fan Damage With Measured Damage Over a Range of Engine Cycles

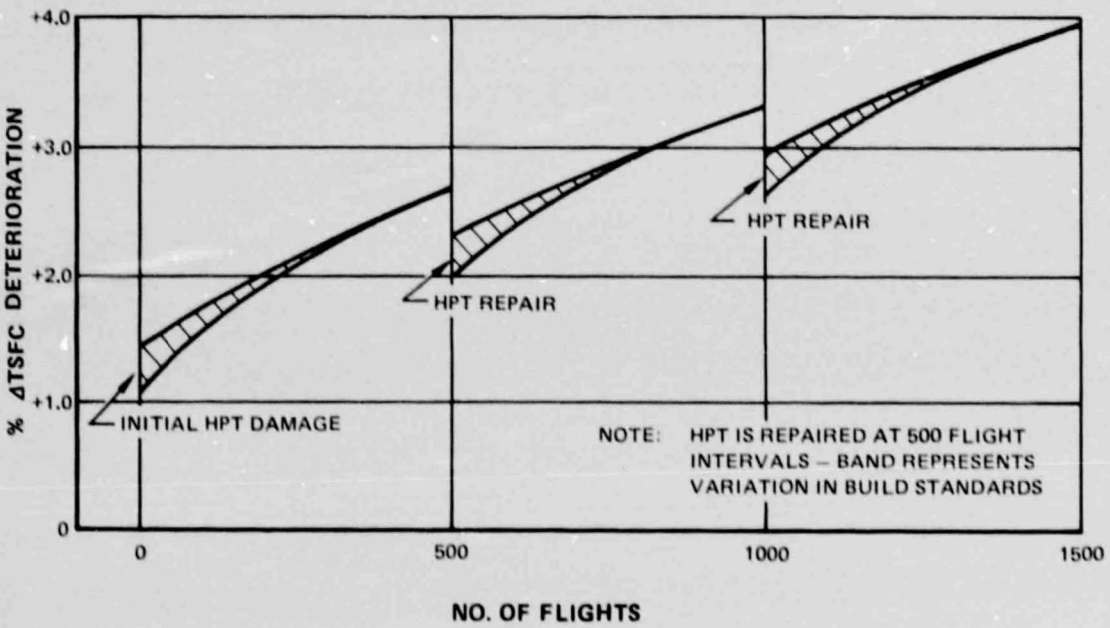

Figure 57 High-Pressure Turbine Deterioration and Repair Effects

APPENDIX

NOMENCLATURE

a_T	–	Stagnation speed of sound (ft/sec)
A	–	Arbitrary constant for curve fitting
A_f	–	Inlet flow area at the fan face (ft^2)
A^*	–	Critical flow area (ft^2)
B	–	Arbitrary constant for curve fitting
BID	–	Blow-in door inlet configuration
c	–	Distance from highlight plane to fan face (inches)
$\bar{c}_j$	–	Average clearance change for stage j (inches)
C_L	–	Coefficient of lift
C.G.	–	Center of gravity
EGT	–	Exhaust gas temperature (°K)
EPR	–	Engine pressure ratio
flap	–	Airplane wing flap
FAA	–	Federal Aviation Administration
Fixed Lip	–	Fixed lip inlet configuration
F_n	–	Engine net thrust (pounds)
F_x, F_y, F_z	–	Cowl load pressure force resultants (pounds)
G	–	Gravity, gravitational field
h	–	Airplane altitude (feet)
HPC	–	High-pressure compressor
HPT	–	High-pressure turbine
ILS	–	Instrument landing system
KEAS	–	Knots equivalent air speed (knots)
Kips	–	Thousand pounds
KTAS	–	Knots true air speed (knots)
KTS	–	Knots
LPC	–	Low-pressure compressor
LPT	–	Low-pressure turbine
$\dot{m}$	–	Fan mass flow (lbm/sec)
MCP	–	Maximum continuous power
MCT	–	Maximum continuous thrust
M_{MAX}	–	Airplane maximum Mach number
M_n	–	Mach number
M_x, M_y, M_z	–	Cowl load pressure moment resultants (in-lb)
n_z	–	Airplane load factor
N_1	–	Low-pressure rotor speed (rpm)

NOMENCLATURE (Cont'd.)

N_2	–	High-pressure rotor speed (rpm)
pack	–	Air conditioning pack
P	–	Pressure (lb/in^2)
PRBC	–	Pressure ratio bleed control
P_T	–	Stagnation pressure (lb/in^2)
q	–	Dynamic pressure ($\frac{1}{2}\rho V_e^2$) (lb/in^2)
s	–	Distance of pressure tap from highlight plane (inches)
Snap	–	Indicates rapid throttle movement
SSLTO	–	Steady sea level take-off
T.O.	–	Take-off
TSFC	–	Thrust Specific Fuel Consumption
T_{T6}	–	Exhaust gas temperature, measured at HPT exit (°K)
V_e	–	Equivalent air speed (ft/sec)
Vs	–	Airplane stall velocity (ft/sec)
Δg	–	Gravity parameter
ξ_{ij}	–	Performance influence coefficient for stage j, condition i
$\dot{\theta}$	–	Airplane pitch rate (radians/sec)
ρ	–	Local free stream mass density ($lb\text{-}sec^2/in.^4$)
σ	–	Ambient density ratio
$\dot{\phi}$	–	Airplane yaw rate (radians/sec)

Subscripts:

airplane	–	B747 airplane
e	–	Equivalent
f	–	Fan face
i	–	Condition
j	–	Stage No.
MAX	–	Maximum
nac	–	Nacelle
s	–	Stall
T	–	Stagnation
x, y, z	–	Directional
1	–	Low-pressue
2	–	High-pressure
6	–	HPT exhaust
∞	–	Infinity